

Electronic Thesis and Dissertation Repository

---

8-3-2023 2:00 PM

## Effect of pharmacological inhibition of endogenous hydrogen sulfide production on bladder cancer progression

Sydney Relouw, *Western University*

Supervisor: Sener, Alp, *The University of Western Ontario*

A thesis submitted in partial fulfillment of the requirements for the Master of Science degree in Microbiology and Immunology

© Sydney Relouw 2023

Follow this and additional works at: <https://ir.lib.uwo.ca/etd>



Part of the [Therapeutics Commons](#)

---

### Recommended Citation

Relouw, Sydney, "Effect of pharmacological inhibition of endogenous hydrogen sulfide production on bladder cancer progression" (2023). *Electronic Thesis and Dissertation Repository*. 9480.  
<https://ir.lib.uwo.ca/etd/9480>

This Dissertation/Thesis is brought to you for free and open access by Scholarship@Western. It has been accepted for inclusion in Electronic Thesis and Dissertation Repository by an authorized administrator of Scholarship@Western. For more information, please contact [wlsadmin@uwo.ca](mailto:wlsadmin@uwo.ca).

## **Abstract**

Present bladder cancer therapies have extremely limited therapeutic impact giving it the highest lifetime treatment cost per patient and leading to an imperative need for investigation of novel therapies. Recent literature suggests hydrogen sulfide (H<sub>2</sub>S), an endogenously produced gaseous signaling molecule, plays a pivotal role in cancer pathophysiology. This study investigated the effect of inhibiting endogenous H<sub>2</sub>S production on bladder cancer progression. We targeted the H<sub>2</sub>S-producing enzyme, cystathionine  $\gamma$ -lyase (CSE), and found that inhibiting its activity significantly attenuated 5637 and MB49 bladder cancer cell viability. Furthermore, an intravesical murine model of bladder cancer was subjected to single and combination intravesical therapies consisting of the CSE inhibitor, propargylglycine (PAG), and gemcitabine (GEM) chemotherapy followed by evaluation of tumor response via magnetic resonance imaging, pathology, and immunohistochemical staining. We observed a significant attenuation of tumor growth and invasion following CSE inhibition and enhanced anti-cancer effects of GEM by PAG, resulting in tumor regression and abrogation of invasion. Our findings suggest that inhibition of endogenous H<sub>2</sub>S production induced apoptosis and an immune response and attenuated VEGF-led neovascularization and proliferation within the bladder tumor. It also enhanced the pro-apoptotic and anti-neovascularization effects of GEM. Therefore, inhibition of endogenous H<sub>2</sub>S production may have antineoplastic potential as well as additive effect with conventional chemotherapy on bladder cancer progression, suggesting H<sub>2</sub>S as a novel target for developing improved combination therapies against bladder cancer.

## **Keywords**

Bladder cancer, hydrogen sulfide (H<sub>2</sub>S), murine model, magnetic resonance imaging (MRI), intravesical therapy, propargylglycine (PAG), sodium hydrosulfide (NaHS), gemcitabine (GEM)

## **Summary for Lay Audience**

Bladder cancer is the 10<sup>th</sup> most common cancer worldwide with almost 600,000 new cases and over 200,000 associated deaths occurring in 2020 alone. Current bladder cancer therapies are inadequate and associated with high failure and complication rates, lengthy treatment times, and are extremely costly. Therefore, novel therapies need to be investigated. Hydrogen sulfide (H<sub>2</sub>S), a gas produced within all mammalian cells, has been shown to play an important role in the development and progression of cancer. This study investigated the effect of inhibiting H<sub>2</sub>S production on bladder cancer progression in combination with a clinically used chemotherapy using a mouse model. Mice with bladder cancer received single and combination therapies consisting of an inhibitor of H<sub>2</sub>S production and chemotherapy. Therapies were administered directly into the mouse bladder and tumor growth was evaluated by magnetic resonance imaging and pathology. We reported that inhibition of H<sub>2</sub>S production slowed the growth of the bladder tumors and reduced their invasiveness. Moreover, we reported that inhibition of H<sub>2</sub>S production increased the anti-cancer effects of chemotherapy as a reduction in both bladder tumor size and invasiveness was observed compared to chemotherapy alone. Therefore, we conclude that inhibiting H<sub>2</sub>S production in conjunction with chemotherapy may serve as an improved combination therapy for bladder cancer.

## Co-Authorship Statement

**Section 1 (1.6.1, 1.6.2, and 1.6.3): Relouw, S., Dugbartey, G.J., Sener, A. Non-invasive imaging modalities in intravesical murine models of bladder cancer. *Cancers*, 2023. 15: 2381. doi: 10.3390/cancers15082381**

Relouw, S. and Sener, A. conceptualized the review. Relouw, S. wrote the manuscript and created figures. Relouw, S., Sener, A., and Dugbartey, G.J. reviewed and edited the manuscript. Final form of the manuscript was approved by all authors.

**Section 2, 3, and 4: Relouw, S., McLeod, P., Knier, N., Martinez Santiesteban, F., Foster, P., Cadieux-Pitre, H.A., Hague, N., Major, S., O'Neil, C., Gabril, M., Moussa, M., Huynh, M., Haeryfar, M., Dugbartey, G.J., Sener, A. Pharmacological inhibition of endogenous hydrogen sulfide production on bladder cancer progression in an intravesical murine model. 2023. [Unpublished manuscript].**

Sener, A. and Dugbartey, G.J. conceptualized and Sener, A. supervised the study. Huynh, M. and Haeryfar, M. assisted with conceptualization. Relouw, S. executed all experiments, curated, and analyzed all data, wrote the manuscript, and created figures. McLeod, P. assisted with all *in vitro* experiments. Major, S. assisted with establishing the Animal Use Protocol. Cadieux-Pitre, H.A. and Hague, N. performed the intravesical therapy methodology. Knier, N., Martinez Santiesteban, F., and Foster, P. performed and assisted with the magnetic resonance imaging methodology. Gabril, M. and Moussa, M. performed pathology. O'Neil, C. performed immunohistochemistry and slide visualization. Relouw, S., Dugbartey, G.J., and Sener, A. reviewed and edited the manuscript.

## **Acknowledgments**

First, I would like to thank Dr. Sener for providing me with the opportunity to join this lab and to take on this project. Dr. Sener's positivity and drive are contagious and paired with the independence and freedom he provided, permitted me to develop my passion for research. He provided constant guidance, support, and encouragement throughout every aspect of this project (especially the stressful times). Overall, this lab has provided me with numerous amazing experiences and has allowed me to develop skills and make connections that are imperative to my previous successes and that I will be able to use in future endeavors.

I would also like to thank my Advisory Committee members, Dr. Huynh and Dr. Haeryfar, who provided me with insight and guidance imperative to the success of this research. The combination of Dr. Huynh's clinical expertise and Dr. Haeryfar's cancer immunology expertise was not only invaluable to my learning experience but also allowed me to approach this project from many different perspectives, which improved this project immensely.

I would also like to thank the other members of the lab, past and present, for their support. I am forever grateful for the friendships and memories we formed as well as for everything we taught and learned from one another. Maria and I joined this lab and went through this experience together and I could not have asked for a better companion throughout this program.

I would also like to thank Patrick McLeod, Sally Major, and Katherine Branton who made the Matthew Mailing Centre an exceptionally welcoming and affirming environment. The *in vitro* portion of this project would not exist without the guidance and technical expertise of Patrick. Nor would the *in vivo* portion exist without Sally, who worked laboriously on the Animal Use Protocol and provided insight into animal care. Katherine helped with all grants received and kept me on track with all associated reports. But what I am most grateful for is her help with ordering my lab supplies, guaranteeing the best price, and tracking down every lost or wrong order. Without this I simply could not have completed

my experiments. I could never thank these three individuals enough for the support they provided me with throughout this program.

Moreover, I would also like to thank Heather-Anne Cadieux-Pitre, Nicole Hague and the rest of the ACVS team. Together they successfully developed and performed the transurethral administration technique, which was completely new to this facility, for the purpose of this research. I cannot fathom the number of hours this required but I am extremely grateful. I would also like to thank them for their assistance and guidance on the welfare of the mice used in this experiment and for making me feel a part of the team.

I would also like to thank Dr. Foster, Dr. Knier, and Francisco (Paco) for collaborating with me on the MRI portion of this research. I would like to thank them for taking numerous hours out of their already incredibly busy schedules to develop the protocol and to help with imaging - everything I know about performing MRI and analyzing the images is owed to this team. I am also grateful for the enlightening conversations we had during the scanning times.

I would also like to thank Dr. Gabriel, Dr. Moussa, and Caroline O'Neil for their assistance and insights with the pathology and immunohistochemistry portion of this research. Caroline and her team were imperative to the completion of this research as they worked tirelessly to complete the immunohistochemical staining in such a short period of time.

Finally, I would like to thank all my family and friends for their love, support, and encouragement. They truly are the reason I was able to accomplish this program. Namely I would like to thank my parents, Mark and Patty Relouw, for their endless support and making me feel as if I can accomplish anything. I would also like to thank my partner Nicholas Rizzo for being by my side throughout this experience and helping me troubleshoot even when he had no idea what I was talking about.

I cannot thank the individuals mentioned above enough for everything they did for me over these past two years. I will be forever grateful for my time at Western University and in the Sener Lab.

## Tables of Contents

<i>Abstract</i> .....	<i>II</i>
<i>Keywords</i> .....	<i>II</i>
<i>Summary for Lay Audience</i> .....	<i>III</i>
<i>Co-Authorship Statement</i> .....	<i>IV</i>
<i>Acknowledgments</i> .....	<i>V</i>
<i>List of Tables</i> .....	<i>IX</i>
<i>List of Figures</i> .....	<i>X</i>
<i>List of Appendices</i> .....	<i>XI</i>
<i>List of Abbreviations</i> .....	<i>XII</i>
<b>1 Introduction</b> .....	<b>1</b>
<b>1.1 Bladder Cancer</b> .....	<b>1</b>
1.1.1 <i>Current standard of care for high-grade NMIBC</i> .....	1
1.1.2 <i>Current standard of care for MIBC</i> .....	3
1.1.3 <i>Economic cost burden of bladder cancer</i> .....	3
<b>1.2 Bladder Cancer Tumor Microenvironment</b> .....	<b>4</b>
<b>1.3 Hydrogen Sulfide</b> .....	<b>5</b>
1.3.1 <i>H<sub>2</sub>S metabolism</i> .....	7
<b>1.4 H<sub>2</sub>S in Cancer</b> .....	<b>7</b>
1.4.1 <i>Sodium hydrosulfide: an exogenous H<sub>2</sub>S donor</i> .....	8
1.4.2 <i>Propargylglycine: an endogenous H<sub>2</sub>S synthesis inhibitor</i> .....	8
<b>1.5 The Role of H<sub>2</sub>S in DNA Repair, Neovascularization, Apoptotic Escape, and Immune Evasion in Cancer Cells</b> .....	<b>9</b>
<b>1.6 H<sub>2</sub>S in Bladder Cancer</b> .....	<b>12</b>
1.6.1 <i>Limitations of current bladder cancer models</i> .....	13
1.6.2 <i>Intravesical murine models of bladder cancer</i> .....	14
1.6.3 <i>Non-invasive imaging modalities for intravesical models of bladder cancer</i> .	15
<b>1.7 Rationale and Hypothesis</b> .....	<b>19</b>
<b>1.8 Aims and Objectives</b> .....	<b>20</b>
<b>2 Methods</b> .....	<b>21</b>
<b>2.1 In vitro model of bladder cancer</b> .....	<b>21</b>
2.1.1 <i>Cell culture</i> .....	21
2.1.2 <i>Quantitative PCR analysis</i> . .....	21
2.1.3 <i>Dose response curves and treatments</i> . .....	22
2.1.4 <i>Flow cytometry</i> .....	24

<b>2.2 <i>In vivo</i> model of bladder cancer .....</b>	<b>24</b>
2.2.1 <i>Experimental animals.</i> .....	24
2.2.2 <i>Murine bladder cancer model.</i> .....	24
2.2.3 <i>Magnetic resonance imaging.</i> .....	26
2.2.4 <i>Tumor analysis.</i> .....	26
2.2.5 <i>Intravesical therapy.</i> .....	28
2.2.6 <i>Histological staining.</i> .....	28
2.2.7 <i>Microscope image analysis.</i> .....	29
2.3 <i>Statistical analysis.</i> .....	29
<b>3 Results.....</b>	<b>30</b>
<b>3.1 <i>CSE gene expression is less downregulated in MB49 cells and upregulated in 5637 cells under hypoxic conditions.</i> .....</b>	<b>30</b>
<b>3.2 <i>Optimal treatment doses were determined as 100 μM NaHS, 20 mM PAG, and 100 μM GEM in vitro.</i> .....</b>	<b>32</b>
<b>3.3 <i>Inhibiting CSE activity attenuates cell viability and further reduces cell viability in the presence of chemotherapy.</i>.....</b>	<b>34</b>
<b>3.4 <i>BBN induces bladder cancer in an intravesical murine model as detected by MRI.</i>.....</b>	<b>38</b>
<b>3.5 <i>Inhibiting CSE activity attenuates tumor progression and invasion and results in tumor regression and abrogates invasion in the presence of chemotherapy.</i>.....</b>	<b>40</b>
<b>3.6 <i>Inhibiting CSE activity induces bladder tumor apoptosis, attenuates neovascularization and proliferation, alters the bladder tumor immune response and potentiates the pro-apoptotic and anti-neovascularization effects of chemotherapy.</i>.....</b>	<b>44</b>
<b>4 Discussion.....</b>	<b>51</b>
<b>4.1 <i>Limitations and future directions</i>.....</b>	<b>61</b>
<b>5 Conclusion.....</b>	<b>62</b>
<b>References .....</b>	<b>64</b>
<b>Appendix A -Animal ethics approval.....</b>	<b>81</b>
<b>Curriculum Vitae .....</b>	<b>82</b>

**List of Tables**

Table 1: List of qPCR primer sequences..... 22

## List of Figures

Figure 1: Schematic of endogenous H <sub>2</sub> S metabolism.....	6
Figure 2: Accumulation of H <sub>2</sub> S, due to the upregulation of H <sub>2</sub> S-producing enzymes in cancerous tissue, promotes pro-cancerous pathways.....	10
Figure 3: Non-invasive imaging in intravesical murine models of bladder cancer. ....	16
Figure 4: <i>In vitro</i> model of bladder cancer workflow.....	23
Figure 5: <i>In vivo</i> model of bladder cancer workflow.....	25
Figure 6: Representative images of tumor burden analysis using MRI.....	27
Figure 7: CSE gene expression is less downregulated in MB49 cells and upregulated in 5637 cells under hypoxic conditions.....	31
Figure 8: Optimal doses are 100 $\mu$ M NaHS, 20 mM PAG, and 100 $\mu$ M GEM as determined by dose response curves.....	33
Figure 9: Inhibiting CSE activity attenuates cell viability and further reduces cell viability in the presence of chemotherapy.....	36
Figure 10: BBN induces bladder cancer in an intravesical murine model as detected by MRI.....	39
Figure 11: Inhibiting CSE activity attenuates tumor progression and invasion and results in tumor regression and abrogates invasion in the presence of chemotherapy.....	42
Figure 12: CSE inhibition induces presence of the apoptotic marker cleaved-PARP-1 but not caspase-9 and further induces PARP-1 <sup>+</sup> cells in combination with chemotherapy.....	47
Figure 13: CSE inhibition reduces presence of the proliferation marker Ki67 and the neovascularization marker VEGF and further reduces VEGF <sup>+</sup> cells in combination with chemotherapy.....	48
Figure 14: CSE inhibition potentiates presence of macrophage marker F4/80.....	49
Figure 15: CSE inhibition induces presence of T cell marker CD8 and further induces presence of CD8 <sup>+</sup> T cells in combination with chemotherapy and reduces the presence of T cell marker CD4.....	50
Figure 16: Proposed mechanisms of H <sub>2</sub> S synthesis inhibition and GEM combination intravesical therapy resulting in bladder tumor progression.....	58

**List of Appendices**

Appendix A: Animal ethics approval..... 81

## List of Abbreviations

Abbreviation	Definition
<sup>18</sup> F-FDG	2- <sup>18</sup> F-fluoro-2-deoxy-glucose
3-MST	3-mercaptopyruvate sulfrtransferase
Bax	Bcl-2-associated x protein
BBN	N-butyl-N-(4-hydroxybutyl)-nitrosamine
BBN <sup>-</sup>	mice without BBN treatment
BBN <sup>+</sup>	mice with BBN treatment
BCG	Bacillus Calmette-Guerin
Bcl-2	B cell lymphoma 2
BLI	bioluminescence imaging
BW	bandwidth
CBS	cystathionine β-synthase
CCL1	chemokine (C-C motif) ligand 1
ccRCC	clear cell renal cell carcinoma
CSE	cystathionine γ-lyase
CTLA-4	cytotoxic T-lymphocyte antigen 4
DMEM	Dulbecco's Modified Eagle media
ERK1/2	extracellular signal-regulated kinase 1/2
FA	flip angle
FBS	fetal bovine serum
FIESTA	Fast Imaging Employing Steady State Acquisition

GEM	gemcitabine
H&E	hematoxylin and eosin
H <sub>2</sub> S	hydrogen sulfide
HIF-1 $\alpha$	hypoxia-inducible factor-1 $\alpha$
IHC	immunohistochemistry
LP	lamina propria
MEK1	mitogen-activated protein kinase kinase 1
MIBC	muscle-invasive bladder cancer
MMC	mitomycin C
MP	muscularis propria
MRI	magnetic resonance imaging
MUI	micro-ultrasound imaging
MVAC	methotrexate, vinblastine, doxorubicin, plus cisplatin
NaHS	sodium hydrosulfide
NMIBC	non-muscle invasive bladder cancer
P/S	penicillin/streptomycin
PAG	propargylglycine
PARP-1	Poly (ADP-ribose) polymerase 1
PBS	phosphate-buffered saline
PET	positron emission tomography
PLP	pyridoxal 5-phosphate
ROI	region of interest

---

RPMI	Roswell Park Memorial Institute
SEM	standard error of mean
TAM	tumor-associated macrophage
TE	echo time
TME	tumor microenvironment
TR	repetition time
TURBT	transurethral resection of the bladder tumor
VEGF	vascular endothelial growth factor
VHL	von Hippel–Lindau

---

## **1 Introduction**

### **1.1 Bladder Cancer**

Bladder cancer is the 10<sup>th</sup> most common malignancy worldwide with almost 600,000 new cases and over 200,000 associated deaths occurring in 2020 alone [1]. Seventy-five percent of patients have non-muscle invasive bladder cancer (NMIBC) at the time of diagnosis [2]. This is when the cancer is present on or within the superficial layers of the bladder urothelium. The remaining 25% have muscle-invasive bladder cancer (MIBC), where the cancer has invaded the detrusor muscle and/or has spread beyond the bladder [2]. Despite the majority of bladder cancer cases being superficial, patients who have and have not received intravesical therapy have a 78% chance of recurrence and 45% chance of progression after 5 years [3]. Moreover, bladder cancer can be further categorized as low- or high-grade. Thirty percent of NMIBC patients have high-grade bladder cancers which consist of poorly differentiated cells. This type of cancer is much more aggressive compared to lower grade pathologies as it has a higher tendency to recur, progress, and metastasize [4].

#### *1.1.1 Current standard of care for high-grade NMIBC*

The current standard of care for high-grade NMIBC is a transurethral resection of the bladder tumor (TURBT) followed by intravesical therapy, which involves administration of immunotherapy or chemotherapy directly into the bladder. This allows the active drug to come into direct contact with the cancer cells and the rest of the urothelium. A typical treatment course consists of six weekly induction sessions followed by one to three years of maintenance doses depending on the risk stratification of the tumor [5]. Bacillus Calmette-Guerin (BCG) immunotherapy is the most common first line intravesical therapy [6]. It works by binding fibronectin, activating the patient's immune system, and inducing an inflammatory response, reducing the risk of progression by 30% [7]. Unfortunately, after one to two years of treatment 40% of patients experience recurrence [8] and 70% experience adverse local and systemic effects [9] such as dysuria, hematuria, or BCG sepsis where an infection occurs within the blood stream [8]. Furthermore, an ongoing worldwide shortage of BCG was declared in 2018, further limiting the number of patients who

could receive full dose BCG. Current salvage intravesical chemotherapies include gemcitabine (GEM) and mitomycin C (MMC), which work by inhibiting DNA synthesis of actively dividing cells. Namely, GEM results in the addition of GEM diphosphate and GEM triphosphate into DNA whereas MMC results in crosslinks within the DNA. A prospective trial using patients who progressed after, or failed BCG immunotherapy treated 54 patients with GEM and 55 patients with MMC and found the rate of recurrence and progression to be less for GEM (28% and 11%, respectively) than MMC (39% and 18%, respectively) [10]. The time to recurrence was also longer for GEM; however, no statistical significance was found for any of these findings ( $p>0.05$ ). Notably, the overall incidence of adverse events was significantly less for GEM than MMC (38.8% vs. 72.2%;  $p=0.021$ ). These findings suggest GEM may be the superior option of the two chemotherapeutic agents. Two other studies compared GEM to BCG in high-grade NMIBC patients. The first study found the recurrence rate to be significantly less for BCG (28.1% vs. 53.1%;  $p=0.037$ ) which also had a significantly longer time to recurrence compared to GEM (39.4 vs. 25.6 months;  $p=0.042$ ) [11]. However, neither treatment resulted in cancer progression and GEM resulted in slightly less local or systemic toxicity (12.5% vs. 9.3% and 0% vs. 6.2%, respectively). The second study made this same comparison in high-risk NMIBC patients declared BCG non-responders [12]. The authors reported that GEM was associated with a significantly lower recurrence rate (52.5% vs. 87.5%;  $p=0.002$ ), but similar progression rates (33% vs. 37.5%;  $p=0.12$ ) compared to BCG. These studies demonstrate a favorable efficacy and toxicity profile of GEM as a salvage high-grade NMIBC therapy.

When NMIBC patients no longer respond to intravesical therapy and/or have progressed, and are eligible and willing to accept urinary diversion, the next line of treatment is a radical cystectomy, which includes complete removal of the bladder along with surrounding lymph nodes and potentially other organs such as the prostate, seminal vesicles, fallopian tubes, ovaries, uterus, and urethra [13]. Complete removal of the bladder significantly impacts the patient's quality of life and has an associated complication rate of approximately 60% and a perioperative death rate of approximately 3% within 90 days [14].

### *1.1.2 Current standard of care for MIBC*

The current standard of care for MIBC consists of neoadjuvant chemotherapy and radical cystectomy. Neoadjuvant chemotherapy is administered systemically, where treatment is injected intravenously and travels throughout the body. This allows the treatment to come into contact with cancer cells that have spread from the initial site. Two main neoadjuvant regimens include cisplatin-based treatments, including cisplatin plus GEM, as well as methotrexate, vinblastine, doxorubicin, plus cisplatin (MVAC). Cisplatin-based neoadjuvant chemotherapy was found to be associated with absolute improvement in overall patient survival, recurrence-free survival, locoregional recurrence-free survival, and metastasis-free survival at 6%, 11%, 11%, and 8%, respectively [15]. MVAC was found to be associated with improved survival (77 vs. 46 months;  $p=0.06$ ) and lower residual disease (38% vs. 15%;  $p<0.001$ ) compared to radical cystectomy alone [16]. Furthermore, cisplatin plus GEM is also used specifically in metastatic disease due to its low toxicity profile compared to MVAC [17], further highlighting the use of GEM in bladder cancer therapies.

### *1.1.3 Economic cost burden of bladder cancer*

Due to the high rates of progression and recurrence, lengthy treatment times, and associated complications, bladder cancer requires lifetime surveillance giving it one of the highest lifetime treatment costs per patient compared to other malignancies [18]. This includes both direct medical costs due to repeat cystoscopic examinations and treatments, as well as indirect costs, such as monetary losses due to time receiving cancer treatments and morbidity and mortality costs. Total costs for bladder cancer were calculated to be \$4.7 billion per year in the US and almost \$5.5 billion per year in Europe in 2014 and 2016, respectively, with expectations that these costs will continue to rise [19, 20].

Overall, current bladder cancer therapies have extremely limited impact. Therefore, development of a novel efficacious intravesical therapy is imperative to preventing progression and permitting bladder preservation. The extremely high-cost burden further underscores this need.

## 1.2 Bladder Cancer Tumor Microenvironment

The tumor microenvironment (TME) consists of all cellular and noncellular components within a tumor that interact and influence tumor formation, progression, and metastasis. Despite the bladder TME remaining poorly characterized, immune cells are notable cellular components [21]. The TME modulates tumor activity by regulating immune responses and as a result, the presence of immune cells. Major immune cells in the bladder TME include CD8<sup>+</sup> cytotoxic T cells, CD4<sup>+</sup> regulatory T cells, and tumor-associated macrophages (TAMs). CD8<sup>+</sup> cytotoxic T cells directly target and destroy cancer cells by inducing apoptosis. Due to their anti-cancer properties, their presence is positively associated with therapeutic response in NMIBC patients [22]. Under healthy conditions, CD4<sup>+</sup> regulatory T cells work by regulating the immune system and preventing overactivity. Under cancerous conditions, they suppress anti-tumor immune responses through the activation of anti-inflammatory molecules such as cytotoxic T-lymphocyte antigen 4 (CTLA-4) which inhibits cytotoxic and helper T cell activation [23]. Therefore, CD4<sup>+</sup> regulatory T cells are elevated within the tumor of bladder cancer patients [24] and their presence is associated with poor patient prognosis [25, 26]. Finally, TAMs are macrophages that have infiltrated the TME. They are phagocytic immune cells responsible for removing dead cells and regulating immune responses including CD8<sup>+</sup> cytotoxic T cell and CD4<sup>+</sup> regulatory T cell activity [27]. TAMs exist on a continuum of activation states with M1 TAMs, which are pro-inflammatory, on one end and M2 TAMs, which are anti-inflammatory, on the other [28]. M1 TAMs inhibit pro-tumor pathways and promote adaptive immune responses through pro-inflammatory cytokines and upregulation of CD8<sup>+</sup> and CD4<sup>+</sup> cell activity leading to cancer cell apoptosis [29]. M2 TAMs stimulate pro-tumor pathways through cell growth factors and angiogenic molecules and are the most abundant macrophage type in the bladder TME [30, 31]. They promote immune evasion through suppression of T cell activity via CTLA-4 and promotion of CD4<sup>+</sup> cell differentiation into regulatory T cells through chemokine (C-C motif) ligand 1 (CCL1) which further contribute to immune response suppression [32, 33]. In bladder cancer, TAM infiltration has been shown to be associated with worse tumor stage and poor therapeutic patient outcomes [34-37].

### 1.3 Hydrogen Sulfide

Hydrogen sulfide (H<sub>2</sub>S) is a key signaling molecule and one of three gasotransmitters within mammalian cells alongside carbon monoxide and nitric oxide. It is membrane-permeable and regulates protein function through persulfidation, otherwise known as S-sulfhydration, which is a post-translational modification involving the addition of a sulfur molecule onto a thiol group of cysteine(s) of a targeted protein [38] (Fig 1A).

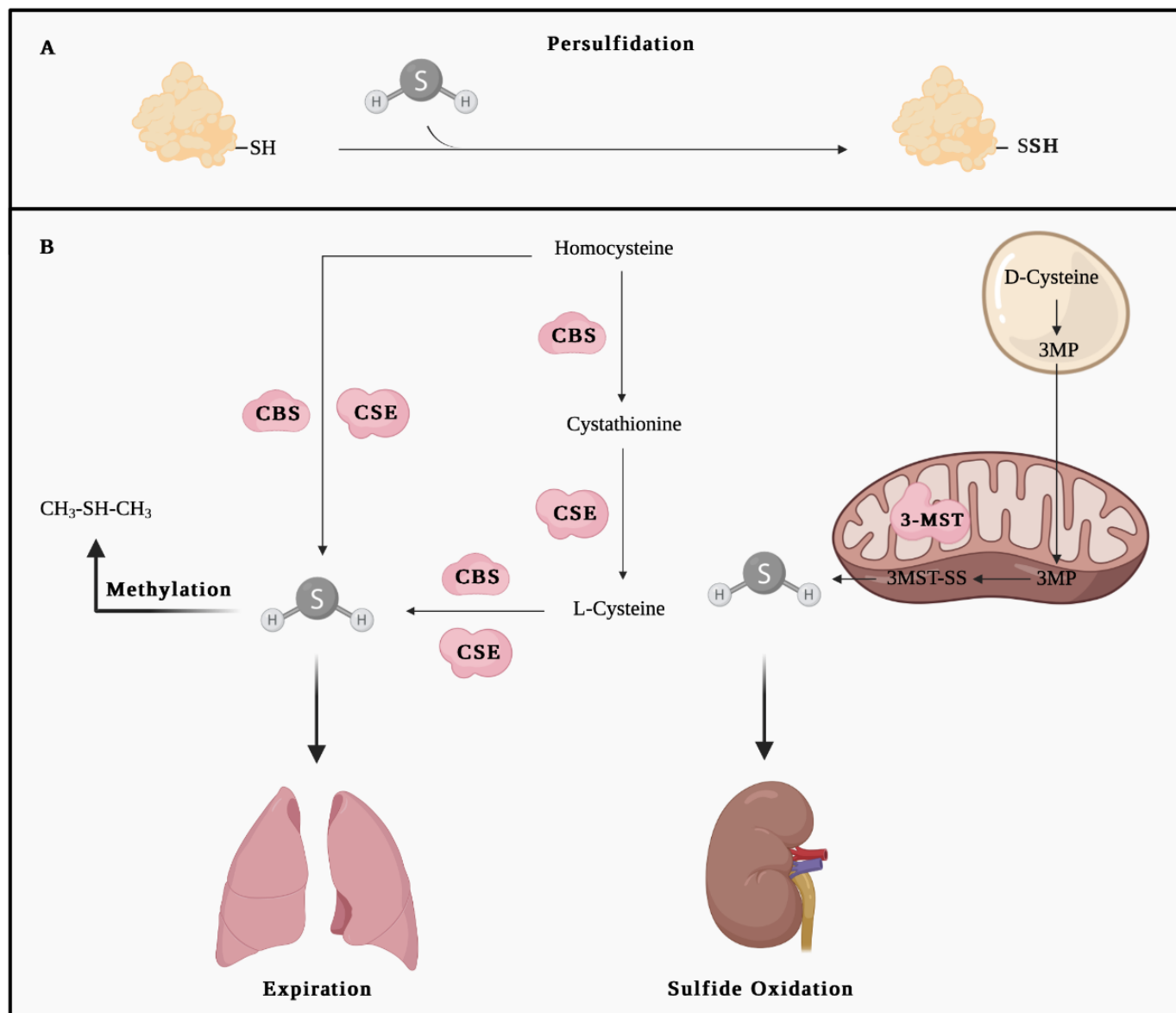


**Figure 1. Schematic of endogenous H<sub>2</sub>S metabolism.** (A) H<sub>2</sub>S regulates protein activity via persulfidation; the addition of a sulfur molecule onto a thiol group of cysteine(s) of a targeted protein. (B) Anabolism of H<sub>2</sub>S within mammalian cells occurs by three independent enzymes: CBS and CSE within the cytosol and 3-MST within the mitochondria. H<sub>2</sub>S catabolism occurs by three routes: methylation within the cytosol, expiration via the lungs, and oxidation within the mitochondria. H<sub>2</sub>S, hydrogen sulfide; CBS, cystathionine  $\beta$ -synthase; CSE, cystathionine  $\gamma$ -lyase; 3-MST, 3-mercaptopyruvate sulftransferase. Figure prepared with BioRender (biorender.com).

### 1.3.1 H<sub>2</sub>S metabolism

Endogenous H<sub>2</sub>S levels are tightly and precisely regulated by several mechanisms, as depicted in Figure 1B. It is endogenously produced in all mammalian cells through the reverse transsulfuration pathway by three independent enzymes: cystathionine  $\beta$ -synthase (CBS), cystathionine  $\gamma$ -lyase (CSE), and 3-mercaptopyruvate sulftransferase (3-MST). CBS, a cytosolic enzyme, catalyzes the condensation of homocysteine with cysteine to produce cystathionine and H<sub>2</sub>S [39]. CSE, also a cytosolic enzyme, catalyzes the conversion of L-cysteine to thiocysteine which breaks down into pyruvate and H<sub>2</sub>S nonenzymatically [40]. After cysteine is converted to mercaptopyruvate, the enzyme 3-MST, localized in the mitochondria, further breaks the substrate down into H<sub>2</sub>S and pyruvate [41]. In contrast, three catabolic routes exist to eliminate excess H<sub>2</sub>S: oxidation, methylation, and expiration. The majority of H<sub>2</sub>S is disposed of through the kidneys via the sulfide oxidation system in the mitochondria. Sulfide quinone oxidoreductase oxidizes H<sub>2</sub>S into persulfide, which is subsequently catalyzed into thiosulfate [42]. Minimal amounts of H<sub>2</sub>S are degraded through methylation within the cytosol. During this process, H<sub>2</sub>S is methylated into non-toxic dimethyl sulfide, which can be further metabolized by the body [43]. Finally, H<sub>2</sub>S can also be eliminated in extremely small quantities through expiration from the lungs [44, 45].

### 1.4 H<sub>2</sub>S in Cancer

Dysregulation of H<sub>2</sub>S metabolism, mainly by the dysregulation of the H<sub>2</sub>S-producing enzymes, has been shown by our group and others to be associated with cancer pathogenesis [46-48]. For example, Sonke *et al* [46] found endogenous levels of H<sub>2</sub>S to be elevated in von Hippel–Lindau-deficient clear cell renal cell carcinoma cells (VHL-ccRCC) compared to nonmalignant renal cells. Subsequently, Sogutdelen *et al* [47] found protein expression of CSE, CBS, and 3-MST to be upregulated in human renal cell carcinoma tissue compared to normal tissue. These studies suggest H<sub>2</sub>S accumulation by the upregulation of H<sub>2</sub>S-producing enzymes may have salient implications in cancer development and growth.

Interestingly, H<sub>2</sub>S appears to have a biphasic dose-dependent effect on cancer cells; moderate to high concentrations of H<sub>2</sub>S are cytoprotective and promote pro-cancerous pathways whereas negligible or extremely high concentrations are toxic and attenuate pathophysiologic pathways [49, 50]. Therefore, experimental manipulation of H<sub>2</sub>S levels in both *in vitro* and *in vivo* settings has been a prominent approach to gain further understanding of how H<sub>2</sub>S modulates carcinogenesis, tumor growth, and invasion. This is accomplished by using both exogenous donors of H<sub>2</sub>S to elevate H<sub>2</sub>S levels as well as inhibitors of H<sub>2</sub>S-producing enzymes to reduce or abrogate H<sub>2</sub>S levels.

#### *1.4.1 Sodium hydrosulfide: an exogenous H<sub>2</sub>S donor*

Several exogenous H<sub>2</sub>S donors exist to investigate the influence of H<sub>2</sub>S on cancer pathogenesis with one of the most commonly used donors being sodium hydrosulfide (NaHS). As a solid analog of H<sub>2</sub>S, NaHS releases large amounts of H<sub>2</sub>S quickly and directly once dissolved in solution. It does so by dissociating into Na<sup>+</sup> and HS<sup>-</sup> which then partially binds to H<sup>+</sup>. To highlight this quick release, a study treated the human breast cancer MCF-7 cell line with 400 μM NaHS and recorded peak concentrations of H<sub>2</sub>S after 20 minutes, which was then depleted to undetectable levels after 90 minutes [51]. Exogenous NaHS has uncovered several pro-cancerous mechanisms promoted by H<sub>2</sub>S. For instance, Cai *et al* [52] found NaHS to promote cellular proliferation in human colon cancer HCT 116 cells, which they attributed to increased Akt and ERK phosphorylation. They also demonstrated that 50 μM NaHS potentiated cell viability but 1000 μM attenuated cell viability compared to the control underscoring the biphasic effect of H<sub>2</sub>S. Moreover, cell proliferation was also increased in human head and neck squamous cell carcinoma cell lines SWU-HN6 and CAL27 after NaHS treatment further underscoring the pro-cancer effects of H<sub>2</sub>S [53].

#### *1.4.2 Propargylglycine: an endogenous H<sub>2</sub>S synthesis inhibitor*

Endogenous H<sub>2</sub>S levels have been attenuated by pharmacologically inhibiting the activity of the H<sub>2</sub>S-producing enzymes. For instance, the small molecule propargylglycine (PAG) is a well-known selective inhibitor of CSE [54]. PAG indirectly targets the pyridoxal 5-phosphate (PLP) cofactor of CSE by sterically hindering the accessibility of the active site on CSE [55]. It must be noted that there is some concern about the selectivity of PAG as

there are many other PLP-dependent enzymes within mammalian cells vulnerable to inhibition [56, 57]. Nonetheless, PAG has been centrally important to the study of H<sub>2</sub>S-targeted cancer therapies including breast, brain, prostate, and gastric cancers [58-60]. Khan *et al* [58] treated human breast cancer cell lines MCF-7 and MDA-MB-231 with PAG and found it to significantly reduce H<sub>2</sub>S levels, as well as cell viability, migration, and invasion. They also investigated the *in vivo* effects of PAG using a subcutaneous xenograft murine model of breast cancer where they observed a significant reduction in tumor volume and weight. PAG also significantly attenuated brain tumor growth in an orthotopic xenograft murine model [59] and significantly reduced human prostate cancer RWPE-1 and C4-2 cell invasion [60]. Nasopharyngeal cancer is also sensitive to PAG *in vitro* and *in vivo* with a significant reduction in cell survival and promotion of apoptosis in human CNE-1 and C666-1 cells and a reduction in subcutaneous xenograft tumor volume and weight [61].

#### 1.5 The Role of H<sub>2</sub>S in DNA Repair, Neovascularization, Apoptotic Escape, and Immune Evasion in Cancer Cells

As briefly mentioned in the previous section, H<sub>2</sub>S influences cancer cell viability, proliferation, migration, and invasion. This section will focus on several of the underlying mechanisms including DNA repair, neovascularization, apoptotic escape, and immune evasion, as shown in Figure 2.

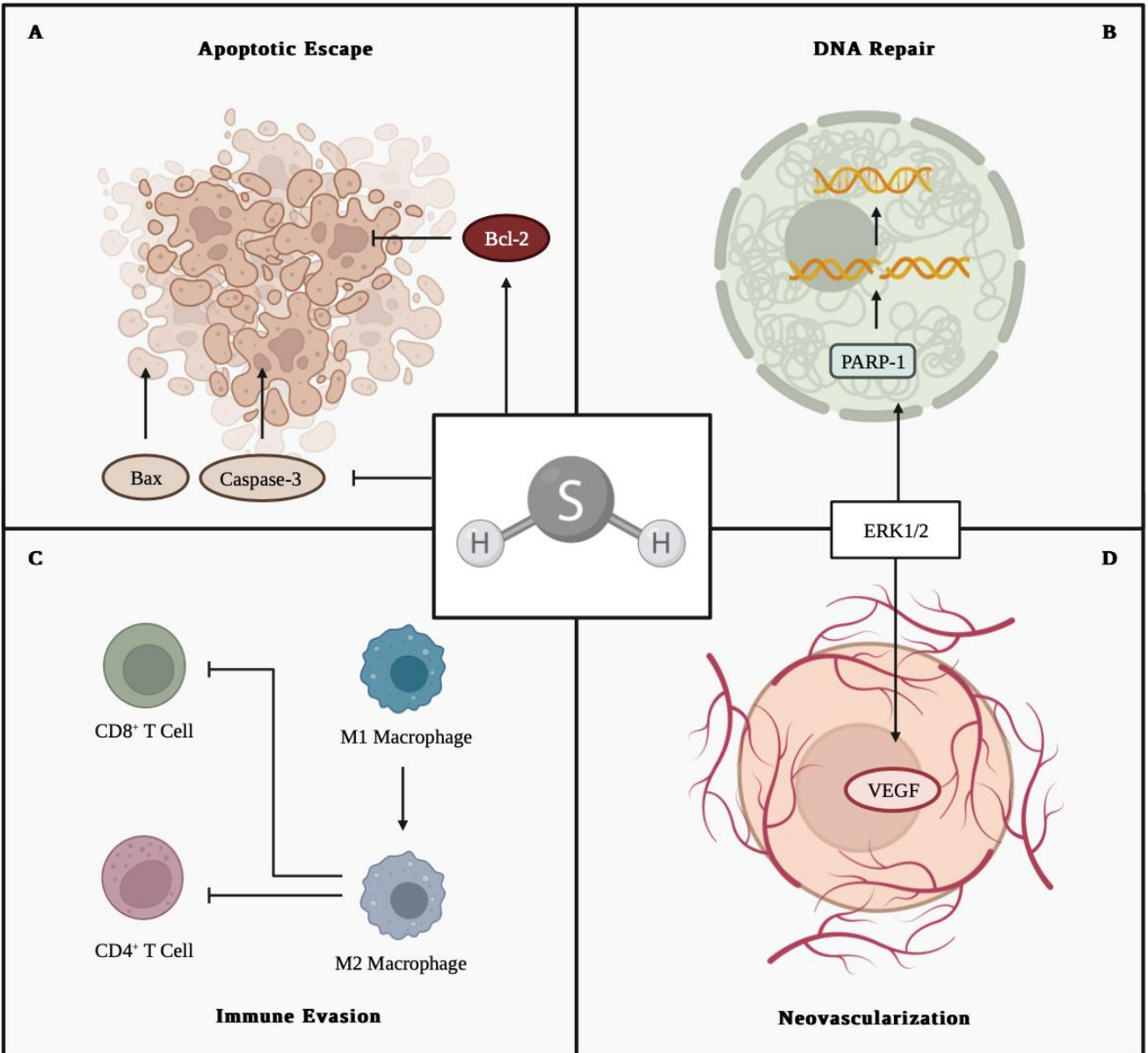


**Figure 2. Accumulation of H<sub>2</sub>S, due to the upregulation of H<sub>2</sub>S-producing enzymes in cancerous tissue, promotes pro-cancerous pathways.** (A) H<sub>2</sub>S downregulates pro-apoptotic proteins Caspase-3 and Bax expression and upregulates anti-apoptotic protein Bcl-2 expression. H<sub>2</sub>S promotes the ERK1/2 pathway leading to (B) PARP-1-led DNA repair and (D) VEGF-led neovascularization. (C) H<sub>2</sub>S promotes M1 to M2 polarization leading to suppression of CD8<sup>+</sup> T cell and CD4<sup>+</sup> T cell proliferation. H<sub>2</sub>S, hydrogen sulfide; Bax, bcl-2-associated X protein; Bcl-2, B cell lymphoma 2; ERK1/2, extracellular signal-regulated kinase 1/2; PARP-1, Poly (ADP-ribose) polymerase 1, VEGF, vascular endothelial growth factor. Figure prepared with BioRender (biorender.com).

Apoptosis is imperative for removing abnormal cells, such as those capable of becoming cancerous. Apoptotic pathways typically target proteins known as caspases. For instance, caspases 2, 8, and 9 are required for the initiation phase and caspases 3, 6, and 7 are required for the execution phase of apoptosis [62]. H<sub>2</sub>S has been shown to exert anti-apoptotic effects on cancer cells (Fig 2A). For example, exogenous H<sub>2</sub>S upregulates B cell lymphoma 2 (Bcl-2) and downregulates active caspase-3 and Bcl-2-associated X protein (Bax) expression through HSP90 regulation in the human esophageal squamous cell cancer cell line EC109 [63]. Furthermore, in human myeloma NCI-H929 cells, exogenous H<sub>2</sub>S aids in apoptotic escape by stimulating Akt signaling and upregulating Bcl-2 and downregulating caspase-3 expression [64]. Finally, human PLC/PFR/5 hepatoma cells also demonstrate a downregulation of caspase-3 and amplification of the activation of the NF-κB pathway following exogenous H<sub>2</sub>S administration [65].

Moreover, H<sub>2</sub>S has been implicated in promoting DNA repair in cancer cells. It does so by activating Poly (ADP-ribose) polymerase 1 (PARP-1), an ADP-ribosylating enzyme and a component of the earliest responses to DNA damage (Fig 2B). This activation is a downstream effect of mitogen-activated protein kinase kinase 1 (MEK1) persulfidation and subsequent extracellular signal-regulated kinase 1/2 (ERK1/2) phosphorylation, which then directly interacts with PARP-1 [66]. Interestingly, it has also been shown that detection of DNA damage by PARP-1 stimulates an increase in H<sub>2</sub>S levels, suggesting a reciprocal relationship [67]. Moreover, DNA damage is less prevalent in mitochondrial DNA of human lung cancer tissue than adjacent healthy tissue [68]. Inhibition of CSE activity in human A549 lung cancer cells resulted in DNA damage accumulation and a reduced repair rate. Conversely, exogenous H<sub>2</sub>S was shown to enhance the formation of mitochondria-specific DNA repair enzymes.

We have previously investigated the role of H<sub>2</sub>S in neovascularization in ccRCC using chick chorioallantoic membrane [46]. Inhibition of H<sub>2</sub>S synthesis significantly decreased the number of blood vessels, whereas exogenous H<sub>2</sub>S increased the number of blood cells compared to the control. Papapetropoulos *et al* [69] implicated H<sub>2</sub>S in neovascularization through vascular endothelial growth factor (VEGF), suggesting H<sub>2</sub>S promotes angiogenesis via ERK1/2 phosphorylation potentiating VEGF signaling (Fig 2D). It was

also found that VEGF promotes H<sub>2</sub>S in return, suggesting a positive feedback mechanism. Wang *et al* [70] investigated this in the context of breast cancer metastasis where the H<sub>2</sub>S-producing enzyme, CSE, was shown to promote human MDA-MB-231 breast cancer cell growth, migration, and invasion via VEGF downstream signaling pathway as indicated by an increase in ERK1/2 protein levels.

H<sub>2</sub>S also regulates immune responses resulting in a pro-tumor environment. Specifically, H<sub>2</sub>S influences macrophage polarization by suppressing M1 macrophage activation and polarizing macrophages toward the M2 inflammatory type [71] (Fig 2C). The downstream effect of this is suppression of T cell proliferation by M2 macrophage. Exogenous H<sub>2</sub>S has been shown to increase the percentage of M2 macrophage in bone marrow-derived macrophages, whereas H<sub>2</sub>S synthesis inhibition decreased this percentage [72]. Limited research has focused specifically on H<sub>2</sub>S and its effect on macrophage regulation under cancerous conditions. However, it is highly plausible that H<sub>2</sub>S regulates TAM activity due to its ability to upregulate M2 macrophage presence and therefore M2-associated tumor-promoting pathways. Moreover, H<sub>2</sub>S regulates CD4<sup>+</sup> regulatory T cell differentiation and function by promoting the Ten eleven translocation family contributing to the anti-inflammatory environment [73].

### 1.6 H<sub>2</sub>S in Bladder Cancer

As demonstrated, H<sub>2</sub>S plays a pivotal role in pro-cancerous pathways; however, its effects in bladder cancer is a relatively new topic in research. For instance, the mere presence of the H<sub>2</sub>S-producing enzymes, CSE, CBS, and 3-MST, had not been reported in human bladder cancer tissue until 2016 [74]. This was also the first study to demonstrate H<sub>2</sub>S metabolism dysregulation in bladder cancer. In line with the previously reported cancers, they revealed a positive correlation between enzyme expression and H<sub>2</sub>S productivity and bladder cancer stage, with low expression and productivity in healthy bladder tissues, moderate expression and productivity in NMIBC tissues, and high expression and productivity in MIBC tissues. This same correlation was replicated in a subsequent study further validating these findings [75]. Others found exogenous H<sub>2</sub>S, by NaHS administration, potentiated the proliferation activity and invasion ability of invasive bladder cancer cells *in vitro* [76]. Likewise, a study demonstrated a similar effect with

DATS, another H<sub>2</sub>S donor. They also found that overexpression of CSE and CBS inhibited cell proliferation and promoting apoptosis of cancer cells, exhibiting the bimodal effect of H<sub>2</sub>S within bladder cancer [77].

Recently, investigation of H<sub>2</sub>S in bladder cancer has been performed *in vivo* [75]. Using a subcutaneous model, where invasive human bladder cancer EJ cells were injected into the flank of nude mice, it was found that PAG or NaHS alone did not significantly alter cell viability. However, they did show potentiation of cisplatin chemotherapy by PAG as a further reduction of tumor size compared to cisplatin chemotherapy alone was observed. They also found that NaHS partially recovered tumor volume, counteracting the cytotoxicity of cisplatin chemotherapy. These findings are the first to suggest H<sub>2</sub>S synthesis inhibition as a potential target in the development of a novel combination therapy for bladder cancer.

#### *1.6.1 Limitations of current bladder cancer models*

(Sections 1.6.1, 1.6.2, and 1.6.3 have been adapted from Relouw *et al* [78])

The previously mentioned studies investigating H<sub>2</sub>S in bladder cancer are very promising; however, there are several limitations that need to be addressed before this research can be conducted in the clinical setting. For instance, *in vitro* models of bladder cancer do not suffice as they are unable to recapitulate human bladder cancer etiology and progression, and they lack many of the defining features of cancer [79]. *In vivo* models, on the other hand, have been developed in an attempt to closely replicate the progression, genomic profile, and histology of human bladder cancer [80, 81]. Previous models include subcutaneous tumors, where human bladder cancer cells are implanted into the shoulder or flank of mice [82, 83]. The attractiveness of this model includes the ease of implantation, a high tumor-take rate, and the ease of tumor growth assessment [84, 85]. However, this model is limited by the assumption that the structure and environment of the skin and epithelium mimics that of the bladder to appropriately apply these findings [86]. Moreover, current bladder cancer studies do not administer treatment in a clinically relevant manner. For example, Wahafu *et al* [75] treated mice via abdominal cavity injections which do not mimic NMIBC nor MIBC therapy administration in humans. Yet, murine models of bladder cancer are critical to this investigation, as they provide a means for translational

research of potential therapies and allow for a more comprehensive exploration of *in vitro* findings prior to clinical testing.

### *1.6.2 Intravesical murine models of bladder cancer*

Requirements of an ideal murine model of bladder cancer have recently been established as (1) tumors being of urothelial origin to mimic human bladder cancer progression, encapsulating all different stages of the tumor, (2) tumors being able to grow within the bladder to interact with other layers of the bladder wall and for direct exposure to therapeutic agents, and (3) tumors being relatively easy to develop within a reasonable time period, making them reproducible and reliable [86, 87]. Following these criteria, an intravesical murine model, rather than a subcutaneous model, facilitates the opportunity for a successful pre-clinical model.

Current intravesical murine models of bladder cancer includes orthotopic, transgenic and carcinogen-induced approaches [88-91]. Orthotopic models require inoculation of bladder cancer tumors into the bladder wall. This model can be further categorized as syngeneic or xenogeneic, which consists of inoculation of mouse or human bladder cancer cells, respectively. Because these cells are already cancerous at the time of inoculation, they do not encapsulate the most primitive stages of bladder cancer. However, this model does allow the cells to continue to develop within the bladder wall for interaction with other tissue types and exposure to therapeutic agents, satisfying criterion 2, but not criterion 1. Moreover, upon successful establishment of bladder cancer cells, tumor formation is rapid and only takes days to form therefore satisfying the final criteria [92].

Transgenic models of bladder cancer involve alterations of the mouse genome and allow investigation of individual gene functions [90]. Despite seeing an imperative advancement in the investigation of human diseases, this model is not as established as the others. Furthermore, transgenic models are very costly and do not mimic the complexity of the microenvironment and interactions during the development of human bladder cancer [93]. Therefore, this model does not fulfill criteria 1 or 3.

Carcinogenic models can be developed by oral administration of carcinogens. A common carcinogen is N-butyl-N-(4-hydroxybutyl)-nitrosamine (BBN), which has been reported to

recapitulate the progression of human bladder cancer induced by tobacco [94-96]. This is highly relevant as approximately half of patients develop bladder cancer due to smoking [97], which satisfies criterion 1. To induce cancer, BBN is first activated in the liver and enters the bladder via urine causing DNA damage and initiating carcinogenesis in an organ specific manner [98]. This allows the cancer to develop on the inner lining of the bladder and allows for direct exposure to therapeutic agents, sufficing criterion 2. A consequence of carcinogen-induced models is that they require an extensive amount of time to develop bladder cancer. Several months of carcinogen exposure may be required depending on the desired cancer stage [99, 100]. However, this model is reliable with 100% of mice developing dysplasia after 16 weeks of 0.05% BBN exposure and 100% of mice developing carcinoma *in situ* after 20 weeks of exposure, satisfying criterion 3 [101].

Overall, several successful intravesical models exist; however, a carcinogen-induced model is the only one to satisfy all three requirements of an ideal murine model of bladder cancer.

### *1.6.3 Non-invasive imaging modalities for intravesical models of bladder cancer*

As tumor formation and progression occur within the bladder of intravesical models, bladder cancer is not readily detectable like it is in subcutaneous models. This provides an obstacle for confirming and monitoring bladder cancer response when investigating novel therapies. Recent studies have demonstrated bioluminescence imaging (BLI), micro-ultrasound imaging (MUI), positron emission tomography (PET), and magnetic resonance imaging (MRI) as non-invasive imaging modalities allowing for initial and repeat assessment of bladder cancer presence facilitating longitudinal investigation [78]. These modalities are depicted in Figure 3.

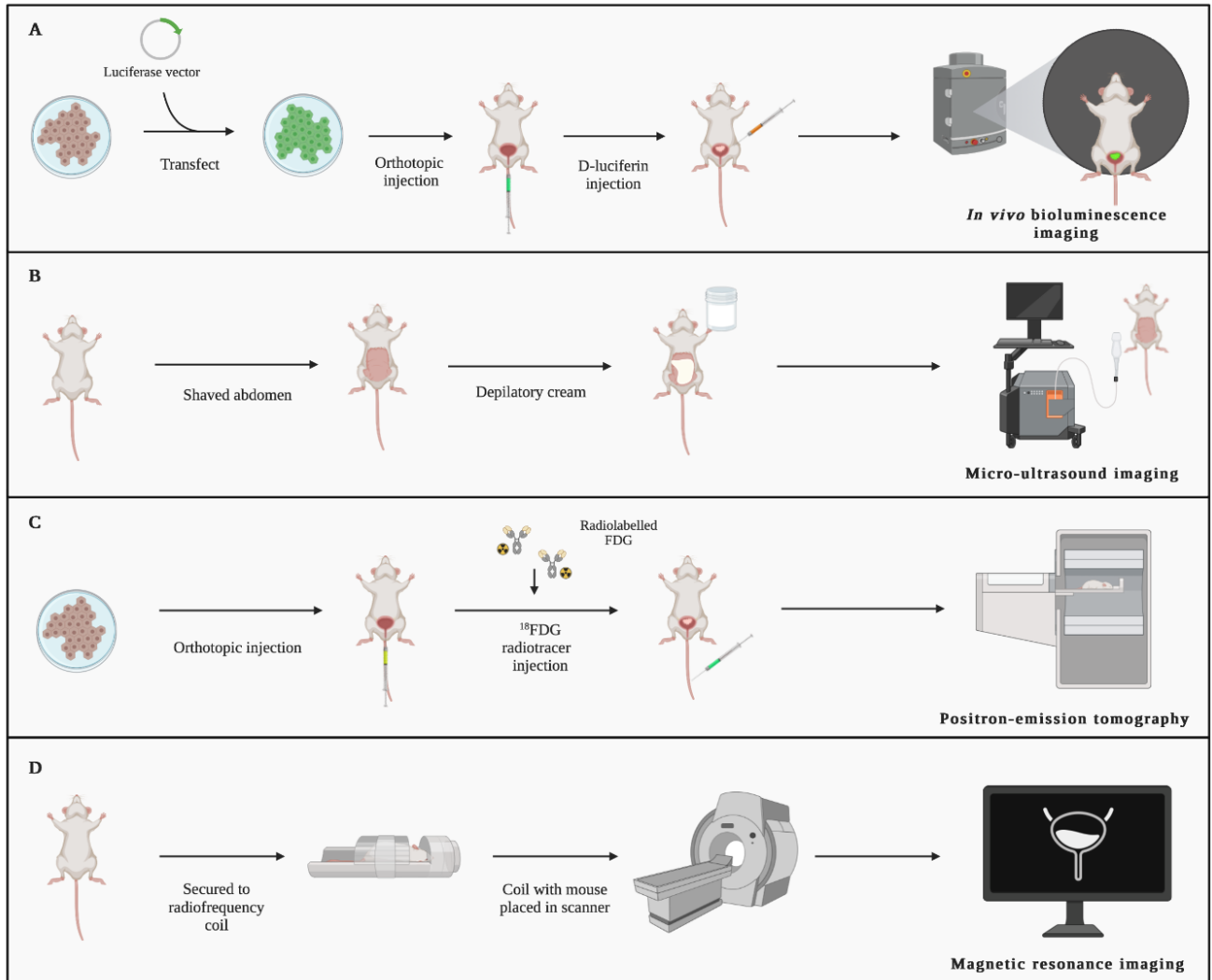


**Figure 3. Non-invasive imaging in intravesical murine models of bladder cancer. (A)**

During BLI, cancer cells are transfected with a luciferase vector and inoculated into the bladder wall. D-luciferin substrate is administered via intravenous or intraperitoneal injection to stimulate the reporter system which is detected by an *in vivo* imaging system.

(B) During MUI, the mouse abdomen is shaved, depilatory cream is applied to remove fine hairs, and high viscosity ultrasound gel is used to enhance image resolution.

(C) During PET imaging, cancer cells are inoculated into the bladder wall, FDG are radiolabeled producing  $^{18}\text{F}$ -FDG and are administered intravenously prior to imaging.

(D) During MRI, mice are secured to a radiofrequency coil and subsequently placed within a mouse or clinical MRI scanner.

BLI, bioluminescence imaging; MUI, micro-ultrasound imaging; PET, positron emission tomography;  $^{18}\text{F}$ -FDG; 2- $^{18}\text{F}$ -fluoro-2-deoxy-glucose MRI, magnetic resonance imaging.

Figure prepared with BioRender (biorender.com).

BLI allows for visualization of bladder cancer cells through the detection of light emission using an *in vivo* imaging system. Bladder cancer cell lines are transfected with a luciferase vector and subsequently inoculated into the bladder wall of a murine model. Subsequent intravenous or intraperitoneal administration with D-luciferin substrate stimulates the reporter system to produce luciferase, which converts D-luciferin to oxyluciferin, resulting in the emission of green light. As genetic engineering of cells is required, this imaging modality is limited to an orthotopic bladder cancer model. BLI is unable to detect the presence of cancer cells immediately after inoculation but can confirm tumor presence as early as 4 days post-inoculation [102]. Authors reported varying tumor size and bioluminescence intensity, which correlated over time with  $R^2$  values ranging from 0.75 to 0.92 [102]. However, this was followed by a decline in bioluminescence over an extended period of time. Jurczok *et al* [103] denoted the loss of bioluminescence in large tumors to be due to necrosis and hemorrhage within the tumor core, which inhibited D-luciferin uptake. In conclusion, BLI is a reliable modality to confirm and quantitatively evaluate early-stage bladder cancer presence but can only qualitatively assess bladder cancer presence in advanced stages.

MUI utilizes soundwaves to produce 2D images of organs and other tissues, such as the bladder wall. MUI is independent of tumor origin, whether orthotopically, carcinogen, or genetically induced, making it suitable for use in conjunction with all intravesical bladder cancer models. Mean bladder cancer tumor detection time in a syngeneic orthotopic model using MUI was found to be 10 days, ranging from 8 to 17 days, whereas that for clinical symptoms of bladder cancer was 20.8 days, ranging from 14 to 28 days [92, 104, 105]. Subsequent studies were able to detect orthotopic bladder cancer tumors as early as 4 [102], 7 [106] and 11 days [105, 107, 108]. However, reported disadvantages of MUI are the lack of 3D imaging [109] and reliance on a skilled operator to detect bladder cancer tumors, as well as the restricted availability of this technology [109, 110].

PET evaluates metabolic activity of organs and tissues providing information on physiology and anatomy. Molecules naturally used by the organs or tissues of interest are tagged by radioactive atoms, producing radiotracers, allowing for detection and evaluation of diseases such as cancer. A widely used radiotracer is 2- $^{18}\text{F}$ -fluoro-2-deoxy-glucose ( $^{18}\text{F}$ -

FDG).  $^{18}\text{F}$ -FDG is a glucose analogue and works based on the premise that cancer cells, which are more metabolically active than non-cancerous cells, will uptake glucose at a higher rate. This uptake is detected by PET, thus identifying cancerous regions. The attractiveness of PET is attributed to its ability to identify protein dysregulation, as indicated by changes in glucose metabolism [111]. Unfortunately, evaluation of bladder cancer with PET imaging is difficult due to the accumulation of  $^{18}\text{F}$ -FDG within the bladder from renal excretion. This excretion obstructs delineation of the tumor from the bladder wall and hinders the detection of primary bladder tumors [112]. This limitation currently makes PET a less appealing option for bladder cancer imaging. However, its unique ability to detect phenotypic changes has encouraged several studies to investigate modifications to potentially improve detection in intravesical murine bladder cancer models [106, 113].

MRI produces high-resolution 3D images of anatomical structures via a strong magnetic field and radio waves. Several studies have investigated the feasibility of MRI as a method for identification and quantitative analysis of murine bladder cancer tumors. In a carcinogen induced bladder cancer murine model, MRI was used to calculate bladder wall and tumor area [109]. In this study, MRI produced T1 and T2 weighted images with  $\sim 100$   $\mu\text{m}$  spatial resolution in less than 10 minutes per mouse. Bladder wall measurements, representative of tumor burden, were calculated by subtracting the area of the inner lumen from the area of the outer edge of the bladder using single axial images. The area of the bladder wall was found to be strongly associated with tumor stage despite being weakly correlated with *ex vivo* bladder weight. Interestingly, bladder wall area was also strongly associated with both NMIBC and MIBC, whether grouped as individual stages or invasiveness. An acknowledged limitation of this study was the use of one axial image in the calculation of the bladder wall area. Multiple sections are recommended for a more complex analysis. Nonetheless, MRI is a reliable modality for repeat assessment of bladder cancer burden in an intravesical murine model.

In conclusion, BLI, MUI, PET, and MRI all offer a means to detect bladder cancer presence and longitudinally follow tumor growth. However, given the loss of BLI signal overtime and requirement of an orthotopic model, the lack of 3D imaging and restricted availability of MUI, and accumulation of radiotracers within the bladder during PET, the 3D imaging

and ease of tumor burden evaluation of MRI makes it the current superior method for cancer evaluation in an intravesical murine model.

### 1.7 Rationale and Hypothesis

Given the limited therapeutic impact and high-cost burden of current bladder cancer treatments, investigation of novel therapeutics is required. H<sub>2</sub>S plays an important role in pathophysiological pathways and supports the development and growth of cancer. Very recently, research has been conducted on H<sub>2</sub>S in bladder cancer and the results are promising; inhibiting H<sub>2</sub>S synthesis potentiates the anti-cancer effects of cisplatin chemotherapy, whereas exogenous H<sub>2</sub>S attenuates these effects *in vitro* and in a subcutaneous murine model [75]. However, it cannot be assumed that these findings will translate into the clinical setting, as the current models are not clinically relevant.

To address the current limitations of this research, an intravesical murine model is required. More specifically, a carcinogen-induced model using BBN should be used, as it satisfies all requirements of an ideal model: it mimics human bladder cancer progression, allows tumors to grow within the bladder wall for direct exposure to therapeutic agents, and it is relatively simple to develop resulting in a reproducible and reliable model. To further mimic the clinical setting, intravesical therapy should be performed to deliver the treatments, as this is the standard for NMIBC. Moreover, an established non-invasive imaging modality, such as MRI, should be used to accurately detect and evaluate bladder tumor response to potential therapies.

Therefore, the purpose of this project is to investigate the effect of inhibiting endogenous H<sub>2</sub>S synthesis on the progression of bladder cancer progression in an intravesical murine model using MRI. With this, we hypothesize that inhibiting H<sub>2</sub>S synthesis will attenuate bladder cancer progression and potentiate the anti-cancer effects of the established chemotherapeutic agent GEM.

## 1.8 Aims and Objectives

**Aim 1:** Investigate the effect of the H<sub>2</sub>S synthesis inhibitor PAG, and the exogenous H<sub>2</sub>S donor NaHS, on bladder cancer cell viability in conjunction with GEM in an *in vitro* model of bladder cancer.

*Objective 1:* Identify a H<sub>2</sub>S-producing enzyme for subsequent targeting.

*Objective 2:* Determine optimal dosage of PAG, NaHS, and GEM for use in subsequent *in vitro* and *in vivo* experiments.

*Objective 3:* Investigate the effects of single and combination treatments of PAG, NaHS, and GEM on bladder cancer cell viability.

**Aim 2:** Explore the effect of H<sub>2</sub>S synthesis inhibition with and without GEM chemotherapy on bladder tumor progression using MRI.

*Objective 1:* Establish a carcinogen-induced intravesical murine model of bladder cancer with BBN.

*Objective 2:* Investigate the effects of single and combination intravesical therapies consisting of PAG, NaHS, and GEM on bladder tumor progression and invasion.

*Objective 3:* Investigate the effect of single and combination intravesical therapies on markers of bladder cancer progression and H<sub>2</sub>S activity.

## 2 Methods

### 2.1 *In vitro* model of bladder cancer

2.1.1 *Cell culture.* Mouse bladder cancer cells (MB49 cell line; MilliporeSigma, USA) were used as they were developed from C57BL/6 mice, keeping in line with our *in vivo* experiments. They were maintained in Dulbecco's modified eagle media (DMEM) containing 10% fetal bovine serum (FBS) and 1% penicillin/streptomycin (P/S). Human bladder cells (5637 cell line; generously donated by the Burton Lab, Western University, ON, Canada) were used as they possess similar molecular features as high-grade NMIBC. They were maintained in Roswell Park Memorial Institute (RPMI) 1640 media containing 10% FBS and 1% P/S. Both cell lines were maintained under normal growth conditions of 21% O<sub>2</sub> and 5% CO<sub>2</sub> at 37°C.

2.1.2 *Quantitative PCR analysis.* An *in vitro* model of bladder cancer that simulates the hypoxic TME was used to quantify mRNA expression of the H<sub>2</sub>S producing enzymes, CSE, CBS, and 3-MST. MB49 and 5637 cells were seeded on 6-well plates (2 × 10<sup>5</sup> cells/well). Following, cells were subjected to 0, 8, or 36 h of hypoxia (5% CO<sub>2</sub>, 0.5% O<sub>2</sub>, 95% N<sub>2</sub>) at 37°C. Hypoxic conditions were created using the HypOxystation H85 hypoxia chamber (HYPO<sub>2</sub>YGEN, USA). Cell lysate was homogenized using QIAshredder (Qiagen, ON, Canada) and total RNA was isolated using RNeasy® Mini Kit (Qiagen, ON, Canada) and reverse transcribed into cDNA using OneScript® Plus cDNA synthesis Kit (ABM, Canada) in conjunction with Oligo(dT)<sub>12-18</sub> primers as per manufacturer protocol. The reaction mixture of each qPCR sample had a volume of 20 µL and was composed as per BlastTaq™ 2X qPCR MasterMix (ABM, Canada) protocol and analyzed using QuantStudio™ 3 Real-Time PCR System (Thermo Fisher Scientific, CA). Primer sequences, shown in Table 1, for human (h) β-actin, mouse (m) β-actin and mCBS were designed using Primer-BLAST software (NCI), primer sequences for mMST and mCSE were generously donated by Adam Greasley from the Zhang lab, and sequences for hCSE, hCBS, and hMST were designed as previously described [77]. All genes of interest were normalized against β-actin from the appropriate species. Fold changes of gene expression were compared to 0 h hypoxia cells and were calculated using the ΔΔCt method.

Table 1. List of qPCR primer sequences.

Primer	Forward Sequence (5' → 3')	Reverse Sequence (5' → 3')
Mouse $\beta$ -actin	CAGCTGACAGGGAAATCGTG	CATTGCCAATAGTGATGACC
Mouse CSE	TCTTGCTGCCACCATTACGA	GTGGTGTAATCGCTGCCTCT
Mouse CBS	GTGGCATGGCGACTGAAGAACGAA	ATGCGGGCAAAGGCCGAAGGAAT
Mouse 3-MST	TGTCTAAGCCCTTGGTAGCC	CCACTCTACCCAGGAGCCAT
Human $\beta$ -actin	AGCACAGAGCCTCGCCTTT	ATCATCATCCATGGTGAGCTGG
Human CSE	AGGTTTAGCAGCCACTGTAAAC	GGGGTTTCGATCCAAACAAGC
Human CBS	GGCCAAGTGTGAGTTCTTCAA	GGCTCGATAATCGTGTCCCC
Human 3-MST	CATTCGCGGAGTACGCAG	GCTGGCGTCGTAGATCACG

**2.1.3 Dose response curves and treatments.** An *in vitro* model of bladder cancer that simulates the hypoxic TME was used to assess the effects of H<sub>2</sub>S on bladder cancer cell viability (Fig 4). To determine optimal doses of NaHS (Thermo Fisher Scientific, CA), PAG (MilliporeSigma, USA), and GEM (MilliporeSigma, USA) for subsequent *in vitro* and *in vivo* experiments, dose response curves were generated. MB49 cells were seeded on 6-well plates ( $2 \times 10^5$  cells/well). Following, cells were subjected to 8 h of hypoxia (5% CO<sub>2</sub>, 0.5% O<sub>2</sub>, 95% N<sub>2</sub>) at 37°C. Cells were then washed with phosphate-buffered saline (PBS) and treated with a gradient of concentrations of NaHS (0 – 300  $\mu$ M), PAG (0 – 80 mM), and GEM (0 – 100 mM). Control cells received untreated media. Cells were then subjected to an additional 24 h of hypoxia (5% CO<sub>2</sub>, 0.5% O<sub>2</sub>, 95% N<sub>2</sub>) at 37°C. These hypoxic conditions were created using the HypOxystation H85 hypoxia chamber (HYPO<sub>2</sub>YGEN, USA). Additionally, the monotherapy and combination treatment effects of PAG + NaHS and PAG + GEM were investigated using MB48 and 5637 cell lines using 20 mM PAG, 100  $\mu$ M NaHS, and 100  $\mu$ M GEM under the same sequence of conditions.

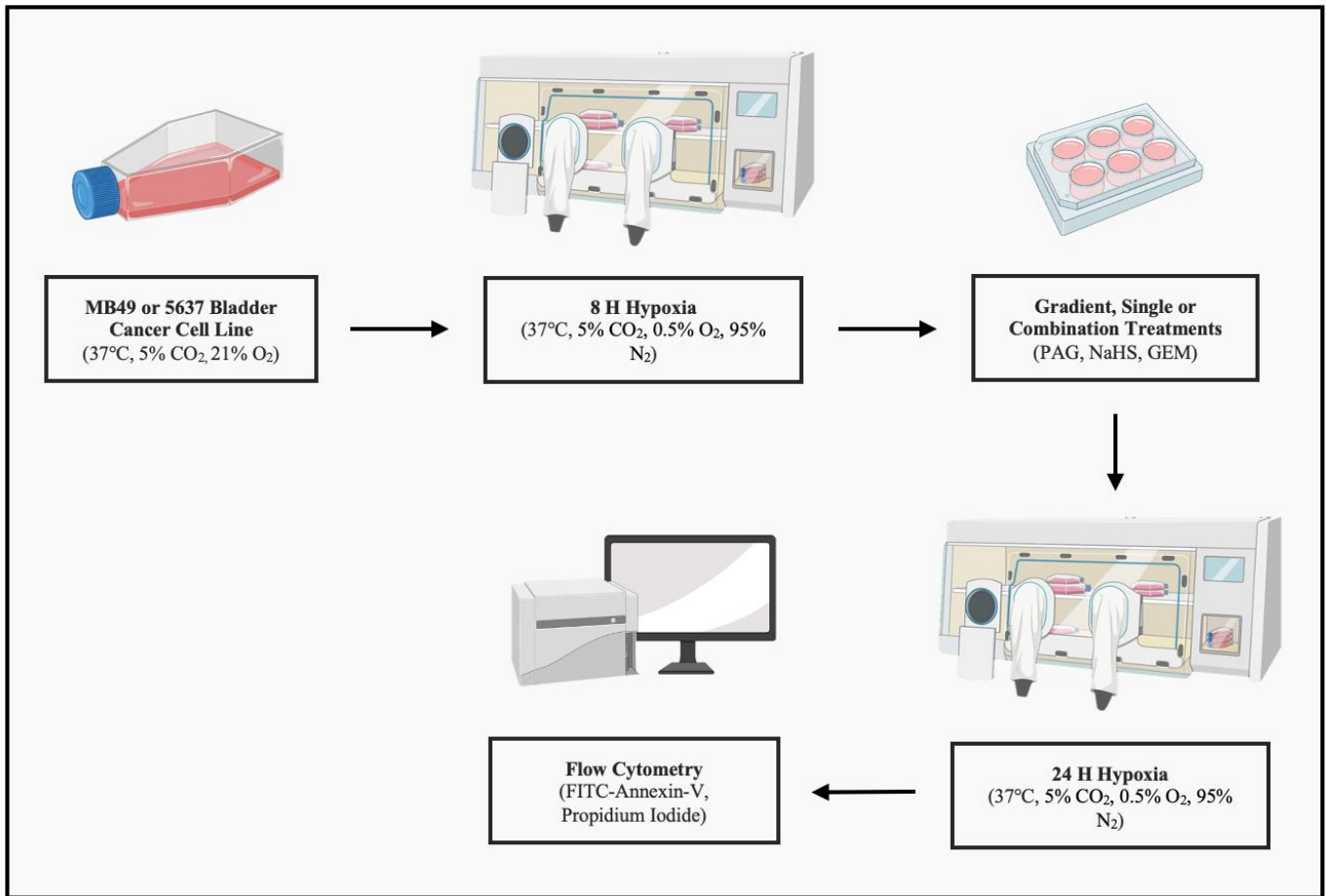


**Figure 4. *In vitro* model of bladder cancer workflow.** MB49 and 5637 cells were first subjected to 8 hr of hypoxia. They were then treated with gradient, single, or combination therapies of NaHS, PAG, and GEM depending on the objective and subjected to an additional 24 hr of hypoxia. Cellular viability was assessed via staining of cells with FITC-Annexin-V and propidium iodide, which measures apoptosis and necrosis, respectively. NaHS, sodium hydrosulfide; PAG, propargylglycine; GEM, gemcitabine. Figure prepared with BioRender (biorender.com).

*2.1.4 Flow cytometry.* Cellular viability was assessed via staining of cells with FITC-conjugated Annexin-V (FITC-Annexin-V; BioLegend, USA) and propidium iodide (BioLegend, USA), which measure cellular apoptosis and necrosis, respectively. Cells were analyzed using the CytoFLEX S (Beckman Coulter, USA) and CytExpert Software (Beckman Coulter, USA) was used to appropriately gate the data for statistical analysis.

## *2.2 In vivo model of bladder cancer*

*2.2.1 Experimental animals.* Thirty-six 6-week-old C57BL/6 male mice were purchased from Charles River Canada (St. Constant, QC, Canada) and maintained in the Animal Care and Veterinary Services facility at Western University (London, ON) under standard conditions. Animal studies were approved by the Animal Care Committee of the University Council on Animal Care (AUP Number: 2022-021; refer to Appendix A).

*2.2.2 Murine bladder cancer model.* Thirty mice were fed 0.05% BBN tap water (BBN<sup>+</sup>; TCI America, USA) for 12-weeks to induce bladder cancer development [114]. BBN-treated water was replaced twice weekly, as BBN is light sensitive. Following 12 weeks of carcinogen exposure, the mice were fed untreated water for the remainder of the experiment. Six mice were fed regular tap water (BBN<sup>-</sup>) for the entire duration of the experiment to act as a healthy control. The experimental timeline is depicted in Figure 5.

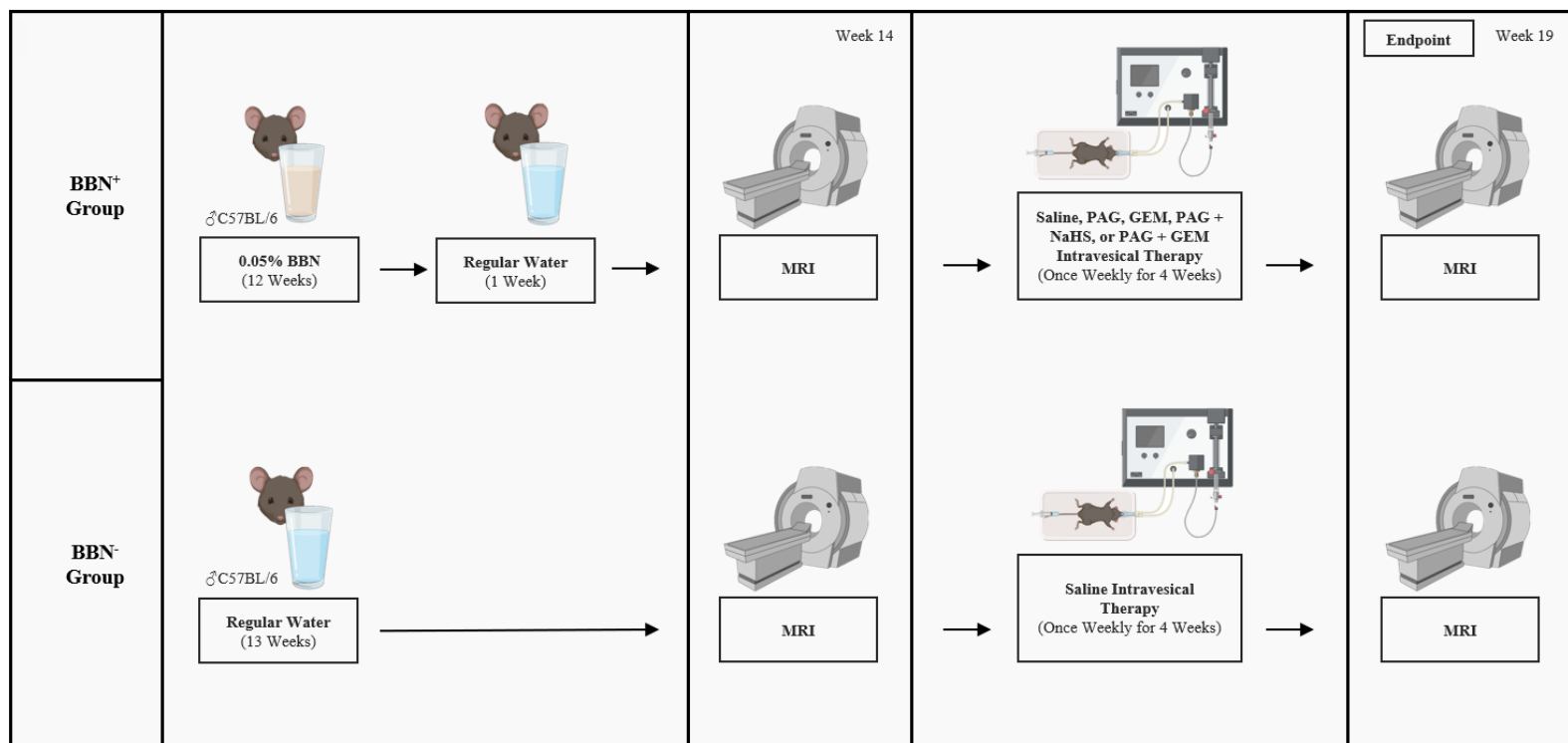


**Figure 5. *In vivo* model of bladder cancer workflow.** Thirty mice were treated with 0.05% BBN tap water for 12 weeks and regular tap water for one week to initiate bladder cancer development. Concurrently, six mice were fed regular water to act as a healthy control. On the 14<sup>th</sup> week, mice underwent MRI to confirm cancer development. Mice then underwent four weekly sessions of intravesical therapy consisting of saline, PAG, or GEM monotherapies or PAG + NaHS or PAG + GEM combination therapies and the healthy control group received saline. Tumor response was evaluated by a second MRI performed after the treatment course. BBN, N-butyl-N-(4-hydroxybutyl)-nitrosamine; MRI, magnetic resonance imaging; NaHS, sodium hydrosulfide; PAG, propargylglycine; GEM, gemcitabine. Figure prepared with BioRender (biorender.com).

2.2.3 *Magnetic resonance imaging.* MRI was performed at week 14 to confirm the presence of bladder tumors prior to beginning intravesical therapy, and again at week 19 to evaluate tumor progression following intravesical therapy (Fig 5). All bladder MRI examinations were acquired on a 3.0T GE MR750 clinical MR scanner (General Electric, Mississauga, ON, Canada) using a custom-built gradient and radio frequency coils. Mice were anesthetized in an anesthesia induction chamber with 2.5% isoflurane and an O<sub>2</sub> flow rate of 2L/min. During the scan, the mice were transferred to a nose cone which supplied 2.5% isoflurane and heart rate and temperature were monitored throughout. *In vivo* bladder images were acquired using the GE system 3D steady-state free precession imaging sequence, Fast Imaging Employing Steady State Acquisition (FIESTA) and produced T2/T1 weighted images. Scanning parameters were as follows: in plane spatial resolution = 200 x 200 μm, repetition time (TR) = 6.5 ms, echo time (TE) = 2.3 ms, bandwidth (BW) = 31.25 kHz, flip angle (FA) = 35°, scan time = approximately 36 minutes per mouse.

2.2.4 *Tumor analysis.* MRI images were analyzed using Horos imaging software, version 3.3.6. Images were evaluated for bladder cancer presence by detecting thickening of the bladder wall and protrusions into the bladder lumen. Total tumor burden was represented as bladder wall volume, which was a modification from a previously described method that used bladder wall area [109]. To quantify tumor bladder wall volume, nine coronal slices were used; the middle slice was determined by the slice with the largest bladder diameter, then four slices, 3 slices apart, were selected posterior and anterior to the middle slice. Two regions of interest (ROI) were manually segmented on all slices, the first being around the outer bladder wall and the second being around the inner bladder lumen (Fig 6A). 3D images were reconstructed to quantify volumes of each ROI and bladder wall volume was calculated as the difference as shown in equation 1.

$$\text{Volume}_{\text{Bladder Wall}} = \text{Volume}_{\text{Outer Wall}} - \text{Volume}_{\text{Inner Lumen}} \quad (1)$$

To evaluate tumor growth following intravesical therapy, mice underwent a second scan on week 19. Tumor growth was calculated as the difference in bladder wall volume from the first MRI to the second MRI as shown in Figure 6A and 6B and in equation 2.

$$\Delta \text{Volume}_{\text{Bladder Wall}} = \text{Volume}_{\text{Bladder Wall MRI 2}} - \text{Volume}_{\text{Bladder Wall MRI 1}} \quad (2)$$

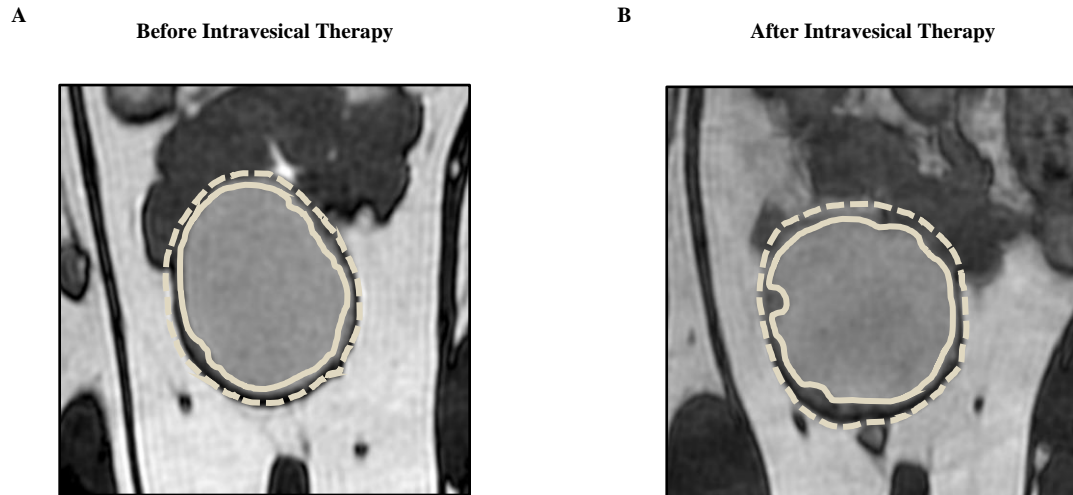


**Figure 6. Representative images of tumor burden analysis using MRI.** (A) MRI image of BBN<sup>+</sup> bladder before PAG + NaHS intravesical therapy and (B) MRI image of the same BBN<sup>+</sup> bladder after PAG + NaHS intravesical therapy. The dashed lines represent the outer bladder wall ROI, and the solid lines represent the inner bladder lumen ROI. MRI, Magnetic resonance imaging; BBN, N-butyl-N-(4-hydroxybutyl)-nitrosamine; PAG, propargylglycine; NaHS, sodium hydrosulfide; ROI, region of interest.

*2.2.5 Intravesical therapy.* BBN<sup>+</sup> mice were randomly assigned to an intravesical therapy group (n=6 mice per group) where they received 80  $\mu$ L of monotherapy (saline, PAG (20 mM), NaHS (100  $\mu$ M), or GEM (100  $\mu$ M)) or 80  $\mu$ L of combination therapy (PAG (20 mM) + NaHS (100  $\mu$ M) or PAG (20 mM) + GEM (100  $\mu$ M)). The BBN<sup>-</sup> control group received 80  $\mu$ L of saline. Therapies began during week 15 and were administered once a week for four weeks as previous studies demonstrated this to be sufficient in observing tumor response [115, 116]. This procedure was performed as described previously [117] and as depicted in Figure 4. Mice were anesthetized in an anesthesia induction chamber with 5% isoflurane and an O<sub>2</sub> flow rate of 2L/min. Mice were then transferred to a nose cone which supplied 2.5% isoflurane throughout the session and received a subcutaneous injection of meloxicam. Mice were then placed in a supine position and the abdomen was shaved. Treatment was delivered via transurethral instillation where the penile body was exposed and a lubricated 26-gauge angiocatheter was inserted into the urethra and treatment was delivered into the bladder lumen. Eighty microliter of treatment was delivered as the average mouse bladder can hold up to 150  $\mu$ L of urine [118]. This minimized the risk of therapy expulsion without utilizing invasiveness methods such as purse string sutures to occlude the urethra as done in previous studies [116]. An ultrasound-guided technique was used to locate the bladder and verify treatments were properly delivered into the bladder lumen, as indicated by swelling of the organ.

*2.2.6 Histological staining.* Bladders were removed after sacrificing the mice at the experimental endpoint (post-second MRI) and placed in 10% formalin for paraffin embedding and sectioning. Histological sections were stained with hematoxylin and eosin (H&E) and scored by an independent and blinded genitourinary pathologist to assess cancer presence and level of invasion. Histological sections also underwent immunohistochemical (IHC) staining where they were incubated with antibodies against the apoptotic markers caspase-9 and cleaved PARP-1, neovascularization marker VEGF, proliferation marker Ki67, macrophage marker F4/80, M2 macrophage marker CD163, and T cell markers CD8 and CD4 (Abcam, Toronto, Canada) and visualized with secondary antibodies.

*2.2.7 Microscope image analysis.* Immunohistochemically stained sections were analyzed at 40x magnification. Five randomly selected fields, which is in line with previous studies [48, 116], were analyzed per section of caspase-9, cleaved PARP-1, VEGF, Ki67, F4/80, CD163, CD8, and CD4 analysis and percent (%) staining per field of view was quantified by Image J version 1.51 (National Institutes of Health, Bethesda, MD).

*2.3 Statistical analysis.* Data are expressed as mean +/- standard error of mean (SEM). Data were analyzed via ANOVA and performed using the Graphpad (LA Jolla, CA) Prism statistical software package, version 9.0. Statistical significance was accepted at the 95% confidence interval.

### 3 Results

#### *3.1 CSE gene expression is less downregulated in MB49 cells and upregulated in 5637 cells under hypoxic conditions.*

To investigate the expression of the H<sub>2</sub>S-producing enzymes under hypoxic conditions MB49 and 5637 cell lines were subjected 0, 8, or 36 h of hypoxia and mRNA levels were quantified using qPCR (Fig 7A and B). Genes were normalized against  $\beta$ -actin and fold changes of gene expression were compared to 0 h hypoxia cells.

In the MB49 cell line, the expression of all genes was downregulated after 8 h of hypoxia compared to 0 h hypoxia. 3-MST gene expression was significantly less downregulated compared to CSE and CBS ( $p < 0.002$  and  $p < 0.0002$ , respectively; Fig 7A). However, after 36 h hypoxia, CSE gene expression was the least downregulated compared to CBS and 3-MST ( $p < 0.002$  and  $p < 0.002$ , respectively; Fig 7A). CSE gene expression was also significantly less downregulated at 36 h compared to 8 h ( $p < 0.0002$ ; Fig 7A). Conversely, CBS gene expression did not significantly change, and 3-MST gene expression were significantly attenuated overtime ( $p > 0.05$  and  $p < 0.05$ , respectively; Fig 7A). These findings suggest hypoxia downregulates CSE gene expression the least compared to CBS and 3-MST in MB49 cells over time.

In the 5637 cell line, the reverse was observed. All genes were upregulated to a similar extent after 8 h of hypoxia compared to 0 h hypoxia. At 36 h hypoxia CSE gene expression was significantly increased by almost 7-fold compared to 0 h hypoxia. CSE gene expression was also significantly upregulated compared to both CBS and 3-MST at this time point ( $p < 0.0001$  and  $p < 0.0001$ , respectively; Fig 7B). Furthermore, CSE gene expression was significantly increased at 36 h hypoxia compared to its expression at 8 h hypoxia, whereas CBS and 3-MST gene expression significantly decreased overtime ( $p < 0.0001$ ,  $p < 0.05$ , and  $p < 0.05$ , respectively; Fig 7B). These findings suggest hypoxia upregulates gene expression of CSE and not of CBS or 3-MST in 5637 cells over time.

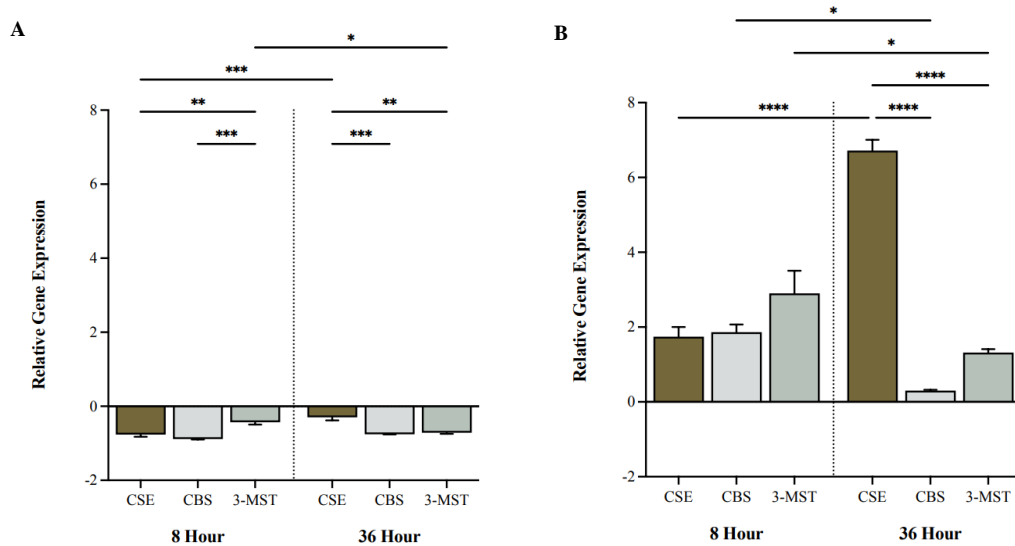


**Figure 7. CSE gene expression is less downregulated in MB49 cells and upregulated in 5637 cells under hypoxic conditions.** qPCR analysis of (A) MB49 and (B) 5637 cells for gene expression levels of CSE, CBS, and 3-MST after 8 and 36 h of hypoxia. Genes were normalized against  $\beta$ -actin and fold changes of gene expression were compared to 0 h hypoxia cells and calculated using the  $\Delta\Delta C_t$  method. Data (n=5) are expressed as mean  $\pm$  SEM. Means were compared using two-way ANOVA followed by Tukey's post-hoc test. \* $p < 0.05$ , \*\* $p < 0.002$ , \*\*\* $p < 0.0002$ , \*\*\*\* $p < 0.0001$ . qPCR, quantitative polymerase chain reaction; CSE, cystathionine  $\gamma$ -lyase; H<sub>2</sub>S, hydrogen sulfide; CBS, cystathionine  $\beta$ -synthase; 3-MST, 3-mercaptopyruvate sulfrtransferase.

**3.2 Optimal treatment doses were determined as 100  $\mu$ M NaHS, 20 mM PAG, and 100  $\mu$ M GEM *in vitro*.**

To determine optimal dosage of NaHS, PAG, and GEM for use in subsequent *in vitro* and *in vivo* experiments, an *in vitro* model was established. Based on the findings in section 3.1, we chose to inhibit H<sub>2</sub>S synthesis by targeting CSE activity using the selective inhibitor, PAG. We also chose NaHS as our exogenous H<sub>2</sub>S donor and GEM as our chemotherapy based on its current success as a salvage intravesical therapy, availability, and relatively low toxicity levels. MB49 cells were subjected to 8 h hypoxia and then treated with a concentration gradient of NaHS (0 – 300  $\mu$ M), PAG (0 – 80 mM), and GEM (0 – 100 mM) and subjected to 24 h more of hypoxia. Cell viability was analyzed using flow cytometry and compared to control cells that underwent hypoxia without treatment. Optimal dose was defined as the dose that resulted in the most significant response on cell viability without exceeding the half maximal inhibitory concentration compared to the untreated control group.

NaHS demonstrated a slight bimodal effect with low (25  $\mu$ M and 50  $\mu$ M) and high concentrations (300  $\mu$ M) either not influencing or slightly, but not significantly, attenuating cell viability compared to the control ( $p > 0.05$ ; Fig 8A). Moderate doses of 100  $\mu$ M and 150  $\mu$ M significantly potentiated cell viability with 100  $\mu$ M resulting in the most significant response compared to the control ( $p < 0.0001$  and  $p < 0.002$ , respectively; Fig 8A). PAG and GEM had opposing effects. Low levels of PAG (5  $\mu$ M and 10  $\mu$ M) did not significantly attenuate cell viability ( $p > 0.05$ ), whereas moderate doses of 20  $\mu$ M and 40  $\mu$ M and a high dose of 80  $\mu$ M significantly attenuated cell viability compared to the control ( $p < 0.0001$ ,  $p < 0.0002$ , and  $p < 0.0002$ , respectively; Fig 8B). Notably, the moderate dose of 20  $\mu$ M elicited the most significant response. All concentrations of GEM significantly attenuated cell viability compared to the control ( $p < 0.0001$ ; Fig 8C). 100 mM elicited the most significant response, exceeding the half maximal inhibitor concentration. Finally, 0.1 mM significantly attenuated cell viability compared to 0.01 mM ( $p < 0.002$ ; Fig 8C).

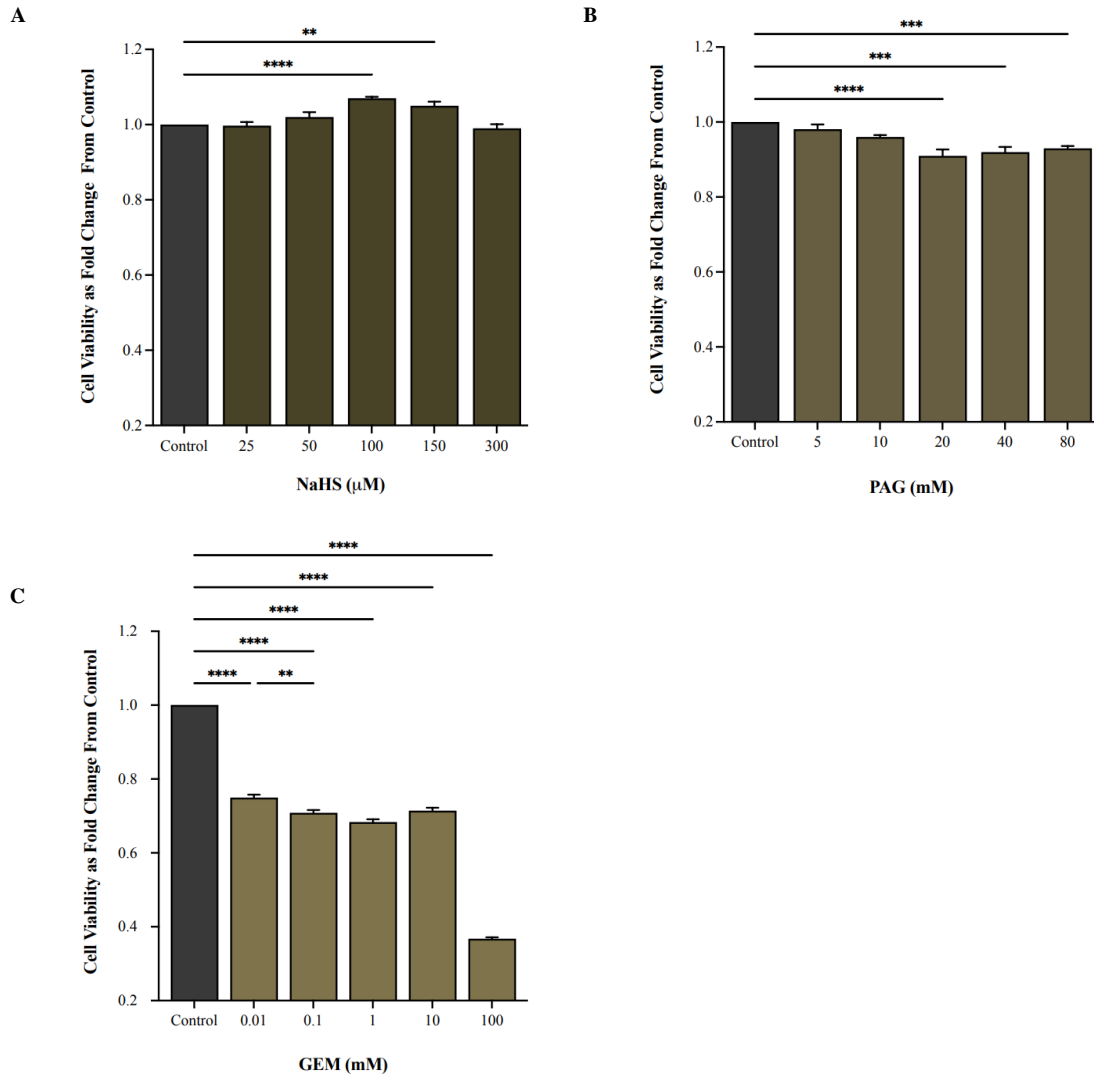


**Figure 8. Optimal doses are 100  $\mu\text{M}$  NaHS, 20 mM PAG, and 100  $\mu\text{M}$  GEM as determined by dose response curves.** Cell viability of MB49 cells following 8 hr of hypoxia, treatment with a gradient of concentrations of (A) NaHS, (B) PAG, and (C) GEM and 24 h more of hypoxia. Flow cytometry was used to quantify cell viability as the portion of cells negative for the apoptosis and necrosis markers, FITC-Annexin-V and propidium iodide, respectively. Cell viability is represented as fold change from control cells that underwent hypoxia without treatment. Data (n=5) are expressed as mean  $\pm$  SEM. Means were compared using one-way ANOVA followed by Tukey's post-hoc test. \* $p$ <0.05, \*\* $p$ <0.002, \*\*\* $p$ <0.0002, \*\*\*\* $p$ <0.0001. NaHS, sodium hydrosulfide; PAG, propargylglycine; GEM, gemcitabine.

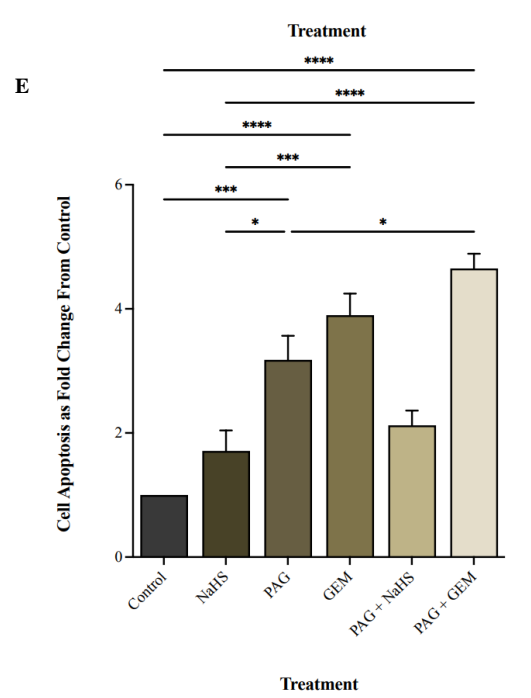
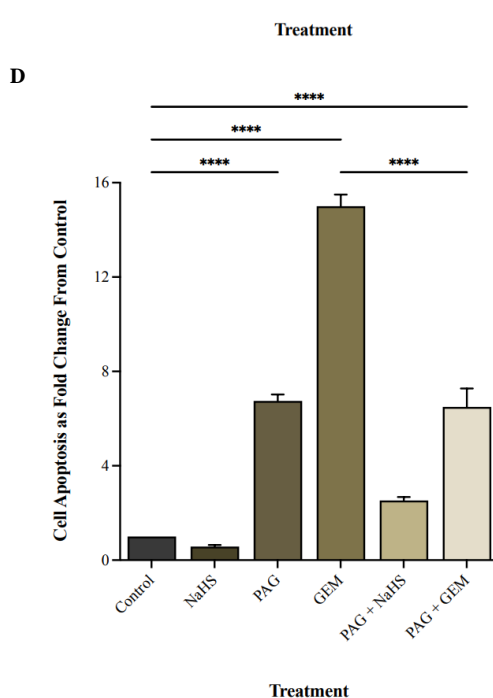
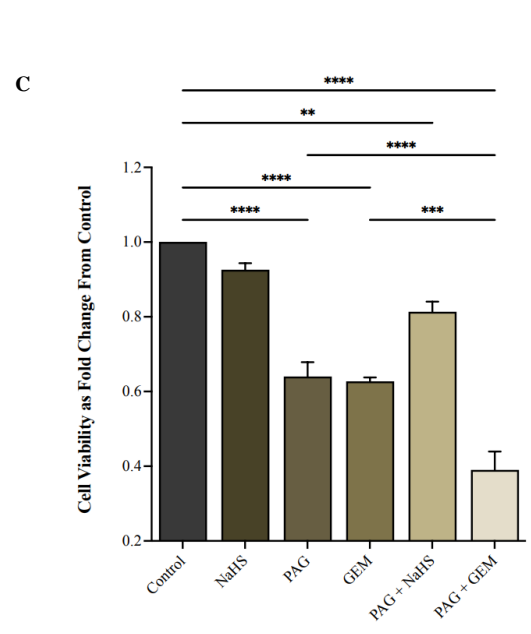
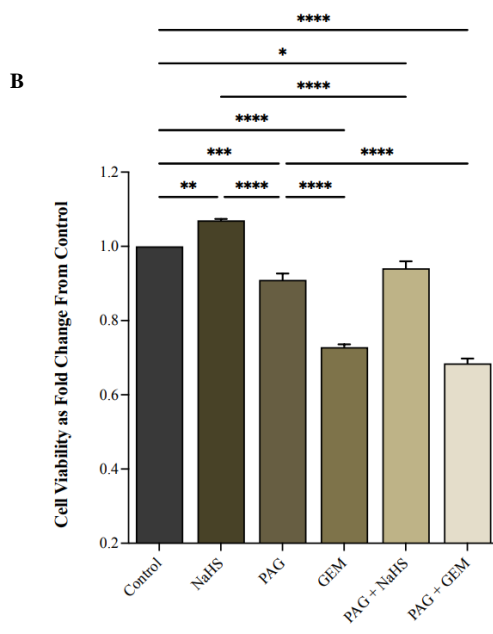
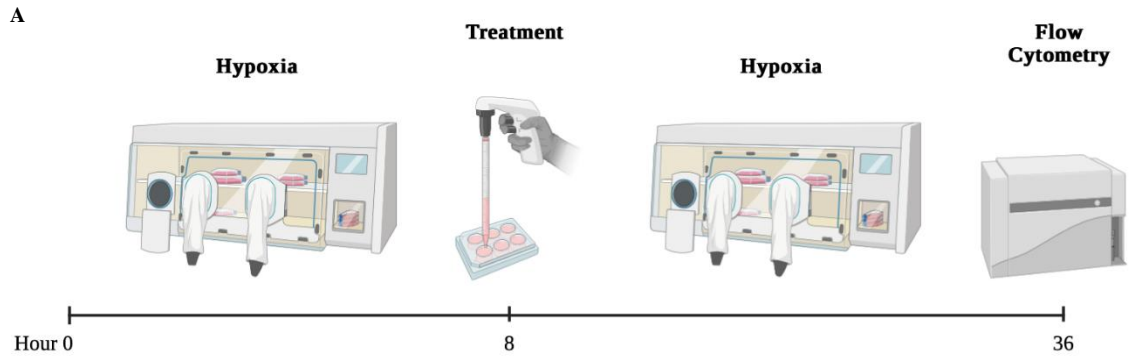
### ***3.3 Inhibiting CSE activity attenuates cell viability and further reduces cell viability in the presence of chemotherapy.***

To investigate the effects of H<sub>2</sub>S synthesis inhibition on bladder cancer cell viability in conjunction with chemotherapy, MB49 and 5637 cells were subjected to 8 h hypoxia followed by treatment with PAG (20 mM), NaHS (100 μM), GEM (100 μM), PAG (20 mM) + NaHS (100 μM) or PAG (20 mM) + GEM (100 μM) and 24 h more of hypoxia (Fig 9A). Cell viability was analyzed using flow cytometry and compared to control cells that underwent hypoxia without treatment.

The MB49 cell line, had a significant increase in cell viability following NaHS monotherapy compared to the control ( $p < 0.002$ ; Fig 9B). However, NaHS had no effect on cell viability of the 5637 cell line ( $p > 0.05$ ; Fig 9C). Conversely, PAG monotherapy significantly attenuated both MB49 and 5637 cell viability ( $p < 0.0002$  and  $p < 0.0001$ , respectively) as did GEM monotherapy compared to the controls ( $p < 0.0001$  and  $p < 0.0001$ , respectively; Fig 9B and 9C). Furthermore, GEM significantly reduced cell viability compared to PAG in MB49 cells but there was no significant difference in cell viability between the two treatments in 5637 cells ( $p < 0.0001$  and  $p > 0.05$ , respectively; Fig 9B and 9C). In terms of combination treatments, NaHS partially recovered cell viability from PAG for both MB49 and 5637 cells compared to the controls ( $p < 0.05$  and  $p < 0.002$ , respectively; Fig 9B and 9C). The PAG + GEM combination treatment further reduced cell viability compared to PAG in both the MB49 and 5637 cells ( $p < 0.0001$  and  $p < 0.0001$ , respectively; Fig 9B and 9C). Compared to GEM monotherapy, cell viability following PAG + GEM combination treatment was not significantly less in MB49 cells, but it was significantly less in 5637 cells ( $p > 0.05$  and  $p < 0.0002$ , respectively; Fig 9B and 9C).

Opposing trends occurred when evaluating cell apoptotic levels. NaHS had an insignificant effect on apoptosis in both MB49 and 5637 cells ( $p > 0.05$  and  $p > 0.05$ , respectively) whereas PAG significantly potentiated apoptosis in both MB49 and 5637 cells ( $p > 0.0001$  and  $p > 0.0002$ , respectively) as did GEM ( $p > 0.0002$  and  $p > 0.0002$  respectively; Fig 9D and 9E). Furthermore, NaHS reduced apoptotic levels of PAG monotherapy to similar levels of the controls in both cell lines ( $p > 0.05$  and  $p > 0.05$ , respectively; Fig 9D and 9E).

Interestingly in the MB49 cells, PAG + GEM combination therapy reduced apoptotic levels from that of GEM monotherapy and to a level similar to PAG monotherapy ( $p < 0.0002$  and  $p > 0.05$ , respectively; Fig 9D). Whereas PAG + GEM combination therapy increased apoptotic levels significantly compared to PAG and insignificantly compared GEM ( $p < 0.05$  and  $p > 0.05$ , respectively; Fig 9E).



Caption on page 37.

**Figure 9. Inhibiting CSE activity attenuates cell viability and further reduces cell viability in the presence of chemotherapy.** (A) Treatment timeline. Cell viability of (B) MB49 and (C) 5637 cells and apoptotic levels of (D) MB49 and (E) 5637 cells following 8 hr of hypoxia, treatment with PAG (20 mM), NaHS (100  $\mu$ M), GEM (100  $\mu$ M), PAG (20 mM) + NaHS (100  $\mu$ M) or PAG (20 mM) + GEM (100  $\mu$ M) and 24 h more of hypoxia. Flow cytometry was used to quantify cell viability as the portion of cells negative for the apoptosis and necrosis markers, FITC-Annexin-V and propidium iodide. Cell viability is represented as fold change from control cells that had underwent hypoxia without treatment. Apoptosis was quantified as the portion of cells positive for FITC-Annexin-V and negative for 7-ADD and represented as fold change from control cells that had underwent hypoxia without treatment. Data (n=5) are expressed as mean  $\pm$  SEM. Means were compared using one-way ANOVA followed by Tukey's post-hoc test. \* $p$ <0.05, \*\* $p$ <0.002, \*\*\* $p$ <0.0002, \*\*\*\* $p$ <0.0001. CSE, cystathionine  $\gamma$ -lyase; NaHS, sodium hydrosulfide; PAG, propargylglycine; GEM, gemcitabine.

### ***3.4 BBN induces bladder cancer in an intravesical murine model as detected by MRI.***

To establish an intravesical murine model of bladder cancer, 30 mice had continuous access to fresh 0.05% BBN tap water for 12 weeks. These mice were designated as BBN<sup>+</sup> mice. Six mice were not treated with BBN to act as a healthy control and were designated as BBN<sup>-</sup> mice. On week 14, all mice underwent MRI to assess for bladder tumor formation. On MRI, bladder cancer can present as thickening of the bladder wall and/or protrusions in the bladder lumen compared to a healthy bladder, where the bladder wall is well-defined with similar thickness throughout, and protrusion free as shown in Figure 10A. These features of bladder cancer were present in all 30 BBN<sup>+</sup> mice suggesting a 100% success rate of bladder cancer development. These features were also absent in all six BBN<sup>-</sup> mice, indicating no spontaneous development of bladder cancer.

As previously reported, tumor burden correlates with bladder wall area [109]. However, this study acknowledges the limitation of using only one axial image to calculate tumor burden and recommends using multiple slices for a more complex analysis. With this in mind, we calculated bladder wall volume using nine coronal slices spaced three slices apart, for a more comprehensive analysis. These slices were used to construct a 3D rendering of the bladder wall which allowed for volume quantification. We reported a significant increase in bladder wall volume in the BBN<sup>+</sup> group compared to the BBN<sup>-</sup> group ( $p < 0.002$ ; Fig 10B). This quantitative finding suggests that bladder wall thickening did occur in the BBN<sup>+</sup> group. BBN<sup>+</sup> mice were then blindly assigned to an intravesical therapy group; saline, PAG, PAG + NaHS, GEM, or PAG + GEM. Figure 10C demonstrates bladder wall volumes of each BBN<sup>+</sup> intravesical therapy group where all groups had a similar mean bladder wall volume prior to beginning intravesical therapy ( $p > 0.05$ ).

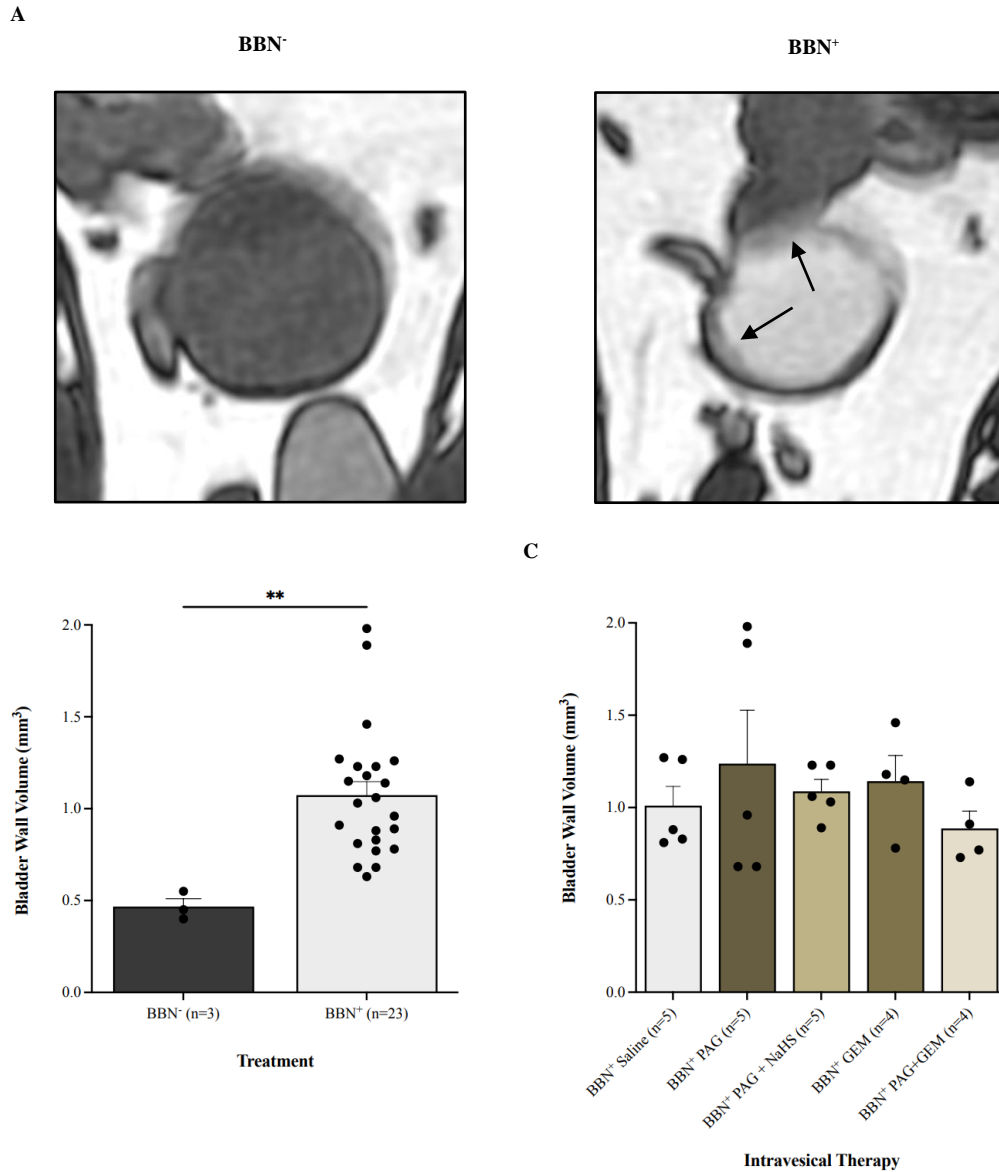


**Figure 10. BBN induces bladder cancer in an intravesical murine model as detected by MRI.** (A) Bladder of BBN<sup>-</sup> mouse compared to bladder of BBN<sup>+</sup> mouse which displays thickening of the bladder wall and protrusions in the bladder space, indicated by arrows. (B) Bladder wall volume (mm<sup>3</sup>) of the BBN<sup>+</sup> group compared to the BBN<sup>-</sup> group. (C) Bladder wall volume (mm<sup>3</sup>) of BBN<sup>+</sup> intravesical therapy groups prior to intravesical therapy. Data are expressed as mean ± SEM. Means were compared using by Tukey's post-hoc test. \* $p < 0.05$ , \*\* $p < 0.002$ , \*\*\* $p < 0.0002$ , \*\*\*\* $p < 0.0001$ . BBN, N-butyl-N-(4-hydroxybutyl)-nitrosamine; MRI, magnetic resonance imaging.

### ***3.5 Inhibiting CSE activity attenuates tumor progression and invasion and results in tumor regression and abrogates invasion in the presence of chemotherapy.***

To investigate the effects of H<sub>2</sub>S synthesis inhibition on bladder cancer progression in conjunction with chemotherapy *in vivo*, we performed MRI and pathology to evaluate tumor response to intravesical therapies consisting of 80  $\mu$ L of saline, PAG (20 mM), NaHS (100  $\mu$ M), or GEM (100  $\mu$ M) monotherapy and 80  $\mu$ L of PAG (20 mM) + NaHS (100  $\mu$ M) or PAG (20 mM) + GEM (100  $\mu$ M) combination therapy.

Changes in the bladder wall volume of the BBN<sup>+</sup> intravesical therapy groups were normalized to the change in bladder wall volume of the BBN<sup>-</sup> saline monotherapy group. In comparison to all other BBN<sup>+</sup> intravesical therapy groups, bladder tumor growth was highest in the BBN<sup>+</sup> saline monotherapy group. In comparison to the BBN<sup>+</sup> saline monotherapy group, the BBN<sup>+</sup> PAG monotherapy group demonstrated significant attenuation of tumor growth ( $p < 0.002$ ; Fig 11). The PAG + NaHS combination therapy group demonstrated attenuation of the anti-cancer effects of PAG, partially recovering tumor growth to a volume similar to the BBN<sup>+</sup> saline monotherapy group ( $p > 0.05$ , Fig 11). Furthermore, the GEM monotherapy group also demonstrated significant attenuation of tumor growth compared to the BBN<sup>+</sup> saline monotherapy group ( $p < 0.0002$ ; Fig 11). The PAG + GEM combination therapy group demonstrated an even further attenuation of tumor growth compared to both the BBN<sup>+</sup> saline monotherapy group and BBN<sup>+</sup> PAG monotherapy group ( $p < 0.0001$  and  $p < 0.002$ , respectively; Fig 11). There was no significant difference between the PAG + GEM combination therapy group and the GEM monotherapy group ( $p > 0.05$ ; Fig 11); however, the PAG + GEM combination therapy group was the only treatment to demonstrate tumor regression.

Figure 11B shows representative images of H&E stained bladder tumor tissue. All BBN<sup>+</sup> intravesical therapy groups were diagnosed with high-grade bladder cancer. Within these images, the BBN<sup>+</sup> saline monotherapy group was diagnosed as MIBC whereas the BBN<sup>+</sup> PAG monotherapy group, BBN<sup>+</sup> PAG + NaHS combination therapy group, BBN<sup>+</sup> GEM monotherapy group, and BBN<sup>+</sup> PAG + GEM combination therapy group were all diagnosed with papillary NMIBC.

Figure 11C shows percentage of mice within each group that had normal tissue, dysplasia, cancer with no invasion or invasion into the lamina propria (LP) or muscularis propria (MP) as determined by pathology. Among the mice that had confirmed bladder tumors, the BBN<sup>+</sup> saline monotherapy group had 33% no invasion and 67% MP invasion (Fig 11D). The BBN<sup>+</sup> PAG monotherapy group had 30% no invasion, 40% LP invasion, and 30% MP invasion (Fig 11D). The BBN<sup>+</sup> PAG + NaHS combination therapy group had 50% LP invasion and 50% MP invasion (Fig 11D). The BBN<sup>+</sup> GEM monotherapy group had 20% no invasion, 60% LP invasion, and 20% MP invasion (Fig 11D). The BBN<sup>+</sup> PAG + GEM combination therapy group had 100% no invasion (Fig 11D).

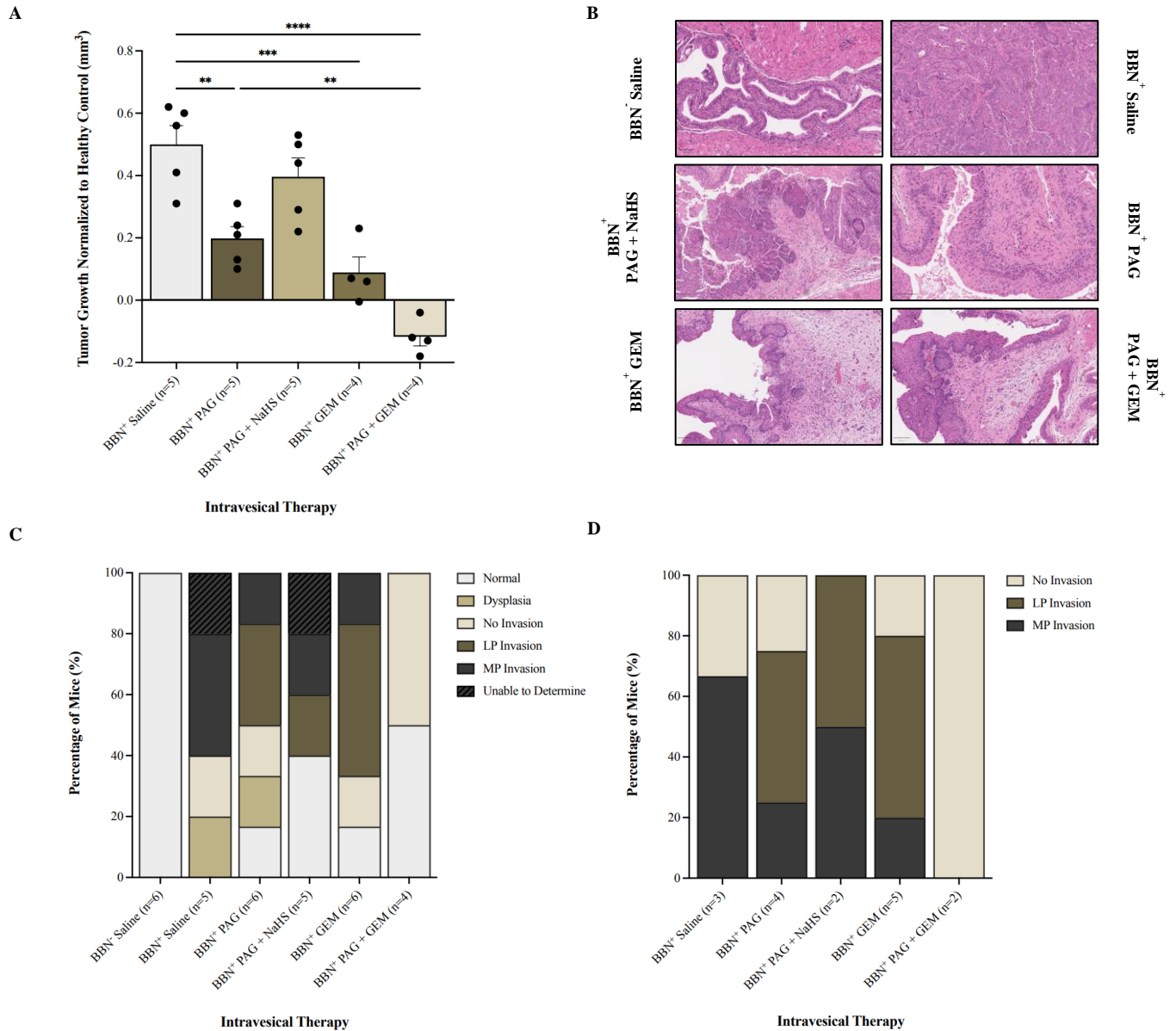


**Figure 11. Inhibiting CSE activity attenuates tumor progression and invasion and results in tumor regression and abrogates invasion in the presence of chemotherapy.**

(A) MRI was used to assess the change in bladder wall volume, representative of tumor progression, before and after intravesical therapy of 80  $\mu$ L of saline, PAG (20 mM), NaHS (100  $\mu$ M), GEM (100  $\mu$ M), PAG (20 mM) + NaHS (100  $\mu$ M) or PAG (20 mM) + GEM (100  $\mu$ M). *Caption continues onto page 43.*

*Caption continued.* Changes in bladder wall volume of the BBN<sup>+</sup> groups were normalized to the change in bladder wall volume of the BBN<sup>-</sup> group. (B) Representative images of H&E stained bladder tumor tissue. (C) Percentage of mice within each group that had normal tissue, dysplasia, cancer with no invasion, LP invasion, or MP invasion. (D) Percentage of mice with no invasion, LP invasion, or MP invasion among the mice that had bladder tumors. Data are expressed as mean  $\pm$  SEM. Means were compared using one-way ANOVA followed by Tukey's post-hoc test. \* $p < 0.05$ , \*\* $p < 0.002$ , \*\*\* $p < 0.0002$ , \*\*\*\* $p < 0.0001$ . CSE, cystathionine  $\gamma$ -lyase; MRI, magnetic resonance imaging; PAG, propargylglycine; NaHS, sodium hydrosulfide; GEM, gemcitabine; BBN, N-butyl-N-(4-hydroxybutyl)-nitrosamine; LP, lamina propria; MP, muscularis propria.

### ***3.6 Inhibiting CSE activity induces bladder tumor apoptosis, attenuates neovascularization and proliferation, alters the bladder tumor immune response and potentiates the pro-apoptotic and anti-neovascularization effects of chemotherapy.***

To investigate the mechanisms by which H<sub>2</sub>S synthesis inhibition attenuates bladder tumor growth and invasion and potentiates the anti-cancer effects of chemotherapy, bladder tumors underwent IHC staining for markers of apoptosis, neovascularization, proliferation, macrophages, and T cells. Staining for the apoptotic marker caspase-9 revealed a significant increase in caspase-9<sup>+</sup> cells in the bladder tumor tissue of the BBN<sup>+</sup> saline monotherapy group compared to the bladder tissue of the BBN<sup>-</sup> saline monotherapy group ( $p < 0.05$ ; Fig 12C). However, caspase-9<sup>+</sup> cells were not significantly altered in any of the BBN<sup>+</sup> intravesical therapy groups compared to the BBN<sup>+</sup> saline monotherapy group (Fig 12C).

Staining for the apoptotic marker PARP-1 revealed that PARP-1<sup>+</sup> cells were not altered in the bladder tumor tissue of the BBN<sup>+</sup> saline monotherapy group compared to the bladder tissue of the BBN<sup>-</sup> saline monotherapy group ( $p > 0.05$ ; Fig 12D). PARP-1<sup>+</sup> cells were induced in the BBN<sup>+</sup> PAG monotherapy group, BBN<sup>+</sup> GEM monotherapy group, and BBN<sup>+</sup> PAG + GEM combination therapy group compared to the BBN<sup>+</sup> saline monotherapy group ( $p < 0.05$ ,  $p < 0.0001$ , and  $p < 0.0002$ , respectively; Fig 12D). PARP-1<sup>+</sup> cells were induced in the BBN<sup>+</sup> PAG + GEM combination therapy group compared to the BBN<sup>+</sup> PAG monotherapy group ( $p > 0.002$ ; Fig 12D). PARP-1<sup>+</sup> cells were not altered in the BBN<sup>+</sup> PAG + NaHS combination therapy group compared to the BBN<sup>+</sup> saline monotherapy group ( $p > 0.05$ ; Fig 12D).

Staining for the proliferation marker Ki67 revealed a significant increase in Ki67<sup>+</sup> cells in the bladder tumor tissue of the BBN<sup>+</sup> saline monotherapy group compared to the bladder tissue of the BBN<sup>-</sup> saline monotherapy group ( $p < 0.002$ ; Fig 13C). Ki67<sup>+</sup> cells were reduced in the BBN<sup>+</sup> PAG monotherapy group, BBN<sup>+</sup> GEM monotherapy group, and BBN<sup>+</sup> PAG + GEM combination therapy group compared to the BBN<sup>+</sup> saline monotherapy group ( $p < 0.002$ ,  $p < 0.002$ , and  $p < 0.0001$ , respectively; Fig 13C). Ki67<sup>+</sup> cells were not altered in the BBN<sup>+</sup> PAG + NaHS combination therapy group compared to the BBN<sup>+</sup> saline

monotherapy group but were induced compared to the BBN<sup>+</sup> PAG monotherapy group ( $p>0.05$  and  $p<0.05$ , respectively; Fig 13C).

Staining for the neovascularization marker VEGF revealed a significant increase in VEGF<sup>+</sup> cells in bladder tumor tissue of the BBN<sup>+</sup> saline monotherapy group compared to the bladder tissue of the BBN<sup>-</sup> saline monotherapy group ( $p<0.0001$ ; Fig 13D). VEGF<sup>+</sup> cells were reduced in the BBN<sup>+</sup> PAG monotherapy group, BBN<sup>+</sup> PAG + NaHS combination therapy group, BBN<sup>+</sup> GEM monotherapy group, and BBN<sup>+</sup> PAG + GEM combination therapy group compared to the BBN<sup>+</sup> saline monotherapy group ( $p<0.0002$ ,  $p<0.05$ ,  $p<0.0002$ , and  $p<0.0002$ , respectively; Fig 13D). VEGF<sup>+</sup> cells were reduced in the BBN<sup>+</sup> PAG + GEM combination therapy group compared to the BBN<sup>+</sup> PAG monotherapy group ( $p>0.05$ ; Fig 13D).

Staining for the macrophage marker F4/80 revealed F4/80<sup>+</sup> macrophage were not altered in bladder tumor tissue of the BBN<sup>+</sup> saline monotherapy group compared to the bladder tissue of the BBN<sup>-</sup> saline monotherapy group ( $p>0.05$ ; Fig 14C). F4/80<sup>+</sup> macrophage were induced in the BBN<sup>+</sup> PAG monotherapy group compared to the BBN<sup>+</sup> saline monotherapy group ( $p<0.002$ ; Fig 14C). F4/80<sup>+</sup> macrophage were reduced in the BBN<sup>+</sup> PAG + NaHS combination therapy group compared to the BBN<sup>+</sup> PAG monotherapy group ( $p>0.002$ ; Fig 14C). F4/80<sup>+</sup> macrophage were not altered in the BBN<sup>+</sup> PAG + NaHS combination therapy group, BBN<sup>+</sup> GEM monotherapy group, and BBN<sup>+</sup> PAG + GEM combination therapy group compared to the BBN<sup>+</sup> saline monotherapy group ( $p>0.05$ ,  $p>0.05$ , and  $p>0.05$ , respectively; Fig 14C).

Staining for the macrophage marker CD163<sup>+</sup> revealed no significant changes in CD163<sup>+</sup> M2 macrophage presence in any group (Fig 14D).

Staining for the T cell marker CD8 revealed no change in CD8<sup>+</sup> T cell presence in the bladder tumor tissue of the BBN<sup>+</sup> saline monotherapy group compared to the bladder tissue of the BBN<sup>-</sup> saline monotherapy group ( $p>0.05$ ; Fig 15C). CD8<sup>+</sup> T cells were induced in the BBN<sup>+</sup> PAG monotherapy group and BBN<sup>+</sup> PAG + GEM combination therapy group compared to the BBN<sup>+</sup> saline monotherapy group ( $p>0.05$  and  $p>0.0001$ , respectively; Fig 15C). CD8<sup>+</sup> T cells were also induced in the BBN<sup>+</sup> PAG + GEM combination therapy group

compared to the BBN<sup>+</sup> GEM monotherapy group ( $p>0.002$ ; Fig 15C). CD8<sup>+</sup> T cells were not altered in the BBN<sup>+</sup> PAG + NaHS combination therapy group and BBN<sup>+</sup> GEM monotherapy group compared to the BBN<sup>+</sup> saline monotherapy group (Fig 15C).

Staining for the helper T cell marker CD4 revealed a significant increase in CD4<sup>+</sup> T cell presence in the bladder tumor tissue of the BBN<sup>+</sup> saline monotherapy group compared to the bladder tissue of the BBN<sup>-</sup> saline monotherapy group ( $p<0.0002$ ; Fig 15D). CD4<sup>+</sup> T cells were reduced in the BBN<sup>+</sup> PAG monotherapy group compared to the BBN<sup>+</sup> saline monotherapy group ( $p<0.05$ ; Fig 15D). CD4<sup>+</sup> T cells were not significantly altered in any other group compared to the BBN<sup>+</sup> saline group (Fig 15D).

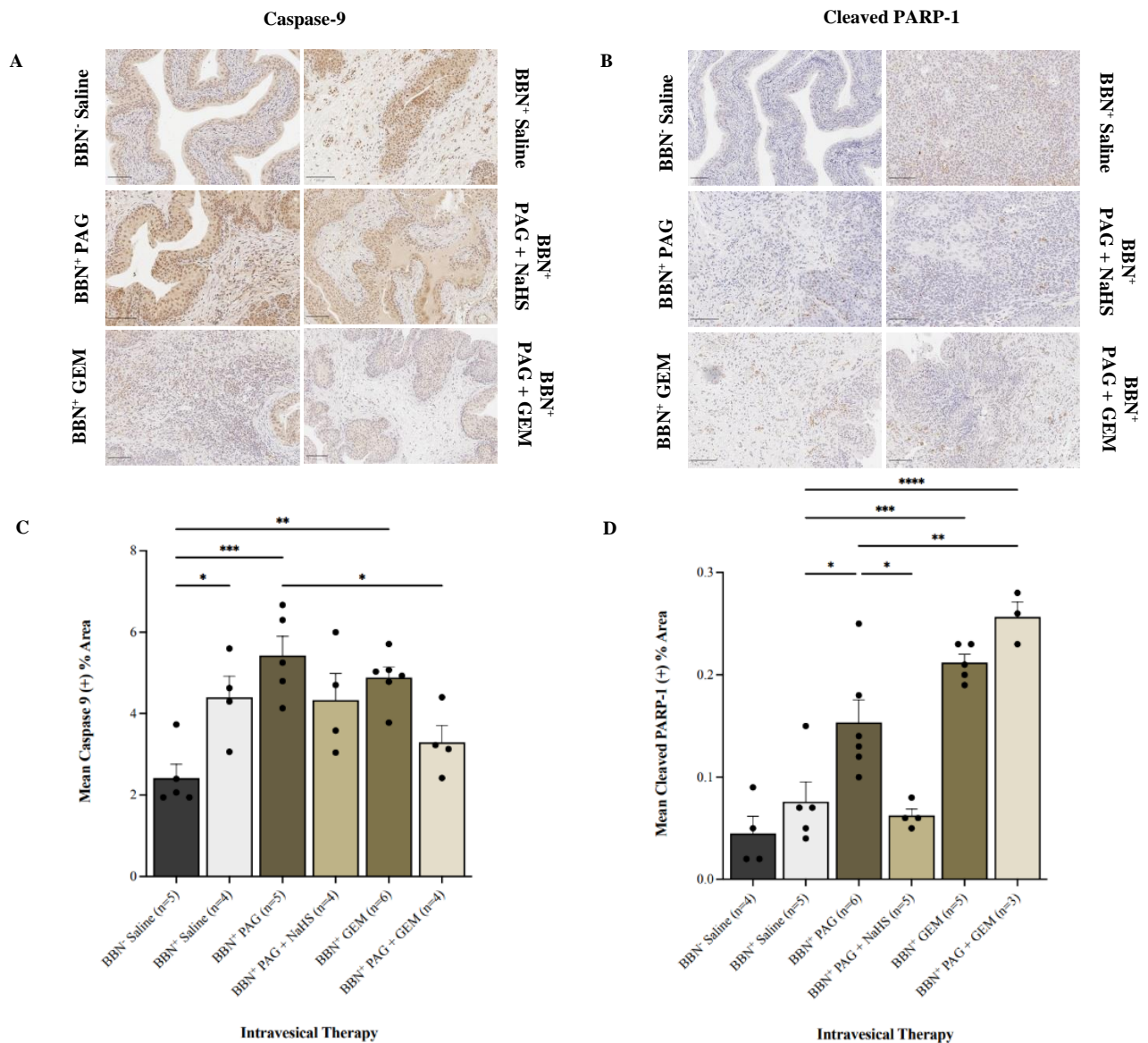


**Figure 12. CSE inhibition induces presence of the apoptotic marker cleaved-PARP-1 but not caspase-9 and further induces PARP-1<sup>+</sup> cells in combination with chemotherapy.** Representative images of immunohistochemical staining of apoptotic markers (A) caspase-9 and (B) cleaved PARP-1 of bladder tumors treated with saline, PAG, PAG + NaHS, GEM, and PAG + GEM intravesical therapy; 40x magnification. Line represents 100  $\mu$ m. Corresponding digital analysis show percent area of sections positive for (C) caspase-9 and (D) cleaved PARP-1. Data are expressed as mean  $\pm$  SEM. Means were compared using one-way ANOVA followed by Tukey's post-hoc test. \* $p < 0.05$ , \*\* $p < 0.002$ , \*\*\* $p < 0.0002$ , \*\*\*\* $p < 0.0001$ . CSE, cystathionine  $\gamma$ -lyase; PARP-1, Poly (ADP-ribose) polymerase 1; PAG, propargylglycine; NaHS, sodium hydrosulfide; GEM, gemcitabine.

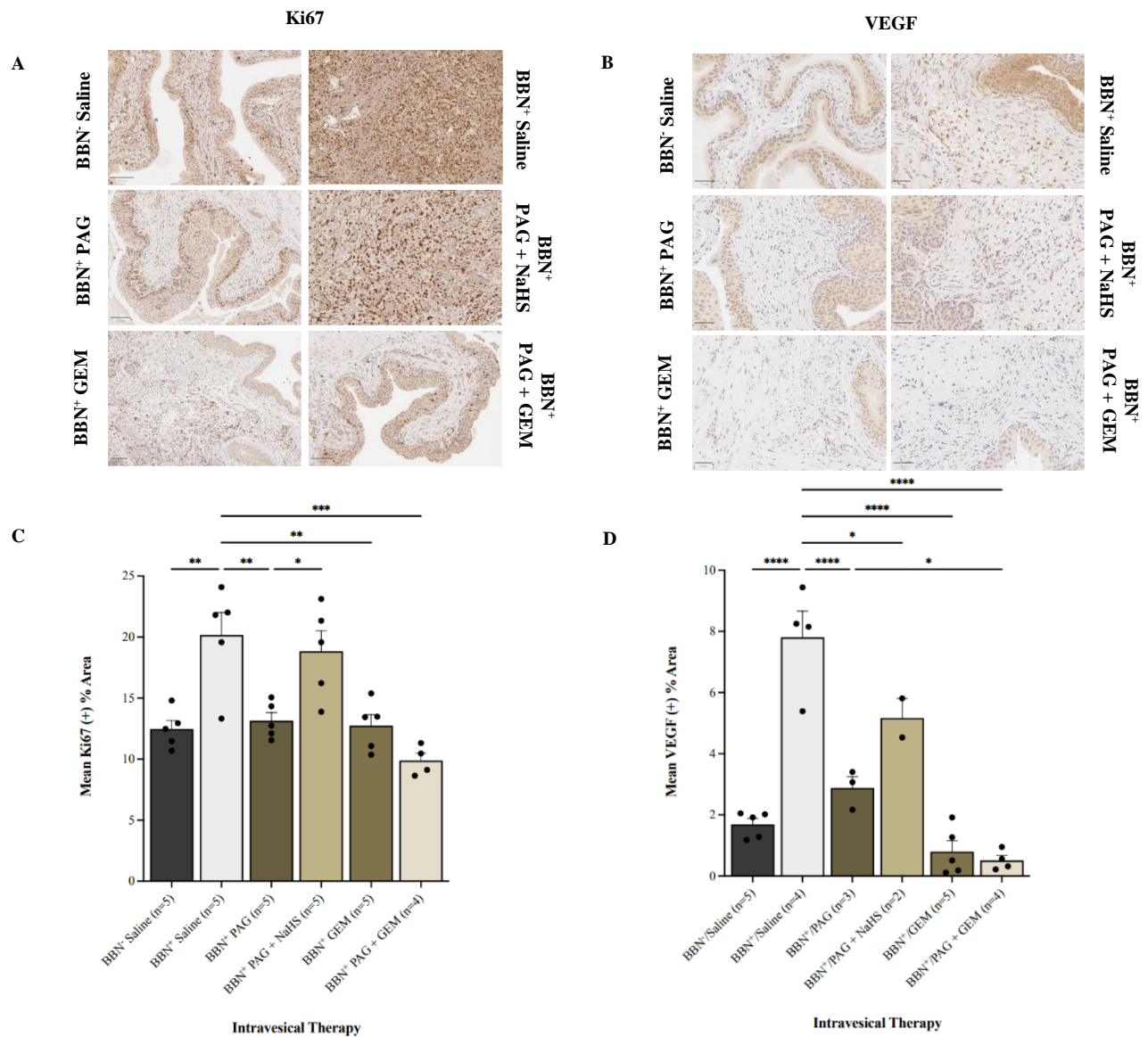


**Figure 13. CSE inhibition reduces presence of the proliferation marker Ki67 and the neovascularization marker VEGF and further reduces VEGF<sup>+</sup> cells in combination with chemotherapy.** Representative images of immunohistochemical staining of (A) proliferation marker Ki67 and (B) neovascularization marker VEGF of bladder tumors treated with saline, PAG, PAG + NaHS, GEM, and PAG + GEM intravesical therapy; 40x magnification. Line represents 100  $\mu$ m and 50  $\mu$ m for Fig A and B, respectively. Corresponding digital analysis show percent area of sections positive for (C) Ki67 and (D) VEGF. Data are expressed as mean  $\pm$  SEM. Means were compared using one-way ANOVA followed by Tukey's post-hoc test. \* $p$ <0.05, \*\* $p$ <0.002, \*\*\* $p$ <0.0002, \*\*\*\* $p$ <0.0001. CSE, cystathionine  $\gamma$ -lyase; VEGF, vascular endothelial growth factor; PAG, propargylglycine; NaHS, sodium hydrosulfide; GEM, gemcitabine.

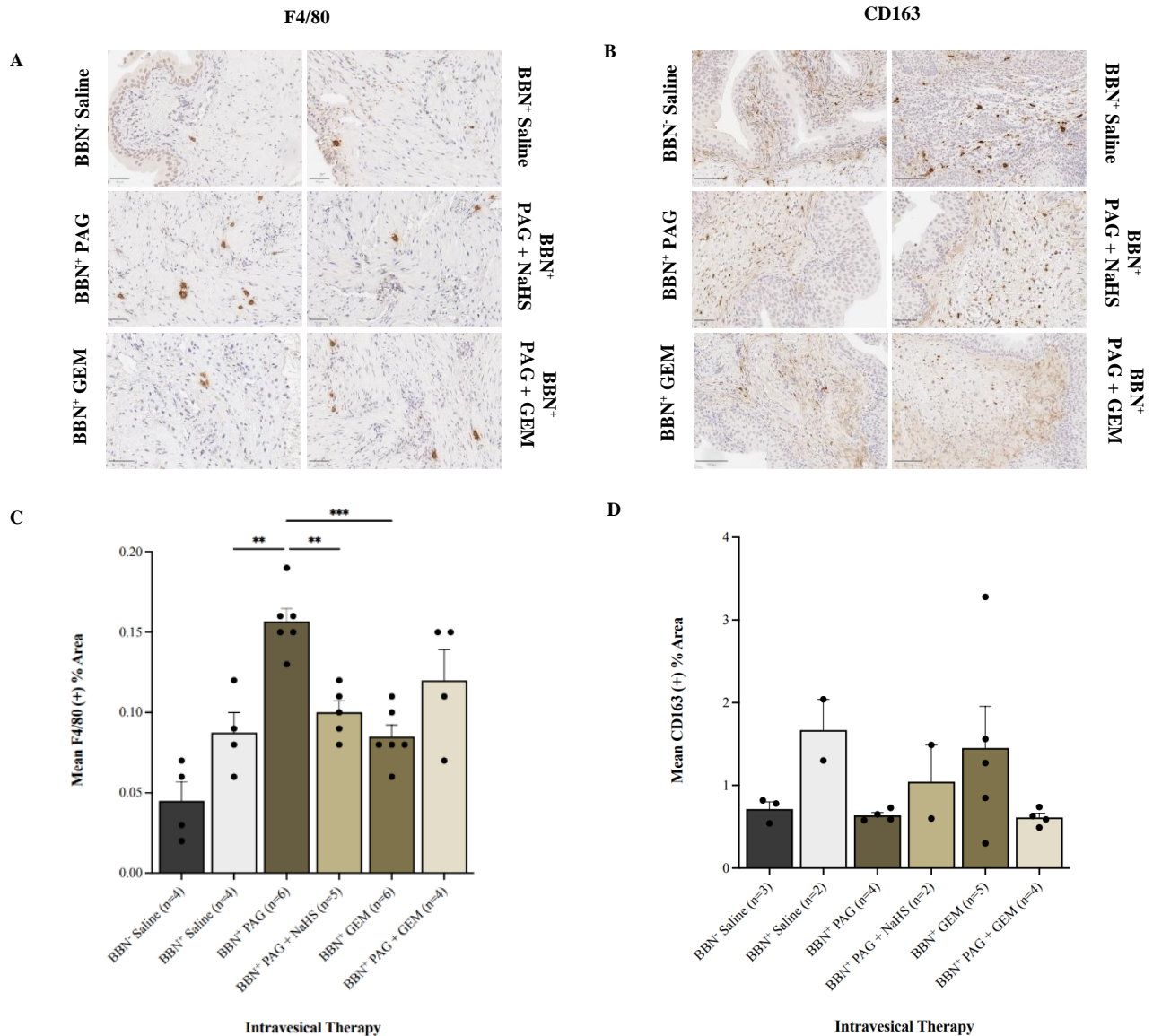


**Figure 14. CSE inhibition potentiates presence of macrophage marker F4/80.** Representative images of immunohistochemical staining for macrophage markers (A) F4/80 and (B) CD163 of bladder tumors treated with saline, PAG, PAG + NaHS, GEM, and PAG + GEM intravesical therapy; 40x magnification. Line represents 50  $\mu$ m. Corresponding digital analysis show percent area of sections positive for (C) F4/80 and (D) CD163. Data are expressed as mean  $\pm$  SEM. Means were compared using one-way ANOVA followed by Tukey's post-hoc test. \* $p$ <0.05, \*\* $p$ <0.002, \*\*\* $p$ <0.0002, \*\*\*\* $p$ <0.0001. CSE, cystathionine  $\gamma$ -lyase; PAG, propargylglycine; NaHS, sodium hydrosulfide; GEM, gemcitabine.

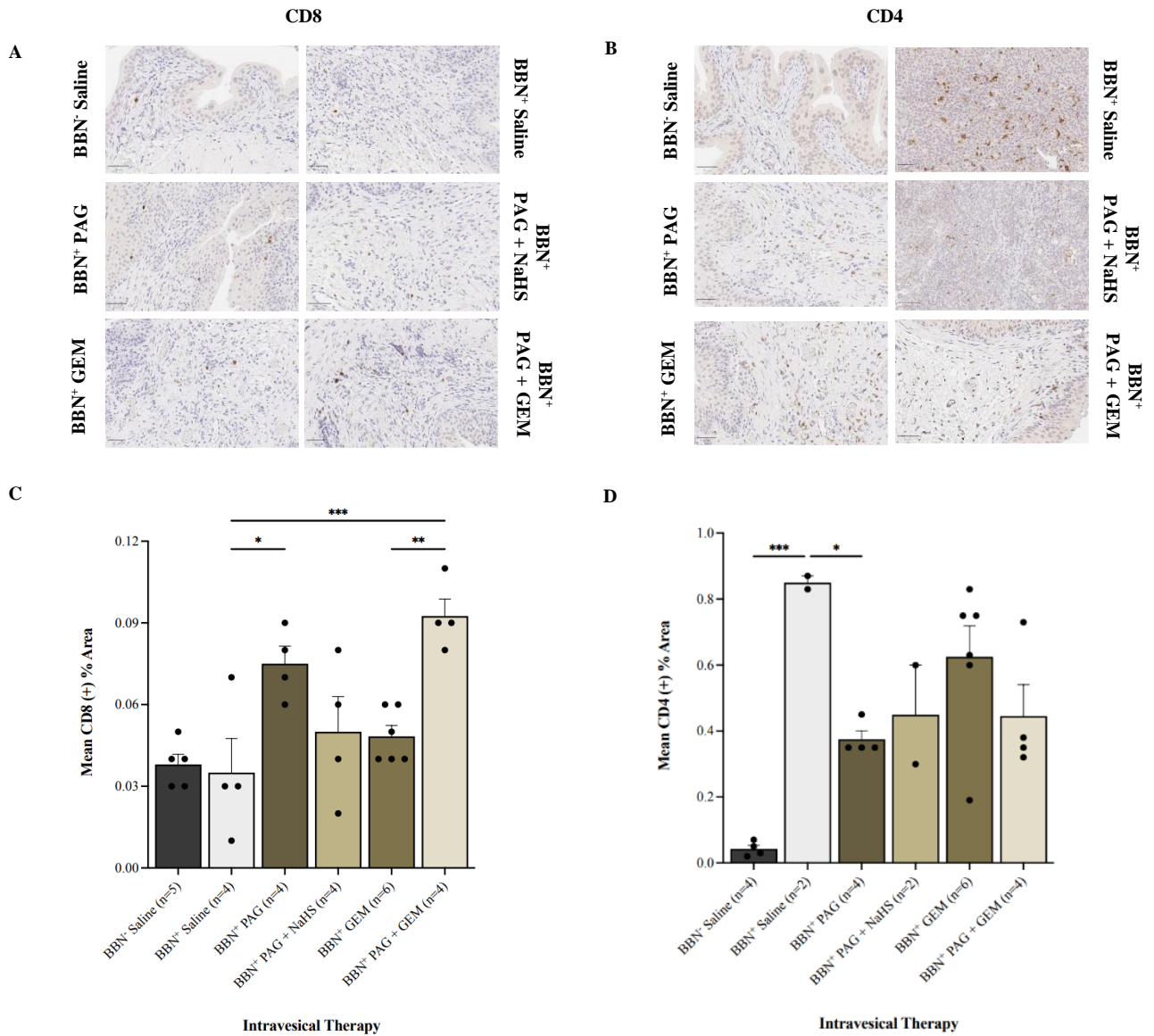


**Figure 15. CSE inhibition induces presence of T cell marker CD8 and further induces presence of CD8<sup>+</sup> T cells in combination with chemotherapy and reduces the presence of T cell marker CD4.** Representative images of immunohistochemical staining for T cell markers (A) CD8 and (B) CD4 of bladder tumors treated with saline, PAG, PAG + NaHS, GEM, and PAG + GEM intravesical therapy; 40x magnification. Line represents 50  $\mu$ m. Corresponding digital analysis show percent area of sections positive for (C) CD8 and (D) CD4. Data are expressed as mean  $\pm$  SEM. Means were compared using one-way ANOVA followed by Tukey's post-hoc test. \* $p$ <0.05, \*\* $p$ <0.002, \*\*\* $p$ <0.0002, \*\*\*\* $p$ <0.0001. CSE, cystathionine  $\gamma$ -lyase; PAG, propargylglycine; NaHS, sodium hydrosulfide; GEM, gemcitabine.

## 4 Discussion

Bladder cancer is the 6th most common cancer in men and 17th most common cancer in women [119]. Current bladder cancer therapies have limited therapeutic impact generating a need for investigation of novel treatments.

H<sub>2</sub>S, an endogenously produced gaseous signaling molecule, has been implicated in the development and progression of cancer [46-48]. Dysregulation of its production, through the experimental use of H<sub>2</sub>S synthesis inhibitors and H<sub>2</sub>S donors, has been shown to contribute to cancer cell viability, invasion, and migration [53, 58-60]. This has most recently been investigated in bladder cancer [74,75, 77]. However, these studies do not successfully mimic the clinical setting, therefore it is difficult to say whether these findings will translate in human subjects. Therefore, this study investigated the therapeutic effect of targeting H<sub>2</sub>S synthesis in a clinically relevant, carcinogen-induced, intravesical murine model of bladder cancer. We showed that inhibiting H<sub>2</sub>S production, by targeting CSE activity, reduced bladder cancer cell viability and tumor progression and strengthened the anti-cancer effects of GEM chemotherapy.

To begin, we performed *in vitro* experiments using both the mouse and human bladder cancer cell lines, MB49 and 5637, respectively. The MB49 cell line was used to develop suitable treatments for the subsequent *in vivo* experiments which utilized a mouse model. The 5637 cell line was used to determine whether these preliminary findings are translatable. We first investigated the dysregulation of H<sub>2</sub>S synthesis in bladder cancer by evaluating the gene expression of the H<sub>2</sub>S-producing enzymes, CBS, CSE, and 3-MST under hypoxic conditions in both cell lines. Gene expression of the H<sub>2</sub>S-producing enzymes have been shown to be downregulated in bladder cancer cells yet, their expression levels are positively correlated with bladder cancer stage suggesting elevated H<sub>2</sub>S levels contribute to the aggressiveness of the disease [75, 77]. Under normoxic conditions, CSE protein levels are the most upregulated compared to CBS and 3-MST in bladder cancer cells [77]. However, these models are missing the hypoxic nature of the bladder cancer microenvironment as hypoxia has been shown to be an integral part of the TME and correlated with worse patient prognosis [120, 121]. Therefore, this should be considered when developing an *in vitro* bladder cancer model.

We found that after hypoxia exposure, H<sub>2</sub>S-producing enzyme gene expression was downregulated in MB49 cells, but more importantly was upregulated in 5637 cells compared to cancer cells without hypoxia. The latter finding may provide an explanation for why previous studies found H<sub>2</sub>S-producing enzyme levels to be positively associated with bladder cancer tumor progression. Hypoxia, which is associated with more progressed stages of bladder cancer, may upregulate H<sub>2</sub>S-producing enzyme expression in bladder cancer. A previous study demonstrates this in the human lung cancer A549 cell line where H<sub>2</sub>S promotes the pro-angiogenic effect of hypoxia-inducible factor-1 $\alpha$  (HIF-1 $\alpha$ ) resulting in increased cancer cell proliferation and invasion [122]. Moreover, they demonstrated that HIF-1 $\alpha$  knockdown reduced H<sub>2</sub>S-induced angiogenesis suggesting a positive feedback mechanism. Therefore, the current study demonstrates that it is plausible that a similar relationship exists in bladder cancer.

CSE is the main H<sub>2</sub>S-producing enzyme present within smooth muscle, which is what the bladder detrusor muscle is composed of [123]. Taking into account the hypoxic nature of the bladder TME, we reported CSE gene expression to be the most upregulated over time compared to the other H<sub>2</sub>S-producing enzymes in 5637 cells suggesting that even under hypoxic conditions CSE may be the most prominent H<sub>2</sub>S-producing enzyme in bladder cancer. This is in line with previous studies as Wahafu *et al* [75] found CSE to be the only H<sub>2</sub>S-producing enzyme to significantly increase from human NMIBC to MIBC tissue samples. Likewise, Panza *et al* [77] showed CSE to have the highest protein expression compared to both CBS and 3-MST in the human bladder cancer cell lines T24 and UMUC3. This highlights the importance of targeting CSE activity when pharmacologically inhibiting H<sub>2</sub>S synthesis.

To further understand the involvement of H<sub>2</sub>S synthesis in mouse and human bladder cancer cell viability, we inhibited endogenous H<sub>2</sub>S synthesis and administered exogenous H<sub>2</sub>S individually and in combination. Based on our previous finding that CSE is the main H<sub>2</sub>S-producing enzyme and the subsequent dose response curves, we used 20 mM PAG, a specific inhibitor of CSE, and 100  $\mu$ M NaHS as the exogenous H<sub>2</sub>S donor.

Compared to the untreated cells exogenous H<sub>2</sub>S has no impact on 5637 cell viability or apoptosis. Wahafu *et al* [75] also reported no effect on human bladder cancer EJ cell viability after 24 h treatment with 100  $\mu$ M NaHS providing support for our findings. Conversely, it has been shown that 100  $\mu$ M NaHS and 50  $\mu$ M NaHS is sufficient to induce a significant increase in human bladder cancer EJ cell and human lung cancer A549 cell viability, respectively [76, 122]. The former study treated cells for 48 h whereas our cells were exposed to NaHS for 24 h so it is plausible that longer exposure is required to induce an effect. Another study investigated this using both exogenous and endogenously generated H<sub>2</sub>S [77]. They found that exogenous H<sub>2</sub>S, by two slow-releasing H<sub>2</sub>S donors DATS and GYY4137, decreased cell viability and induced apoptosis in UMUC3 and T24 human bladder cancer cell lines. Moreover, increasing endogenous H<sub>2</sub>S, by overexpression of CBS and CSE, attenuated human bladder cancer cell viability in the UMUC3 cell line. Therefore, fast and immediate administration of H<sub>2</sub>S may be the key to the observed pro-cancer effects of H<sub>2</sub>S rather than a slow and steady release.

Interestingly, we did see a significant potentiation of cell viability in the MB49 cell line following NaHS administration. This discrepancy from the cell viability of the 5637 cell line may be explained by the difference in H<sub>2</sub>S-producing enzyme gene expression. The downregulation of gene expression levels in MB49 cells may make these cells more sensitive to H<sub>2</sub>S administration. 100  $\mu$ M NaHS may alter these cells into a high H<sub>2</sub>S state, whereas 5637 cells may already be in this high state so they may not be as sensitive to exogenous administration.

In contrast, inhibiting H<sub>2</sub>S synthesis significantly attenuates cell viability and significantly potentiates cell apoptosis in both MB49 and 5637 cells. Wahafu *et al* [75] found that PAG treatment did not impact EJ cell viability after 24 h; however, they used only 100  $\mu$ M PAG, whereas we used 20 mM, therefore our high dose may explain this discrepancy. A breast cancer study also reported 20 mM PAG significantly reduced viability of the human breast cancer cell lines MCF-7 and MDA-MB-231 [58]. Furthermore, they found PAG treatment significantly potentiated the apoptotic index of the breast cancer cells compared to untreated cells. Similar trends have also been shown in human non-small cell lung cancer cells, human gastric AGS cells, and human nasopharyngeal carcinoma cells which suggest

targeting CSE activity is sufficient in restricting human cancer cell viability and inducing cancer cell death [61, 122, 124].

Our study showed a discrepancy in cell viability between cell lines following PAG treatment, whereby the viability of 5637 cells was reduced by over 20% compared to MB49 cells. This may be once again due to the difference in H<sub>2</sub>S-producing enzyme expression, whereby the upregulation and availability of CSE in 5637 cells may make them more sensitive to PAG treatment compared to MB49 cells where CSE is downregulated and therefore less available for PAG interaction. Nonetheless, these findings demonstrate the anti-cancer potential of CSE activity inhibition in human bladder cancer cells.

To corroborate whether it is the inhibition of H<sub>2</sub>S production that is contributing to the observed anti-cancer effects, PAG-treated cells were also supplemented with NaHS. NaHS partially recovers cell viability from PAG and reduces apoptotic levels in both cell lines. Sekiguchi *et al* [124] also reported a reversal of the inhibitory effects of PAG on human gastric AGS cell proliferation by NaHS. Others have attempted to investigate the effect of H<sub>2</sub>S synthesis inhibition and H<sub>2</sub>S donor administration *in vitro* by directly measuring H<sub>2</sub>S production [46, 51]. This was accomplished using a fluorescent-based assay and a colorimetric-based assay, respectively, with other methods being chromatographic-based assays [125] and electrochemical-based assays [126]. If these methodologies were reliable, measuring H<sub>2</sub>S production could further corroborate our findings. Unfortunately, each of these methodologies are associated with their own inherent faults which currently do not allow for selective and sensitive measurements of real-time H<sub>2</sub>S levels. For example, main disadvantages have been identified as fluorescent-based assays having extremely high response times, colorimetric-based assays and chromatographic-based assays being associated with low sensitivity, and electrochemical-based assays having to rely on manipulating pH which results in overestimation of H<sub>2</sub>S levels [127]. Nonetheless, we reported that reintroducing H<sub>2</sub>S in the form of an exogenous donor reversed the anti-cancer effects of CSE activity inhibition supporting our hypothesis that is it the loss of H<sub>2</sub>S, rather than an off-target effect, that attenuates cancer cell viability and potentiates cancer cell death.

Interestingly, we reported that PAG treatment decreased cell viability to a level comparable to GEM treatment in 5637 cells. Therefore, we wanted to investigate the effect of both treatments in combination. We found PAG treatment potentiates the anti-cancer effects of GEM and further increase apoptotic levels in the 5637 cell line compared to GEM treatment alone. Wahafu *et al* [75] also found PAG treatment in combination with cisplatin chemotherapy to further reduced human bladder cancer cell viability compared to both PAG and cisplatin chemotherapy alone. This was attributed to an increase in the level of pro-apoptotic proteins, Bax, Bcl-2, and cleaved PARP-1. Thus, it is plausible that inhibition of CSE activity by PAG may elicit an additive effect with current bladder cancer chemotherapies.

Based on our promising *in vitro* results, we investigated the anti-cancer effects of PAG and its additive relationship with GEM in a clinically relevant, carcinogen-induced, intravesical murine model. Following intravesical therapy, MRI was used to evaluate bladder tumor response to the H<sub>2</sub>S-targeted therapies. Our study shows that inhibiting H<sub>2</sub>S synthesis, by targeting CSE activity, reduced tumor growth compared to saline-treated mice. We also reported an attenuation of tumor invasion following PAG monotherapy, as 30% of PAG-treated tumors had MP invasion compared to the 67% of saline-treated tumors that had MP invasion. Cano-Galiano *et al* [59] and Wang *et al* [61] reported that PAG significantly decreased orthotopic xenogeneic brain and subcutaneous syngeneic nasopharyngeal carcinoma tumor growth, respectively. Wang *et al* [60] also reported suppression of prostate tumor growth in an orthotopic xenograft mouse model following CSE knockdown. Therefore, the current literature in other cancer types supports our finding that PAG monotherapy impedes cancer growth.

In line with our *in vitro* results, PAG + NaHS combination therapy partially recovered tumor growth compared to PAG monotherapy, resulting in bladder wall volume similar to saline-treated tumors. Moreover, 50% of PAG + NaHS-treated tumors had MP invasion compared to the 30% of PAG-treated tumors with MP invasion. These findings further validate our hypothesis that it is the inhibition of H<sub>2</sub>S synthesis that is contributing to the anti-cancer effects observed by PAG treatment rather than being the result of an off-target effect.

To follow this hypothesis further, we investigated whether the anti-cancer effects of PAG monotherapy could potentiate the anti-cancer effects of GEM monotherapy as observed in our *in vitro* findings. Previously, Wahafu *et al* [75] demonstrated that PAG treatment with cisplatin chemotherapy further reduced subcutaneous bladder cancer tumor volume compared to cisplatin chemotherapy alone. Similarly, we reported that PAG in combination with GEM not only reduced tumor growth compared to PAG monotherapy, but it was the only group that resulted in regression of the tumor. We also reported no invasion in the PAG + GEM-treated tumors compared to the 30% and 20% of tumors that had MP invasion in the PAG-treated and GEM-treated tumors, respectively. Therefore, not only does PAG have an additive effect with GEM, but this combination therapy was able to reduce tumor size rather than delay tumor growth and abrogate tumor invasion altogether.

These findings are promising as the model utilized in this study does not reflect clinical reality, yet tumor regression and abrogation of invasion were still observed. Within the clinical setting, patients would first undergo TURBT which would then be followed by intravesical therapy. We forwent the surgery and performed primary intravesical therapy. Therefore, PAG + GEM combination therapy may be even more successful when surgery is performed. It is also important to note that the model utilized in this study was initially meant to target NMIBC. However, we observed a large number of MIBCs suggesting our findings may be more applicable to patients with MIBC. The typical treatment course for MIBC involves neoadjuvant chemotherapy followed by radical cystectomy. However, 50% of patients will experience recurrence within two years of receiving a radical cystectomy [128]. As we observed tumor regression and abrogation of invasion following PAG + GEM combination therapy without any other therapeutic intervention, this may be a promising treatment for MIBC patients, especially those who are unable to undergo radical cystectomy.

H<sub>2</sub>S promotes cancer cell function by promoting anti-apoptotic pathways, DNA repair, proliferation, neovascularization, and evading anti-tumor immune responses. For instance, it has previously been reported that PAG induces apoptosis through cleaved caspase-3 in human breast cancer cell lines MCF-7 and MDA-MB-231 [58]. Caspase-3 is directly cleaved and activated by caspase-9 [129]. GEM has also been reported to induce cancer

cell death by activating caspase-9 [130, 131]. Conversely, we reported no significant change in caspase-9<sup>+</sup> cell infiltration following PAG or GEM monotherapy. Nevertheless, caspases also induce apoptosis by cleaving the DNA repair initiator, PARP-1. GEM also induces apoptosis through PARP-1 degradation as demonstrated by a downregulation of intact PARP-1 following GEM treatment in human KLM1 pancreatic cancer cells [132]. We also demonstrated this as an increase in cleaved PARP-1<sup>+</sup> cells in GEM-treated tumors. In contrast, H<sub>2</sub>S potentiates PARP-1 activity by persulfidation of MEK1 [66]. We found that PAG monotherapy resulted in increased presence of cleaved PARP<sup>+</sup> cells, suggesting high apoptotic activity. Khan *et al* [58] also found an increased level of cleaved PARP-1 following PAG treatment in human breast cancer cell lines MCF-7 and MDA-MB-231. More interestingly, we found an additive effect between PAG and GEM as PAG + GEM combination therapy resulted in a further increase in cleaved PARP-1<sup>+</sup> cells compared to both monotherapies. Therefore, these findings suggest H<sub>2</sub>S synthesis inhibition potentiates the apoptotic effects of GEM through PARP-1 degradation (Fig 16).

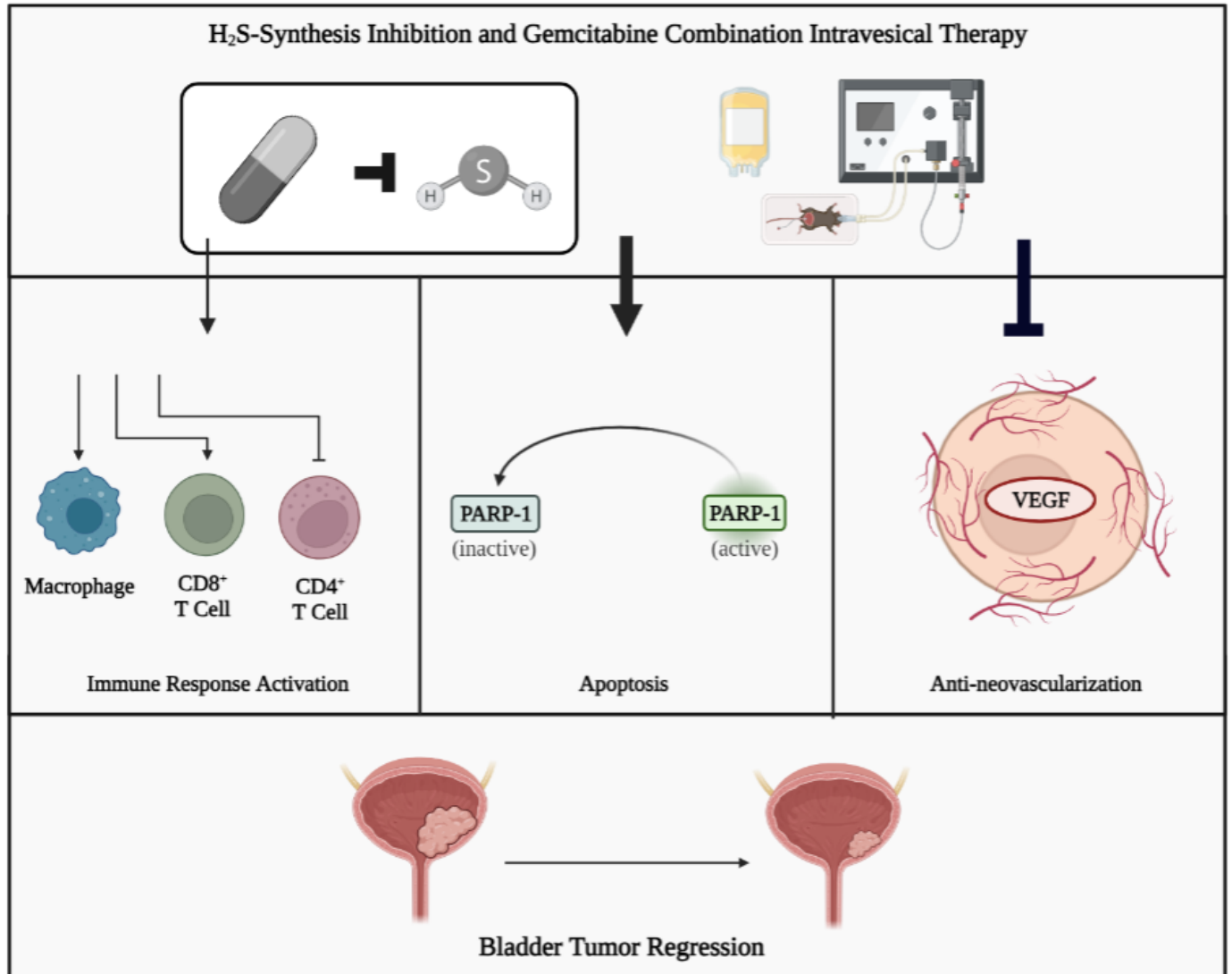


**Figure 16. Proposed mechanisms of H<sub>2</sub>S synthesis inhibition and GEM combination intravesical therapy resulting in bladder tumor regression.** H<sub>2</sub>S synthesis inhibition modifies the immune response, potentiating F4/80<sup>+</sup> macrophage and CD8<sup>+</sup> T cell infiltration and attenuating CD4<sup>+</sup> T cell infiltration. H<sub>2</sub>S synthesis inhibition and GEM potentiate PARP-1 cleavage, resulting in apoptosis. H<sub>2</sub>S synthesis inhibition and GEM attenuate neovascularization reducing the presence VEGF<sup>+</sup> cells. H<sub>2</sub>S, hydrogen sulfide; GEM, gemcitabine; PARP-1, Poly (ADP-ribose) polymerase 1; VEGF, vascular endothelial growth. Figure prepared with BioRender (biorender.com).

Another important marker of bladder cancer prognosis is the proliferation marker Ki67 as high Ki67 levels are indicative of poor bladder cancer patient survival and recurrence [133]. In comparison to saline-treated tumors, we observed a significant decrease in Ki67<sup>+</sup> cells in our PAG and GEM monotherapy groups. Khan *et al* [58] also reported a significant decrease in Ki67 levels following PAG treatment in human breast cancer MCF-7 and MDA-MB-231 cells and subcutaneous tumors. PAG + GEM combination therapy resulted in the lowest number of Ki67<sup>+</sup> cells suggesting a further reduction in bladder tumor proliferation and a better prognosis compared to no therapy, PAG or GEM monotherapy. It may also be of importance to further identify proliferating cells as tumor or immune cells using the marker CD45 to provide a deeper insight into what is occurring within the TME.

Neovascularization is another critical process in cancer as the formation of new blood vessels promotes cancer proliferation and growth. H<sub>2</sub>S is a key mediator of neovascularization as its production by CSE has been shown to promote the ERK1/2 signaling pathway [70]. Our group previously demonstrated a reduction in blood vessels following H<sub>2</sub>S synthesis inhibition in VHL<sup>-</sup> ccRCC [46]. In this study we observed a decrease in VEGF<sup>+</sup> cells following PAG and GEM monotherapy and a further reduction following PAG + GEM combination therapy suggesting another explanation for the observed additive relationship (Fig 16).

Finally, the immune system plays a critical role in eliminating cancer cells. However, the TME evades anti-tumor immune responses through recruitment of TAMs via chemotactic molecules [134] and favoring pro-tumor M2 TAM polarization which in turn dysregulates T cell function [32, 33]. It has been reported that GEM has no effect on immune cell infiltration such as macrophage and T cells within bladder cancer [116], which was also demonstrated in this study. Conversely, GEM appears to play a role in promoting M2 macrophage polarization in the pancreatic cancer cell lines MiaPaCa-2 and Colo-357 [135]. However, T cell infiltration does not appear to be altered by GEM in pancreatic cancer patients [136].

In mice, tumor infiltrating TAMs generally express F4/80 and M2 TAMs specifically express CD163, allowing quantification of total macrophage vs. M2 TAMs. We reported

that PAG monotherapy potentiated macrophage infiltration, as indicated by a significantly higher presence of F4/80<sup>+</sup> macrophage compared to saline monotherapy, suggesting H<sub>2</sub>S synthesis inhibition is capable of evoking an immune response within the bladder tumor (Fig 16). We found no significant changes in the presence of CD163<sup>+</sup> M2 macrophage however, we did observe a slight decrease in CD163<sup>+</sup> M2 macrophage following PAG monotherapy, suggesting PAG may attenuate M2-polarization or infiltration. We also observed a statistically insignificant but noticeable increase in F4/80<sup>+</sup> macrophage presence and decrease in CD163<sup>+</sup> M2 macrophage presence after PAG + GEM combination therapy compared to GEM monotherapy. With that, we hypothesize that the observed increase in F4/80<sup>+</sup> macrophage may be due to an increase in anti-tumor M1 macrophage rather than pro-tumor M2 macrophage. To further investigate this, we suggest using alternative markers for M2 macrophage due to the lack of significance in this study. Although previous literature utilizes CD163 as an M2 macrophage marker [137], Barros *et al* [138] suggest that it may not be reliable. Although CD163 is macrophage specific they demonstrated that it may not be M2-specific. Thus, it may be more dependable to employ a double staining technique such as F4/80 with CD206 or triple staining with F4/80, CD206, and CD111b which has been shown to be M2 macrophage specific [139, 140]. Nonetheless, our findings suggest that PAG adds an immune component to the tumor response to GEM. This addition may be imperative to the attenuation of tumor growth and invasion and potentiation of GEM observed in the murine model.

Moreover, we hypothesized H<sub>2</sub>S synthesis inhibition would modulate T cell infiltration given the observed impact of H<sub>2</sub>S on macrophage. Our study found a significant increase in CD8<sup>+</sup> T cell infiltration in the bladder tumor following PAG monotherapy compared to saline monotherapy. Comparatively, Yue *et al* [141] reported a decrease in CD8<sup>+</sup> T cells following H<sub>2</sub>S treatment in human colon cancer tissue. These findings suggest that H<sub>2</sub>S attenuates CD8<sup>+</sup> T cell infiltration, and inhibiting H<sub>2</sub>S production may rescue this (Fig 16). Furthermore, we reported a significant decrease in CD4<sup>+</sup> T cell infiltration in the bladder tumor following PAG monotherapy compared to saline monotherapy suggesting H<sub>2</sub>S synthesis inhibition attenuates infiltration of CD4<sup>+</sup> cells. CD4<sup>+</sup> T cells are comprised of several subsets including immunosuppressive regulatory T cells, which have been shown to be abundant in bladder cancer [142]. We also demonstrated a significant potentiation of

CD4<sup>+</sup> cells in the BBN<sup>+</sup> saline group compared to the BBN<sup>-</sup> saline group. Therefore, it is possible that what we are seeing is a depletion of regulatory T cells from the bladder tumor following PAG monotherapy. Yue *et al* [141] previously reported a significant decrease in regulatory T cell infiltration following H<sub>2</sub>S depletion in a subcutaneous murine model of colon cancer. We also reported that PAG supplementation with GEM chemotherapy significantly increased CD8<sup>+</sup> T cell presence and insignificantly decreased CD4<sup>+</sup> T cell presence compared to GEM monotherapy underscoring our hypothesis that the addition of an anti-tumor immune response by PAG may be responsible for the increased potency of GEM chemotherapy.

#### 4.1 Limitations and future directions

This study possessed a few limitations. Firstly, as BBN treatment was delivered through a communal water bottle, its consumption by individual mice could not be evaluated. Therefore, its intake among mice may have been inconsistent resulting in variable tumor types at the time intravesical therapy began. Because no mice were sacrificed at this time point, no confirmative pathology could be performed. However, as a previous study has reported [109], bladder wall area significantly correlates with tumor burden therefore cancer type could potentially be interpreted from this data. Another limitation exists within the variability of interpretation of the MRI images. Glaser *et al* [109] suggested using all available MRI slices to give a more thorough evaluation of bladder wall volume. However, utilization of the entire bladder was not possible in this study due to the poor resolution of imaging strictly at the most anterior and posterior parts of the bladder. Image quality and usage was also affected by the movement of the bowel. To overcome this limitation, we utilized four slices on either side of the midpoint of the bladder with each slice being three slices apart, totaling nine slices. This ensured all images used were unobstructed and the amount of bladder analyzed was maximized. However, we would recommend that additional views, such as axial and sagittal, be used during future analysis to avoid bowel impediment and allow utilization of the entire bladder. Finally, doses used in the intravesical therapy were evaluated and determined *in vitro* and were not evaluated *in vivo*. Therefore, it is possible that more effective doses for all three treatments exist, and these

doses should be determined prior to future studies to investigate the full potential of these therapies.

Despite these limitations, our findings are promising and suggest H<sub>2</sub>S as a potential target in developing novel bladder cancer therapies. To improve the quality of this research inhibition of H<sub>2</sub>S synthesis by PAG should be verified by quantifying H<sub>2</sub>S production. We previously performed real-time measurement of H<sub>2</sub>S production in ccRCC cell lines using the H<sub>2</sub>S-specific, fluorescent probe MeRhoAz [46]. Therefore, this methodology may be an appropriate approach to doing so. Future studies should also aim to uncover the specific mechanisms underlying the anti-cancer effects of H<sub>2</sub>S, as well as its additive effects with GEM chemotherapy, such as with M2 macrophage and CD4<sup>+</sup> T cell subtypes. Proliferating immune cells should also be differentiated from other proliferating cells. This may be accomplished by additional pathology or omics techniques to provide a greater insight into what is occurring at the gene and protein levels. Moreover, although the employed model is more clinically relevant than previously used methods, the treatment course should be prolonged to six weekly sessions to better mimic the current treatment course used in clinical practice. Finally, intravesical therapy is specific to NMIBC. However, many of the cancers developed within this experiment were MIBC suggesting intravesical therapy may not be the most appropriate therapeutic choice. Future studies should consider shortening the timeline for BBN treatment to ensure treatment of NMIBCs or consider a more suitable method for MIBC such as intravenous administration. Doing so will better facilitate the clinical translation of our findings.

## **5 Conclusion**

In conclusion, this study reports that pharmacological inhibition of endogenous H<sub>2</sub>S production attenuates bladder cancer progression and potentiates the anti-cancer effects of a clinically used chemotherapeutic in a clinically relevant murine model. Current bladder cancer therapies have limited patient success, lengthy treatment times, and an extremely high cost burden, creating an inescapable need for novel therapies. We have demonstrated the vital role of H<sub>2</sub>S in bladder cancer progression as H<sub>2</sub>S-producing enzyme gene expression is upregulated in bladder cancer cells under hypoxic conditions with specific attention to CSE. Inhibition of CSE activity by PAG monotherapy reduced bladder cancer

viability as well as tumor growth and invasion and has an additive effect with GEM chemotherapy, resulting in tumor regression and abrogation of invasion. Our findings suggest H<sub>2</sub>S synthesis inhibition induces apoptosis, attenuates neovascularization and proliferation, and modulates the tumor immune response. H<sub>2</sub>S synthesis inhibition also potentiates the pro-apoptotic and anti-neovascularization effects and adds an immune component to the response to GEM chemotherapy increasing the number of mechanisms by which this therapy may target and destroy cancer cells. These findings underpin the role H<sub>2</sub>S plays in cancer pathophysiology demonstrated by the current literature and reveals the potential of H<sub>2</sub>S as a target for developing improved bladder cancer combination therapies.

## References

1. Sung, H., Ferlay, J., Siegel, R.L., Laversanne, H., Seorjomataram, I., Jemal, A., Bray, F. Global cancer statistics 2020: GLOBOCAN estimates of incidence and mortality worldwide for 36 cancers in 185 countries. *CA Cancer J Clin.* 2021; 71: 209-249. doi: 10.3322/caac.21660
2. Burger, M., Catto, J. W. F., Dalbagni, G., Grossman, H. B., Herr, H., Karakiewicz, P., Kassouf, W., Kiemeny, L. A., la Vecchia, C., Shariat, S., & Lotan, Y. Epidemiology and risk factors of urothelial bladder cancer. *Eur Urol.* 2013; 63: 234–241. doi: 10.1016/j.eururo.2012.07.033
3. Sylvester, R.J., van der Meijden, A.P., Oosterlinck, W., Witjes, J.A., Bouffieux, C., Denis, L., Newling, D.W.W., Kurth, K. Predicting recurrence and progression in individual patients with stage Ta T1 bladder cancer using EORTC risk tables: a combined analysis of 3596 patients from seven EORTC trials. *Eur Urol.* 2006; 49: 466-744. doi: 10.1016/j.eururo.2005.12.031
4. Hall, M.C., Chang, S.S., Dalbagni, G., Pruthi, R.S., Seigne, J.D., Skinner, E.C., Wolf, J.S., Schellhammer, P.F. Guideline for the management of non-muscle invasive bladder cancer (stages Ta, T1, and Tis): 2007 update. *J Urol.* 2007; 178: 2314-2330. doi: 10.1016/j.juro.2007.09.003
5. Bhindi, B., Kool, R., Kilkarni, G. S., Siemens, D.R., Aprikian, A.G., Breau, R.H., Brimo, F., Fiarey, A., French, G., Hanna, N., Izawa, J.I., Lacombe, L., McPherson, V., Rendon, R.A., Shayegan, B., So, A.I., Zlotta, A.R., Black, P.C., Kassouf, W. Canadian urological association guideline on the management of non-muscle-invasive bladder cancer. *Can Urol Assoc J.* 2021; 14: 424-457. doi: 10.5489/cuaj.7367
6. Babjuk, M., Burger, M., Capoun, O., Cohen, D., Comperat, E.M., Dominguez Escrig, J.L., Gontero, P., Liedberg, F., Masson-Lecomte, A., Mostafid, A.H., Palou, J., van Rhijn, B.W.G., Roupert, M., Shariat, S.F., Seisen, T., Soukup, V., Sylvester, R.J. European association of urology guidelines on non-muscle-invasive bladder cancer (Ta, T1, and carcinoma in situ). *Eur Urol.* 2022; 81, 50-61. doi: 10.1016/j.eururo.2021.09.028
7. Sylvester, R.J. bacillus calmette-guerin treatment of non-muscle invasive bladder cancer. *Int J Urol.* 2011; 18: 113-120. doi: 10.1111/j.1442-2042.2010.02678.x

8. Zlotta, A., Fleshner, N.E., Jewett, M.A. The management of BCG failure in non-muscle-invasive bladder cancer: an update. *Can Urol Assoc J.* 2009; 6: 5199-5205. doi: 10.5489/cuaj.1196
9. Meng, M.V., Gschwend, J.E., Shore, N., Grossfeld, G.D., Mostafid, H., Black, P.C. Emerging immunotherapy options for bacillus calmette-guerin unresponsive non-muscle invasive bladder cancer. *Urol J.* 2019; 202: 1111-1119. doi: 10.1097/JU.0000000000000297
10. Addeo, R., Caraglia, M., Bellini, S., Abbruzzese, A., Vincenzi, B., Montella, L., Miragliuolo, A., Guarrasi, R., Lanna, M., Cennamo, G., Faiola, V., Del Prete, S. Randomized phase III trial on gemcitabine versus mitomycin in recurrent superficial bladder cancer: evaluation of efficacy and tolerance. *J Clin Oncol.* 2010; 28: 543-548. doi: 10.1200/JCO.2008.20.8199
11. Porena, M., Zingaro, M., Lazzeri, M., Mearini, L., Giannantoni, A., Bini, V., Costantini, E. Bacillus Calmette-guerin versus gemcitabine for intravesical therapy in high-risk superficial bladder cancer: a randomized prospective study. *Urol Int.* 2010; 84: 23-27. doi: 10.1159/000273461
12. Lorenzo, G.D., Perdonà, S., Damiano, R., Faiella, A., Cantiello, F., Pignata, S., Ascierio, P., Simeone, E., De Sio, M., Autorino, R. Gemcitabine versus bacilli Calmette-guerin after initial bacilli Calmette-guerin failure in non-muscle-invasive bladder cancer: a multicenter prospective randomized trial. *Cancer.* 2010; 116: 1893-1900. doi: 10.1002/cncr.24914
13. Witjes, J.A., Bruins, H.M., Cathomas, R., Comperat, E.M., Cowan, N.C., Gakis, G., Hernandez, V., Espinos, E.L., Lorch, A., Neuzillet, Y., Rouanne, M., Thalmann, G.N., Veskimäe, E., Ribal, M.J., van der Heijden, A.G. European association of urology guidelines on muscle-invasive and metastatic bladder cancer: summary of the 2020 guidelines. *Eur Urol.* 2021; 79: 82-104. doi: 10.1016/j.eururo.2020.03.055
14. Shabsign, A., Korets, R., Vora, K.C., Brooks, C.M., Cronin, A.M., Savage, C., Paj, G., Bochner, B.H., Dalbagni, G., Herr, H.W., Donat, S. M. Defining early morbidity of radical cystectomy for patients with bladder cancer using a standardized reporting methodology. *Eur Urol.* 2009; 55: 164-176. doi: 10.1016/j.eururo.2008.07.031

15. Advanced Bladder Cancer (ABC) Meta-analysis Collaborators Group. Adjuvant chemotherapy for muscle-invasive bladder cancer: a systemic review and meta-analysis of individual participant data from randomized controlled trials. *Eur Urol.* 2022; 81: 50-61. doi: 10.1016/j.eururo.2021.09.028
16. Grossman, H.B., Natale, R.B., Tangen, C.M., Speights, V.O. Neoadjuvant chemotherapy plus cystectomy compared with cystectomy alone for locally advanced bladder cancer. *N Engl J Med.* 2003; 349: 859-866. doi: 10.1056/NEJMoa022148
17. Sonpavde, G., Watson, D., Tourtellott, M., Cowey, C.L., Hellerstedt, B., Hutson, T.E., Zhan, F., Vogelzang, N.J. Administration of cisplatin-based chemotherapy for advanced urothelial carcinoma in the community. *Clin Genitourin Cancer.* 2012; 10: 1-5. doi: 10.1016/j.clgc.2011.11.005
18. Joyce, D.D., Sharma, V., Williams, S.B. Cost-effectiveness and economic impact of bladder cancer management: an updated review of the literature. *Pharmacoeconomics.* 2023. doi: 10.1007/s40273-023-01273-8
19. Mossanen, M., Gore, J.L. The burden of bladder cancer care: direct and indirect costs. *Curr Opin Urol.* 2014; 24: 487-491. <https://doi.org/10.1097/MOU.0000000000000078>
20. Leal, J., Luengo-Fernandez, R., Sullivan, R., Witjes, J.A. Economic burden of bladder cancer Across the european union. *Eur Urol.* 2016; 69: 438-447. doi: 10.1016/j.eururo.2015.10.024
21. Hatogai, K., Sweis, R.F. The tumor microenvironment of bladder cancer. *Adv Exp Med Biol.* 2021; 1296: 275-260. doi: 10.1007/978-3-030-59038-3\_17
22. Krpina, K., Babarovic, E., Jonjic, N. Correlation of tumor-infiltrating lymphocytes with bladder cancer recurrence in patients with solitary low-grade urothelial carcinoma. *Virchows Arch.* 2015; 467: 443-448. doi: 10.1007/s00428-015-1808-5
23. Togashi, Y., Shitara, K., Nishikawa, H. Regulatory T cells in cancer immunosuppression – implications for anticancer therapy. *Nat Rev Clin Oncol.* 2019; 16: 356–371. doi: 10.1038/s41571-019-0175-7
24. Loskog, A., Ninalga, C., Paul-Wetterberg, G., de la Torre, M., Malmstrom, P.U., Totterman, T.H. Human bladder carcinoma is dominated by T-regulatory cells and Th1 inhibitory cytokines. *J Urol.* 2007; 177: 353–358. doi: 10.1016/j.juro.2006.08.078

25. Miyake, M., Tatsumi, Y., Gotoh, D., Ohnishi, S., Owari, T., Iida, K., Ohnishi, K., Hori, S., Morizawa, Y., Itami, Y., Nakai, Y., Inoue, T., Anai, S., Torimoto, K., Aoki, K., Shimada, K., Konishi, N., Tanaka, N., Fujimoto, K. Regulatory T cells and tumor-associated macrophages in the tumor microenvironment in non-muscle invasive bladder cancer treated with intravesical bacille calmette-guerin: a long-term follow-up study of a Japanese cohort. *Int J Mol Sci.* 2017: 18. doi: 10.3390/ijms18102186
26. Murai, R., Itoh, Y., Kageyama, S., Nakayama, M., Ishigaki, H., Teramoto, K., Narita, M., Yoshida, T., Tomita, K., Kobayashi, K.I., Wada, A., Nagasawa, M., Kubota, S., Ogasawara, K., Kawauchi, A. Prediction of intravesical recurrence of non-muscle-invasive bladder cancer by evaluation of intratumoral Foxp3+ T cells in the primary transurethral resection of bladder tumor specimens. *PLoS One.* 2018: 13: doi: 10.1371/journal.pone.0204745
27. Quaranta, V., Schmid, M.C. Macrophage mediated subversion of anti-tumor immunity. *Cells.* 2019: 8. doi: 10.3390/cells8070747
28. Rhee, I. Diverse Macrophages Polarization in Tumor Microenvironment. *Arch Pharm Res.* 2016: 39: 1588-1596. doi: 10.1007/s12272-016-0820-y
29. Sinha, P., Clements, V.K., Ostrand-Rosenberg, S. Reduction of Myeloid-Derived Suppressor Cells and Induction of M1 Macrophages Facilitate the Rejection of Established Metastatic Disease. *J. Immunol.* 2005: 174: 636–645. doi: 10.4049/jimmunol.174.2.636
30. Takao, S., Smith, E.H., Wang, D., Chan, C.K., Bulkley, G.B., Klein, A.S. Role of reactive oxygen metabolites in murine peritoneal macrophage phagocytosis and phagocytic killing. *Am. J. Physiol. Physiol.* 1996: 271: C1278–C1284. doi: 10.1152/ajpcell.1996.271.4.C1278
31. Mantovani, A., Marchesi, F., Malesci, A., Laghi, L., Allavena, P. Tumour-associated macrophages as treatment targets in oncology. *Nat Rev Clin Oncol.* 2017: 14: 399–416. doi: 10.1038/nrclinonc.2016.217
32. Noy, R., Pollard, J.W. Tumor-Associated Macrophages: From Mechanisms to Therapy. *Immunity.* 2014: 41: 49–61. doi: 10.1016/j.immuni.2014.06.010

33. Mantovani, A., Sica, A., Sozzani, S., Allavena, P., Vecchi, A., Locati, M. The chemokine system in diverse forms of macrophage activation and polarization. *Trends Immunol.* 2004; 25: 677–686. doi: 10.1016/j.it.2004.09.015
34. Huang, C.P., Liu, L.X., Shyr, C.R. Tumor associated macrophage facilitate bladder cancer progression by increasing cell growth, migration, invasion and cytokine expression. *Anticancer Res.* 2020; 40: 2715-2724. doi: 10.21873.anticancer.14243
35. Hanada, T., Nakagawa, M., Emoto, A., Nomura, T., Nasu, N., Nomura, Y. Prognostic value of tumor-associated macrophage count in human bladder cancer. *Int J Urol.* 2000; 7: 263–269. doi: 10.1046/j.1442-2042.2000.00190.x
36. Takeuchi, H., Tanaka, M., Tanaka, A., Tsunemi, A., Yamamoto, H. Predominance of M2- polarized macrophages in bladder cancer affects angiogenesis, tumor grade and invasiveness. *Oncol Lett.* 2016; 11: 3403–3408. doi: 10.3892/ol.2016.4392.
37. Wang, B., Liu, H., Dong, X., Wu, S., Zeng, H., Liu, Z., Wan, D., Dong, W., He, W., Chen, X., Zheng, L., Huang, J., Lin, T. High CD204+ tumor-infiltrating macrophage density predicts a poor prognosis in patients with urothelial cell carcinoma of the bladder. *Oncotarget.* 2015; 6: 20204–20214. doi: 10.18632/onco-target.3887
38. Filipovic, M.R. Persulfidation (s-sulphydration) and H<sub>2</sub>S. *Handb Exp Pharmacol.* 2015; 230: 29-59. doi: 10.1007/978-3-319-18144-8\_2
39. Braunstein, A., Goryachenkova, E., Tolosa, E., Willhardt, I., and Yefremova, L. Specificity and some other properties of liver serine sulphhydrase: evidence for its identity with cystathionine β-synthase. *Biochem Biophys Acta.* 1971; 242: 247–260. doi: 10.1016/0005-2744(71)90105-7
40. Chiku, T., Padovani, D., Zhu, W., Singh, S., Vitvitsky, V., and Banerjee, R. H<sub>2</sub>S biogenesis by human cystathionine γ-lyase leads to the novel sulfur metabolites lantionine and homolantionine and is responsive to the grade of hyperhomocysteinemia. *J Biol Chem.* 2009; 284: 11601–11612. doi: 10.1074/jbc.M808026200
41. Yadav, P.K., Yamada, K., Chiku, T., Koutmos, M., and Banerjee, R. Structure and kinetic analysis of H<sub>2</sub>S production by human mercaptopyruvate sulfurtransferase. *J Biol Chem.* 2013; 288: 20002–20013. doi: 10.1074/jbc.M113.466177

42. Jackson, M.R., Melideo, S.L., Jorns, M.S. Role of human sulfide: quinone oxidoreductase in H<sub>2</sub>S metabolism. *Methods Enzymol.* 2015; 554: 255–270. doi: 10.1016/bs.mie.2014.11.037
43. Weiseger, R., Pinkus, L., Jakoby, W. Thiol-S-methyltransferase: suggested role in detoxification of intestinal hydrogen sulfide. *Biochem Pharmacol.* 1980; 29: 2885–2887. doi: 10.1016/0006-2952(80)90029-5
44. Sun, Y., Wang, X.M., Chen, Y.H., Zhu, R.X., and Liao, C.C. Exhaled hydrogen sulfide in patients with chronic obstructive pulmonary disease and its correlation with exhaled nitric oxide. *Chin Med J (Engl).* 2013; 126: 3240–3244.
45. Toombs, C.F., Insko, M. A., Wintner, E.A., Deckwerth, T.L., Usansky, H., Jamil, K., Goldstein, B., Cooreman, M., Szabo, C. Detection of exhaled hydrogen sulphide gas in healthy human volunteers during intravenous administration of sodium sulphide. *Br J Clin Pharmacol.* 2010; 69: 626-636. doi: 10.1111/j.1365-2125.2010.03636.x
46. Sonke, E., Verrydt, M., Postenka, C.O., Pardhan, S., Willie, C. J., Mazzola, C.R., Hammers, M.D., Pluth, M.D., Lobb, I., Power, N.E., Chambers, A.F., Leong, H.S., Sener, A. Inhibition of endogenous hydrogen sulfide production in clear-cell renal cell carcinoma cell lines and xenografts restricts their growth, survival and angiogenic potential. *Nitric Oxide.* 2015; 49: 26-39. doi: 10.1016/j.noix.2015.06.001
47. Sogutdelen, E., Pacoli, K., Juriasingani, S., Akbari, M., Gabril, M., Sener, A. Patterns of expression of H<sub>2</sub>S-producing enzyme in human renal cell carcinoma specimens: potential for future therapeutics. *In Vivo.* 2020; 24; 2775-2781. doi: 10.21873/invivo.12102
48. Arkbari, M., Sogutdelen, E., Juriasingani, S., Sener, A. Hydrogen sulfide: emerging role in bladder, kidney, and prostate malignancies. *Oxid Med Cell Longev.* 2019; 2019. doi: 10.1155/2019/2360945
49. Hellmich, M.R., Coletta, C., Chao, C., Szabo, C. The therapeutic potential of cystathionine β-synthetase/hydrogen sulfide inhibition in cancer. *Antioxid Redox Signal* 2015; 22: 424–448. doi: 10.1089/ars.2014.5933
50. Hellmich, M.R., Coletta, C., Chao, C., Dikman, A., Szabo, C. P20: pro-and anti-proliferative effects of hydrogen sulfide in colon cancer cells: a unifying hypothesis. *Nitric Oxide.* 2014; 39: S22. doi: 10.1016/j.niox.2014.03.070

51. Lee, Z. W., Zhou, J., Chen, C.S., Zheo, Y., Tan, C.H., Li, L., Moore, P.K., Deng, L.W. The slow releasing hydrogen sulfide donor, GYY4137, exhibits novel anti-cancer effects in vitro and in vivo. *PLoS One*. 2011; 6. doi: 10.1371/journal.pone.0021077
52. Cai, W.J., Wang, M.J., Ju, L.H., Wang, C., Zhu, Y.C. Hydrogen sulfide induces human colon cancer cell proliferation: role of Akt, ERK, and p21. *Cell Biol Int*. 2010; 24: 565-572. doi: 10.1042/CBI20090368
53. Zhang, S., Bian, H., Li, X., Wu, H., Bi, Q., Yan, Y., Wang, Y. Hydrogen sulfide promotes cell proliferation of oral cancer through activation of the COX2/AKT/ERK1/2 axis. *Oncol Rep*. 2016; 35: 2825-2832. doi: 10.3892/or.2016.4691
54. Asimakopoulou, A., Panopoulos, P., Chasapis, C.T., Coletta, C., Zhou, Z., Cirino, G., Giannis, A., Szabo, C., Spyroulias, G.A., Papapetropoulos, A. Selectivity of commonly used pharmacological inhibitors for cystathionine b synthase (CBS) and cystathionine g lyase (CSE). *Br J Pharmacol*. 2013; 169: 922-932. doi: 10.1111/bph.12171
55. Sun, Q., Collins, R., Huang, S., Holmberg-Schiavone, L., Anand, G.S., Tan, C. H., van den Berg, S., Deng, S. W., Moore, P.K., Karlberg, T., Sivaraman, J. Structural Basis for the Inhibition Mechanism of Human Cystathionine  $\gamma$ -Lyase, an Enzyme Responsible for the Production of H<sub>2</sub>S. *J Biol Chem*. 2009; 284: 3076-3085. doi: 10.1074/jbc.M805459200
56. Percundani, R., Peracchi, A. A genomic overview of PLP dependent enzymes. *EMBO Rep*. 2003; 4: 850-854. doi: 10.1038/sj.embor.embor914
57. Liang, J., Han, Q., Tan, Y., Ding, H., Li, H. Current Advances on Structure-Function Relationships of Pyridoxal 5'-Phosphate-Dependent Enzymes. *Front Mol BioSci*. 2019; 6. doi: 10.3389/fmolb.2019.00004
58. Khan, N.H., Wang, D., Wang, W., Shahid, M., Khattak, S., Ngowi, E.E., Sarfraz, M., Ji, X.Y., Zhang, C.Y., Wu, D.D. Pharmacological inhibition of endogenous hydrogen sulfide attenuates breast cancer progression. *Molecules*. 2022; 27: 4049. doi: 10.3390/molecules27134049
59. Cano-Caliano, A., Oudin, A., Fack, F., Allega, M.F., Sumpton, D., Martinez-Garcia, E., Dittmar, G., Hau, A.C., De Falco, A, Herold-Mende, C., Bjerkvig, R., Meiser, J.,

- Tardito, S., Niclou, S.P. CSE drives antioxidant defense in cysteine-restricted IDH1-mutant astrocytomas. *Neurooncol Adv.* 2021: 3. doi: 10.1093/oaajnl/vdab057
60. Wang, Y. H., Huang J.T., Chen, W. L., Wang, R.H., Kao, M.C., Pan, Y.R., Chan, S.H., Tsai, K.W., Kung, H.J., Lin, K.T., Wang, L.H. Dysregulation of CSE promotes prostate cancer progression and metastasis. *EMBO Rep.* 2019: 20. doi: 10.15252/embr.201845986
61. Wang, D. Y., Zhang, J., Li, H.X., Zhang, Y.X., Jing, M.R., Cai, C.B., Wang, D., Qi, H.Q., Wang, Y.Z., Chen, H.J., Li, T., Zhai, Y.K., Ji, X. Y., Wu, D.D. Inhibition of endogenous hydrogen sulfide production suppresses the growth of nasopharyngeal carcinoma cells. *Mol Carcinog.* 2023: 62: 652-664. doi: 10.1002/mc.23513
62. Parrish, A.B., Freel, C.D., Kornbluth, S. Cellular mechanisms controlling caspase activation and function. *Cold Spring Harb Perspect Biol.* 2013: 5. doi: 10.1101/cshperspect.a008672
63. Lei, Y., Zhen, Y., Zhang, W., Sun, W., Lin, W., Feng, J., Luo, H., Chen, Z., Su, C., Zeng, B., Chen, J. Exogenous hydrogen sulfide exerts proliferation, anti-apoptosis, angiopoiesis and migration effects via activating HSP90 pathway in EC109 cells. *Oncol Rep.* 2016: 35: 3714-3720. doi: 10.3892/or.2016.4734
64. Zheng, D., Chen, Z., Chen, J., Zhuang, X., Feng, J., Li, J. Exogenous hydrogen sulfide exerts proliferation, anti-apoptosis, migration effects and accelerates cell cycle progression in multiple myeloma cells via activating the Akt pathway. *Oncol Rep.* 2021: 36: 1909-1916. doi: 10.3892/or.2016.5014
65. Zhen, Y., Pan, W., Hu, F., Wu, H., Feng, J., Zhang, Y., Chen, J. Exogenous hydrogen sulfide exerts proliferation/anti-apoptosis/angiogenesis/migration effects via amplifying the activation of NF-kB pathway in PLC/PRF/f hepatoma cells. *Int J Oncol.* 2015: 2194-2204. doi: 10.3892/ijo.2015.2914
66. Zhao, K., Ju, Y.J., Li, S., Altaany, Z., Wang, R., Yang, G. S-sulfhydration of MEK1 Leads to PARP-1 activation and DNA damage repair. *EMBO Rep.* 2014: 15: 792-800. doi: 10.1002/embr.201338213
67. Jiang, X., MacArthur, M.R., Trevino-Villarreal, J.H., Kip, P., Ozaki, C.K., Mitchell, S.J., Mitchell, J.R. Intracellular H<sub>2</sub>S production is an autophagy-dependent adaptive

- response to DNA damage. *Cell Chem Biol.* 2021: 28: 1669-1678. doi: 10.1016/j.chembiol.2021.05.016
68. Szczesny, B., Marcatti, Zatarain, J.R., Druzhyna, N., Wiktorowicz, J.E., Nagy, P., Hellmich, M.R., Szabo, C. Inhibition of hydrogen sulfide biosynthesis sensitizes lung adenocarcinoma to chemotherapeutic drugs by inhibiting mitochondrial DNA repair and suppressing cellular bioenergetics. *Sci Rep.* 2016:6:36125. doi: 10.1038/srep36125
69. Papapetropoulos, A., Pyriochou, A., Altaany, Z., Yang, G., Marazioti, A., Zhou, Z., Jeschke, M.G., Branksi, L.K., Herndon, D.N., Wang, R., Szabo, C. Hydrogen sulfide is an endogenous stimulator of angiogenesis. *PNAS.* 2019: 106. doi: 10.1073/pnas.0908047106
70. Wang, L., Shi, H., Liu, Y., Zhang, W., Duan, X., Li, M., Shi, X., Wang, T. Cystathionine  $\gamma$ -lyase promotes the metastasis of breast cancer via the VEGF signaling pathway. *Int J Oncol.* 2019: 55: 473-487. doi: 10.3892/ijo.2019.4823
71. Zhuang, R., Guo, L., Du, J., Wang, S., Li, J., Liu, Y. Exogenous hydrogen sulfide inhibits oral mucosal wound-induced macrophage activation via the NK-kB pathway. *Oral Dis.* 2018: 24: 793-801. doi: 10.1111/odi.12838
72. Miao, L., Xin, X., Xin, H., Shen, X., Zhu, Y.Z. Hydrogen sulfide recruits macrophage migration by integrin  $\beta$ 1-*Src*-*FAK*/*Pyk2*-*Rac* pathway in myocardial infarction. *Sci Rep.* 2016: 6. doi: 10.1038/srep22363
73. Yang, R., Qu, C., Zhou, Y., Konkell, J.E., Shi, S., Liu, Y., Chen, C., Liu, S., Liu, D., Chen, Y., Zandi, E., Chen, W., Zhou, Y., Shi, S. Hydrogen sulfide promotes Tet1- and Tet2-mediated Foxp3 demethylation to drive regulatory T cell differentiation and maintain immune homeostasis. *Immunity.* 2015: 43: 251-263. doi: 10.1016/j.immuni.2015.07.017
74. Gai, J.W., Qin, W., Liu, M., Wang, H.F., Zhang, M., Li, M., Zhou, W.H., Ma, W.T., Liu, G.M., Song, W.H., Jin, J., Ma, H.S. Expression profile of hydrogen sulfide and its synthases correlates with tumor stage and grade in urothelial cell carcinoma of bladder. *Urol Oncol.* 2016: 24. doi: 10.1016/j.urolonc.2015.06.020
75. Wahafu, W., Gai, J., Song, L., Ping, H., Wang, M., Yang, F., Niu, Y., Xing, N. Increased H<sub>2</sub>S and its synthases in urothelial cell carcinoma of the bladder, and

- enhanced cisplatin-induced apoptosis following H<sub>2</sub>S inhibition in EJ cells. *Oncol Lett.* 2018; 15: 8484-8490. doi: 10.3892/ol.2018.8373
76. Liu, H., Chang, J., Zhao, Z., Li, Y., Hou, J. Effects of exogenous hydrogen sulfide on the proliferation and invasion of human bladder cancer cells. *J Cancer Res Ther.* 2017; 13: 829-832. doi: 10.4103/jcrt.JCRT\_423\_17
77. Panza, E., Bello, I., Smimmo, M., Brancaleone, V., Mitidieri, E., Bucci, M., Cirino, G., Sorrentino, R., D Emmanuele di Villa Bianca, R. Endogenous and exogenous hydrogen sulfide modulates urothelial bladder carcinoma development in human cell lines. *Biomed Pharmacother.* 2022; 151. doi: 10.1016/j.biopha.2022.113137
78. Relouw, S., Dugbartey, G.J., Sener, A. Non-invasive imaging modalities in intravesical murine models of bladder cancer. *Cancers*, 2023. 15: 2381. doi: 10.3390/cancers15082381
79. Oliveira, P.A., Gil da Costa, R.M., Vasconcelos-Nobrega, C., Arantes-Rodrigues, R., Pinto-Leite, R. Challenges with in vitro and in vivo experimental models of urinary bladder cancer for novel drug discovery. *Expert Opin Drug Discov*, 2016; 11. doi: 10.1080/17460441.2016.1174690
80. Zhang, N., Li, D., Shao, J., Wang, X. Animal models for bladder cancer: the model establishment and evaluation (review). *Oncol Lett.* 2015; 9. doi: 10.3892/ol.2015.2888
81. John, B. A., Said, N. Insights from animal models of bladder cancer: recent advances, challenges, and opportunities. *Oncotarget*, 2017; 8. doi: 10.18632/oncotarget.17714.
82. Zhang, Y., Li, Y. Bladder cancer cells prevent cisplatin-induced oxidative stress by upregulating Nestin1 expression. *Am J Transl Res.* 2021; 13: 11178-11193
83. Wang, Y., Gao, J., Hu, S., Zeng, W., Yang, H., Chen, H., Wang, S. SLC25A21 suppresses cell growth in bladder cancer via an oxidative stress-mediated mechanism. *Front Oncol.* 2021; 11 doi: 10.3389/fonc.2021.682710
84. Gong, Z., Xu, H., Su, Y., Wu, W., Hao, L., Han, C. Establishment of a novel bladder cancer xenograft model in humanized immunodeficient mice. *Cell Physiol Biochem.* 2015; 37. doi: 10.1159/000430401
85. Yang, R., Liu, M., Liang, H., Guo, S., Guo, X., Yuan, M., Lian, H., Yan, X., Zhang, S., Chen, X., Fang, F., Gio, H., Zhang, C. miR-138-5p contributes to cell proliferation

- and invasion by targeting survivin in bladder cancer cells. *Mol Cancer*. 2016: 15. doi: 10.1186/s12943-016-0569-4
86. Raven, P.A., D'Costa, N.M., Moskalev, I., Tan, Z., Frees, S., Chavez-Munoz, C., So, A.I. Development of murine intravesical orthotopic human bladder cancer (mio-hBC) model. *Am J Clin Exp Urol*. 2018: 6: 245-259
87. Seo, H.K., Shin, S.P., Jung, N.R., Kwon, W.A., Jeong, K.C., Lee, S.J. The establishment of a growth-controllable orthotopic bladder cancer model through the downregulation of c-myc expression. *Oncotarget*. 2016: 8: 50500-50509. doi: 10.18632/oncotarget.10784
88. Brown, N.S., Streeter, E.H., Jones, A., Harris, A.L., Bicknell, R. Cooperative stimulation of vascular endothelial growth factor expression by hypoxia and reactive oxygen species: the effect of targeting vascular endothelial growth factor and oxidative stress in an orthotopic xenograft model of bladder carcinoma. *Br J Cancer*. 2005: 92: 1696-1701. doi: 10.1038/sj.bjc.6602522
89. Parada, B., Reis, F., Pinto, A., Sereno, J., Xavier-Cunha, M., Neto, P., Rocha-Pereira, P., Mota, A., Figueiredo, A., Teixeira, F. Chemopreventive efficacy of atorvastatin against nitrosamine-induced rat bladder cancer: antioxidant, anti-proliferative and anti-inflammatory properties. *Int J Mol Sci*. 2012: 31: 8482-8499. doi: 10.3390/ijms13078482
90. Zhu, Z., Ma, A.H., Zhang, H., Lin, T.Y., Xue, X., Farrukh, H., Zhu, S., Shi, W., Yuan, R., Cao, Z., Chittepu, V.C.S.R., Prabhala, R., Li, Y., Lam, K.S., Pan, C. Phototherapy with cancer-specific nanoporphyrin potentiates immunotherapy in bladder cancer. *Clin Cancer Res*. 2022: 28: 4820-4831. doi: 10.1158/1078-0432.CCR-22-1362
91. Garris, G.S., Wong, J.L., Ravetch, J.V., Knorr, D.A. Dendritic cell targeting with Fc-enhanced CD40 agonistic antibodies induced durable bladder cancer immunity. *Sci Transl Med*. 2021: 13. doi:10.1126/scitranslmed.abd1346
92. Chan, E., Patel, A., Heston, W., Larchian, W. Mouse orthotopic models for bladder cancer research. *BJU Int*. 2009: 104: 1286-1291. doi: 10.1111/j.1464-410X.2009.08577.x

93. Ahmed, I., Sansom, O. J., Leung, H.Y. Exploring molecular genetics of bladder cancer: lessons learned from mouse model. *Dis Model Mech.* 2012; 5: 323-332. doi: 10.1242/dmm.008888
94. Oliveira, M.M., Teixeira, J.C., Vasconcelos-Nobrega, C., Felix, L.M., Sardao, V.A., Colaco, A.A., Oliveira, P.A., Peixoto, F.P. Mitochondrial and liver oxidative stress alternations induced by N-butyl-N-(4-hydroxybutyl) nitrosamine: relevance for hepatotoxicity. *J Appl Toxicol.* 2013; 33: 434-443. doi: 10.1002/jat.1763
95. Afify, H., Ghoneum, A., Almousa, S., Abdulfattah, A.Y., Warren, B., Langsten, K., Gonzalez, D., Casals, R., Bharadwaj, M., Kridel, S., Said, N. Metabolic credentialing of murine carcinogen-induced urothelial cancer. *Sci Rep.* 2021; 11. doi: 10.1038/s41598-021-99746-3.
96. Fantini, D., Meeks, J.J. The BBN model: a mouse bladder cancer model featuring basal-subtype gene expressing and MLL3-MLL4 genetic disruption. *Oncoscience.* 2018; 5: 172-173. doi:10.18632/oncoscience.439.
97. Burger, M., Catto, J.W.F., Dalbagni, G., Grossman, H.B., Herr, H., Karakiewicz, P., Kassouf, W., Kiemeny, L.A., La Vecchia, C., Shariat, S., Lotan, Y. Epidemiology and risk factors of urothelial bladder cancer. *Eur Urol.* 2013; 63: 234-241. doi: 10.1016/j.eururo.2012.07.033
98. Oliveira, P.A., Vasconcelos-Nobrega, C., da Costa, R.M.G., Arantes-Rodrigues, R. The N-butyl-N-4-hydroxybutyl nitrosamine mouse urinary bladder cancer model. *Methods Mol Biol.* 2018; 1655: 155-167. doi: 10.1007/978-1-4939-7234-0\_13
99. Smilowitz, H. M., Tarmu, L.J., Sanders, M.M., Taylor III, J.A., Choudhary, D., Xue, C., Dymont, N.A., Sasso, D, Deng, X., Hainfeld, J.F. Biodistribution of gold nanoparticles in BBN-induced muscle-invasive bladder cancer cell line. *Int J Nanomedicine.* 2017; 12. doi: 10.2147/IJN.S140977.
100. He, C., Huang, L., Lei, P., Liu, X., Li, B., Shan, Y. Sulforaphane normalizes intestinal flora and enhances gut barrier in mice with BBN-induced bladder cancer. *Mol Nutr Food Res.* 2018; 62. doi: 10.1002/mnfr.201800427.
101. Ohtani, M., Kakizoe, T., Nishio, Y., Sato, S., Sugimura, T., Fukushima, S., Niijima, T. Sequential changes of mouse bladder epithelium during induction of invasive

- carcinomas by N-butyl-N-(4-hydroxybutyl) nitrosamine. *Cancer Res.* 1986; 46: 2001-2004.
102. Jager, W., Moskalev, I., Janssen, C., Hayashi, T., Awrey, S., Gust, K.M., So, A.I., Zhang, K., Fazli, L., Li, E., Thuroff, J.W., Lange, D., Black, P.C. Ultrasound-guided intramural inoculation of orthotopic bladder cancer xenografts: a novel high-precision approach. *PLoS One.* 2013; 8. doi: 10.1371/journal.pone.0059536.
103. Jurczok, A., Fornara, P., Soling, A. Bioluminescence imaging to monitor bladder cancer adhesion *in vivo*: a new approach to optimize a syngeneic, orthotopic, murine bladder cancer model. *BJU Int.* 2008; 101: 120-124. doi: 10.1111/j.1464-410X.2007.07193.x
104. Patel, A.R., Chan, E.S.Y., Hansel, D.E., Powell, C.T., Heston, W.D., Larchian, W.A. Transabdominal micro-ultrasound imaging of bladder cancer in a mouse model: a validation study. *J Urol.* 2010; 75: 799-804. doi: 10.1016/j.urology.2009.06.047.
105. Chan, E.S.Y., Patel, A.R., Larchian, W.A., Heston, W.D. In vivo targeted contrast enhanced micro-ultrasound to measure intratumor perfusion and vascular endothelial growth factor receptor 2 expression in a mouse orthotopic bladder cancer model. *J Urol.* 2011; 185: 2359-2365. doi: 10.1016/j.juro.2011.02.047.
106. Pereira, P.M.R., Roberts, S., Figueira, F., Tome, J.P.C., Reiner, T., Lewis, J.S. PET/CT imaging with an <sup>18</sup>F-labeled galactodendritic unit in a galectn-1-overexpressing orthotopic bladder cancer model. *J Nucl Med.* 2020; 61: 1369-1375. doi: 10.2967/jnumed.119.236430.
107. Scheepbouwer, C., Meyer, S., Burggraaf, M.J., Jose, J. Molthoff, C.F.M. A multimodal imaging approach for longitudinal evaluation of bladder tumor development in an orthotopic murine model. *PLoS One.* 2016; 11. doi: 10.1371/journal.pone.0161284.
108. Hoang, T.T., Mandleywala, K., Viray, T., Tan, K.V., Lewis, J.S., Pereira, P.M.R. EGFR-targeted immunoPET of UMUC3 orthotopic bladder tumors. *Mol Imaging Biol.* 2022; 24: 511-518. doi: 10.1007/s11307-022-01708-2.
109. Glaser, A.P., Procissi, D., Yu, Y., Meeks, J.J. Magnetic resonance imaging assessment of carcinogen-induced murine bladder tumors. *J Vis Exp.* 2019. doi: 10.3791/59101.

110. Cai, J., Xie, Z., Yan, Y., Huang, Z., Tang, P., Cao, X., Wang, Z., Yang, C., Tan, M., Zhang, F., Shen, B. Establishment of an optimized orthotopic bladder cancer model in mice. *BMC Urol.* 2022; 22. doi: 10.1186/s12894-022-01093-6.
111. Solingapuram Sai, K.K., Zachar, Z., Bingman, P.M., Mintz, A. Metabolic PET imaging in oncology. *Nucl Med Mol Imaging.* 2017; 209: 270-276. doi: 10.2214/AJR.17.18112
112. Vasireddi, A., Nguyen, N.C. PET/CT limitations and pitfalls in urogenital cancers. *Semin Nucl Med.* 2021; 51: 611-620. doi: 10.1053/j.semnuclmed.2021.06.013.
113. Mahendra, I., Hanaoka, H., Yamaguchi, A., Amartuvshin, T., Tsushima, Y. Diagnosis of bladder cancer using <sup>18</sup>F-labeled  $\alpha$ -methyl-phenylalanine tracers in a mouse model. *Ann Nucl Med.* 2020; 34: 329-336. doi: 10.1007/s12149-020-01452-z.
114. Ampona, V.O., Shuman, L., Ellis, J., Wang, E., Walter, V., Owens, R.G., Zaleski, M., Warrick, J.I., Raman, J.D., DeGraff, D.J. Carcinogen-induced bladder cancer in the FVB mouse strain is associated with glandular differentiation and increased Cd274/Pdl-1 expression. *Am J Clin Exp Urol.* 2019; 7: 139-152.
115. Mao, M, H., Huang, H.B., Zhang, X.L., Liu, Y.L., Wang, P. Additive antitumor effect of arsenic trioxide combined with intravesical bacillus calmette-guerin immunotherapy against bladder cancer through blockade of the IER3/Nrf2 pathway. *Biomed Pharmacother.* 2018. 107: 1093-1103. doi: 10.1016/j.biopha.2018.08.057
116. Hori, S., Miyake, M., Tatsumi, Y., Onishi, S., Morizawa, Y., Nakai, Y., Tanaka, N., Fujimoto, K. Topical and systemic immunoreaction triggered by intravesical chemotherapy in N-butyl-N-(4-hydroxybutyl) nitrosamine induced bladder cancer mouse model. *PLoS One.* 2017; 12. doi: 10.1371/journal.pone.0175494
117. Lee, S., Carrasco Jr., A. C., Meachman, R.B., Malykhina, A.P. Transurethral instillation procedure in adult mice. *J Vis Exp.* 2017. doi: 10.3791/56663
118. Reis, L.O., Sopena, J.M.G., Favaro, W.J., Martin, M.C., Simao, A.F.L., dos Reis, R.B., de Andrade, M.F., Domenech, J.D., Cardo, C.C. Anatomical features of the urethra and urinary bladder catheterization in female mice and rats. An essential translational tool. *Acta Cir Bras.* 2011; 26: 106-110. doi: 10.1590/s0102-86502011000800019

119. Ferlay J et al (2018) Global cancer observatory: cancer today. Available from: <https://gco.iarc.fr/today>. Accessed date 20 May 2023
120. Liu, Z., Tang, Q., Qi, T., Othmane, B., Yang, Z., Chen, J., Hu, J., Zu, X. A robust hypoxia risk score predicts the clinical outcomes and microenvironment immune characters in bladder cancer. *Front Immunol.* 2021; 12: 725223. doi: 10.2289/fimmu.2021.725223
121. Cao, R., Ma, B., Wang, G., Xiong, Y., Tian, Y., Yuan, L. Characterization of hypoxia response patterns identified prognosis and immunotherapy response in bladder cancer. *Mol Ther Oncolytics.* 2021; 22: 277-293. doi: 10.1016/j.omto.2021.06.011
122. Wang, M., Yan, J., Cao, X., Hua, P., Li, Z. Hydrogen sulfide modulates epithelial-mesenchymal transition and angiogenesis in non-small cell lung cancer via HIF-1 $\alpha$  activation. *Biochem Pharmacol.* 2020; 172. doi: 10.1016/j.bcp.2019.113775
123. Wang, R. Physiological implications of hydrogen sulfide: a whiff exploration that blossomed. *Physiol Rev.* 2012; 92: 791-896. doi: 10.1152/physrev.00017.2011
124. Sekiguchi, F., Sekimoto, T., Ogura, A., Kawabata, A. Endogenous hydrogen sulfide enhances cell proliferation of human gastric cancer AGS cells. *Biol Pharm Bull.* 2016; 39: 887-890. doi: 10.1248/bpb.b15-01015
125. Kioke, S., Kawamura, K., Kimura, Y., Shibuya, N., Kimura, H., Ogasawara, Y. Analysis of endogenous H<sub>2</sub>S and H<sub>2</sub>S<sub>n</sub> in mouse brain by high-performance liquid chromatography with fluorescence and tandem mass spectrometric detection. *Free Radic.* 2017; 113: 355-362. doi: 10.1016/j.freeradbiomed.2017.10.346
126. Hall, J.R., Taylor, J.B., Bradshaw, T.M., Schoenfisch, M.H. Planar carbon electrode for real-time quantification of hydrogen sulfide release from cells. *Sens Diagn.* 2022; 1: 203-211. doi: 10.1039/d2sd00179a
127. Ibrahim, H., Serag, A., Farag, M.A. Emerging analytical tools for the detection of the third gasotransmitter H<sub>2</sub>S, a comprehensive review. *J Adv Res.* 2021; 27: 137-153. doi: 10.1016/j.jare.2020.05.018
128. Hamid, A.R.A.H., Ridwan, F.R., Parikesit, D., Widia, F., Mochtar, C.A., Umbas, R. Meta-analysis of neoadjuvant chemotherapy compared to radical cystectomy alone in improving overall survival of muscle-invasive bladder cancer patients. *BMC Urol.* 2020; 20: 158. doi: 10.1186/s12894-020-00733-z

129. Srinivasula, S.M., Ahmad, M., Fernandes-Alnemri, T., Alnemri, E.S. Autoactivation of procaspase-9 by Apaf-1-mediated oligomerization. *Mol. Cell.* 1998: 1: 949-958. doi: 10.1016/s1097-2765(00)80095-7
130. Yong-Xian, G., Xiao-Huan, L., Fan, Z., Guo-Fang, T. Gemcitabine inhibits proliferation and induces apoptosis in human pancreatic cancer PANC-1 cells. *J Cancer Res Ther.* 2016: 12: 1-4. doi: 10.4103/0973-1482.191615
131. Gassaniga, P., Silvestri, I., Gradilone, A., Scarpa, S., Morrone, S., Gandini, O., Gianni, W., Frati, L., Angliano, A. A. Gemcitabine-induced apoptosis in 5637 cell line: an in vitro model for high-risk superficial bladder cancer. *Anticancer Drugs.* 2007: 18: 179-185. doi: 10.1097/CAD.0b013e328010ef47
132. Wang, Y., Kuramitsu, Y., Tokuda, K., Baron, B., Kitagawa, T., Akada, J., Maehara, S., Maehara, Y., Nakamura, K. Gemcitabine induces poly (ADP-ribose) polymerase-1 (PARP-1) degradation through autophagy in pancreatic cancer. *PLoS One.* 2014: 9: doi: 10.1371/journal.pone.0109076
133. Ko, K., Jeong, C.W., Kwak, C., Kim, H.H., Ku, J. H. Significance of Ki-67 in non-muscle invasive bladder cancer patients: a systemic review and meta-analysis. *Oncotarget.* 2017: 8: 100614-100630. doi: 10.18632/oncotarget.21899
134. Ge, Z., Ding, S. The crosstalk between tumor-associated macrophages (TAMs) and tumor cells and the corresponding targeted therapy. *Front Oncol.* 2020: 10. doi: 10.2289/fonc.2020.590941
135. Deshmukh, S.K., Tyagi, N., Khan, M.A., Srivastava, S.K., al-Ghadhban, A., Dugger, K., Carter, J.E., Sinh, S., Sinh, A. P. Gemcitabine treatment promotes immunosuppressive microenvironment in pancreatic tumors by supporting the infiltration, growth, and polarization of macrophages. *Sci Rep.* 2018: 8. doi: 10.1038/s41598-018-30437-2
136. Plate, J. M.D., Plate, A.E., Shott, S., Bograd, S., Harris, J.E. Effect of gemcitabine on immune cells in subjects with adenocarcinoma of the pancreas. *Cancer Immunol Immunother.* 2005: 9: 54: 915-925. doi: 10.1007/s00262-004-0638-1
137. Xue, Y., Tong, L., Liu, F., Liu, A., Zeng, S., Xiong, Q., Yang, Z., He, X., Sun, Y., Xu, C. Tumor-infiltrating M2 macrophages driven by specific genomic alterations are

- associated with prognosis in bladder cancer. *Oncol Rep.* 2019; 42: 581-594. doi: 10.3892/or.2019.7196
138. Barros, M.H.M., Hauck, F., Dreyer, J.H., Kempkes, B., Niedobitek, G. Macrophage polarization: an immunohistochemical approach for identifying M1 and M2 macrophages. *PLoS One.* 2013; 8: 390808. doi: 10.1371/journal.pone.0080908
139. Jiang, Z., Zhang, Y., Zhang, Y., Jia, Z., Zhang, Z., Yang, J. Cancer derived exosomes induces macrophages immunosuppressive polarization to promote bladder cancer progression. *Cell Commun Signal.* 2021; 19. doi: 10.1186/s12964-021-00768-1
140. Kong, X., Zhu, M., Wang, Z., Xu, Z., Shao, J. Characteristics and clinical significance of CD163+/CD206+M2 mono-macrophage in the bladder cancer microenvironment. *Turk J Biol.* 2021; 45: 624-632. doi: 10.3906/biy-2014-17
141. Yue, T., Li, J., Zhu, J., Zuo, S., Wang, X., Liu, Y., Liu, J., Liu, X., Wang, P., Chen, S. Hydrogen sulfide creates a favorable immune microenvironment for colon cancer. *Cancer Res.* 2023; 83: 595-612. doi: 20.2258/0008-5472.CAN-22-1837
142. Oh, D.Y., Kewk, S.S., Raju, S.S., Li, T., McCarthy, E., Chow, E., Aran, D., Ilano, A., Pai, C.C.S., Rancan, C., Allaire, K., Burra, A., Sun, Y., Spitzer, M.H., Mangul, S., Porten, S., Meng, M.V., Friendlander, T.W., Ye, C.Y., Fong, W. Intratumoral CD4+ T cells mediate anti-tumor cytotoxicity in human bladder cancer. *Cell.* 2020; 181: 1612-1625. doi: 10.1016/j.cell.2020.05.017

## **Appendix A -Animal ethics approval**

**AUP Number:** 2022-021

**PI Name:** Sener, Alp

**AUP Title:** The effect of pharmacological inhibition of endogenous hydrogen sulfide production on the progression of high-grade bladder cancer

**Approval Date:** 04/01/2022

### **Official Notice of Animal Care Committee (ACC) Approval:**

Your new Animal Use Protocol (AUP) 2022-021:1: entitled " The effect of pharmacological inhibition of endogenous hydrogen sulfide production on the progression of high-grade bladder cancer" has been APPROVED by the Animal Care Committee of the University Council on Animal Care. This approval, although valid for up to four years, is subject to annual Protocol Renewal.

Prior to commencing animal work, please review your AUP with your research team to ensure full understanding by everyone listed within this AUP.

As per your declaration within this approved AUP, you are obligated to ensure that:

1. This Animal Use Protocol is in compliance with:
  - Western's Senate MAPP 7.12 [PDF]; and
  - Applicable Animal Care Committee policies and procedures.
2. Prior to initiating any study-related activities—as per institutional OH&S policies—all individuals listed within this AUP who will be using or potentially exposed to hazardous materials will have:
  - Completed the appropriate institutional OH&S training;
  - Completed the appropriate facility-level training; and
  - Reviewed related (M)SDS Sheets.

Submitted by: Copeman, Laura on behalf of the Animal Care Committee

Dr. Rob Gros,  
Animal Care Committee Chair  
Animal Care Committee  
The University of Western Ontario  
London, Ontario Canada N6A 5C1

## Curriculum Vitae – Sydney Relouw

**Post-secondary  
Education and  
Degrees:** Carleton University  
Ottawa, Ontario, Canada  
2015-2019 B.Sc.

The University of Western Ontario  
London, Ontario, Canada  
2021-2023 M.Sc.

**Honours and  
Awards:** FW Luney Graduate Entrance Scholarship  
The University of Western Ontario  
2021-2023

**Related Work  
Experience:** Teaching Assistant  
MEDSCIEN 3990, MICROIMM 3100, MICROIMM 2500  
The University of Western Ontario  
2021-2023

### Publications:

*Published:*

**Relouw, S.**, Dugbartey, G.J., Sener, A. Non-invasive imaging modalities in intravesical murine models of bladder cancer. *Cancers*, 2023. 15: 2381. doi: 10.3390/cancers15082381

*In Progress:*

**Relouw, S.**, P., McLeod, Knier, N., Martinez Santiesteban, F., Foster, P., Cadieux-Pitre, H.A., Hague, N., O’Neil, C., Gabril, M., Moussa, M., Huynh, M., Haeryfar, M., Sener, A. Pharmacological inhibition of endogenous hydrogen sulfide production on bladder cancer progression in an intravesical murine model. 2023.

### Presentations:

*Oral:*

Effect of pharmacological inhibition of endogenous hydrogen sulfide production on high-grade bladder cancer progression. 78<sup>th</sup> Canadian Urological Association Annual Meeting (International). Montreal, Canada. June 2023.

*Poster:*

The effect of pharmacological inhibition of endogenous hydrogen sulfide production on high-grade bladder cancer progression. Infection and Immunity Research Forum (Institutional). London, Canada. November 2022.

The effect of pharmacological inhibition of endogenous hydrogen sulfide production on high-grade bladder cancer progression. Western Research Forum (Institutional). London, Canada. March 2023.

Effect of pharmacological inhibition of endogenous hydrogen sulfide production on high-grade bladder cancer progression. Immuno-Oncology Symposium (Institutional). London, Canada. March 2023.

Pharmacological inhibition of endogenous hydrogen sulfide production in an intravesical murine model of bladder cancer. Dr. Robert Zhong Surgery Research Day (Institutional). London, Canada. June 2023.